CONTRACT SERIAL NO. 79219-01-SQ
CONTRACT REQUISITION NO. 23440-7-9219
CONTRACTOR: ONTARIO RESEARCH FOUNDATION

Laser Treatment of Al-Bronze

Final Report No. 57-10908A

Metals Technology Laboratories
Engineering Performance Section
CANMET
568 Booth Street
Ottawa, Ontario
K1A 0G1

Attention: Dr. W. Revie

Submitted by:

G. Palumbo
R. T. Lassau
Metals & Corrosion Technologies

T. Kilp
Laser Applications

September 8, 1989

MICROMEDIA

32 pp

ORTECH
INTERNATIONAL
2395 Speakman Drive
Mississauga, Ontario L5K 1B3
(416) 822-4111
Telefax (416) 823-1446

We, ORTECH Corporation, conducting business as "ORTECH International", stipulate that this document is subject to the following terms and conditions:
1. Any proposal contained herein was prepared for the consideration of the addressee only. Its contents may not be used by nor disclosed to any other party without our prior written consent.
2. Any testing, inspection or investigation performed by us will be conducted in accordance with normal professional standards. Neither we nor our employees shall be responsible for any loss or damage resulting directly or indirectly from any default, error or omission.
3. Any report, proposal or quotation prepared by us refers only to the particular material, instrument or other subject referred to in it. No representation is made that similar articles will be of like quality.
4. No report issued by us shall be published in whole or in part without our prior written consent.
5. Our name shall not be used in any way in connection with the sale, offer or advertisement of any article, process or service.
6. We reserve the right not to commence and/or continue any work until payment arrangements satisfactory to us are established.

TABLE OF CONTENTS

Page

EXECUTIVE SUMMARY 1

1. INTRODUCTION 2

2. EXPERIMENTAL 2
    2.1 Sample Preparation
    2.2 Laser Processing
    2.3 Corrosion and Mechanical Tests
    2.4 Metallography and Chemical Analysis

3. RESULTS AND DISCUSSION 6
    3.1 Microstructural and Chemical Characteristics of the Laser Treated Surfaces
    3.2 Mechanical Properties
    3.3 Corrosion Behaviour

4. SUMMARY AND RECOMMENDATIONS 16

APPENDIX A
APPENDIX B
APPENDIX C

EXECUTIVE SUMMARY

Laser processing parameters and procedures for (1) surface alloying and (2) microstructural refinement of a conventional binary aluminum bronze alloy (CDA610) have been established. An optimum treatment depth of ~200 µm was achieved, consisting of a relatively uniform concentration of laser alloyed iron, and a microstructure characteristic of rapid solidification processing. The corrosion and mechanical properties of laser modified specimens were evaluated, and on the basis of the observed performance, these laser modified alloys are considered promising candidate materials for marine (1) erosion and corrosion and (2) cavitation, resistant applications. Application of this technology to service conditions will require further refinement and optimization of laser alloy chemistry and laser treated surface topography.

RESUME - TRAITMENT LASER POUR AL-BRONZE

Les paramètres et procédures d'utilisation du laser pour (1) réduire la surface et (2) raffinement microstructural d'un alliage binaire conventionnel d'aluminium bronze (CDA610) ont été établies. Un traitement optimum a été réalisé à une profondeur de ~200 µm, consistant d'une concentration relativement uniforme de fer diminué par laser et, une caractéristique de microstructure par procédé de solidification rapide. La corrosion et les propriétés mécaniques des spécimens modifiés au laser ont été évalués, et sur les fondements de la performance observée, ces alliages modifiés par laser sont considérés comme étant des materiaux prometteurs pour (1) l'érosion et la corrosion marine et (2) les applications résistantes à la cavitation. L'application de cette technologie en condition de service requérera de plus amples raffinements et une opt chimie d'alliage au laser et surface traitée au laser.

1. INTRODUCTION

This final report provides a comprehensive summary and evaluation of the results derived from the laser surface modification program initially outlined in Proposal No. 87-58-5271. Preliminary results used to establish fundamental laser processing parameters for the laser surface treatment and alloying (Fe) of a binary Al-bronze (Cu-7 wt.% Al) have been previously presented in progress report s numbered 1-3, and have been appended to this report (Appendices A, B, C). This present report will focus on results pertaining to (1) the refinement and optimization of laser processing parameters, and (2) the corrosion and mechanical properties of laser treated Al-bronze specimens.

2. EXPERIMENTAL

2.1 Sample Preparation

Initial attempts at laser alloying a Cu-7 wt.% Al alloy (CDA610 Heat F499 Metal Samples Co. Inc.) were unsuccessful due to intergranular cracking during laser processing (Progress Report No. 2). It was subsequently determined by ORTECH International that this commercial alloy was severely embrittled by trace levels of bismuth. In order to alleviate this cracking problem, a Cu 7 wt.% alloy was cast (2 cm dia. rod) by induction melting high purity grades of Cu (99.999%) and Al (99.,999%). The as-cast microstructure of the alloy is shown in Figure 1. Disc specimens of 5 mm thickness were sectioned from the cast rod, and mechanically polished to a 600 grit finish for subsequent processing.

In this investigation, both vapour and electrochemical deposition techniques were investigated as means for the application of Fe-layers. As discussed in Progress Reports numbered 1 and 2, electrodeposition was determined to provide improved (1) coating integrity, and (2) interfacial adhesion.

Laser processing results presented in Progress Reports numbered 2 and 3 were obtained with specimens having a 15 µm electrodeposited Fe coating. In order to more closely control the Fe concentration in the laser alloyed zone, the following empirical relation was derived, yielding the coating thickness (t) required as a function of desired Fe concentration (C (wt.%)) and laser treatment depth (d).

$$t = 0.011 \cdot C \cdot d \qquad [1.0]$$

Results presented in this final report were obtained with electrodeposited coating thickness of 4.4 µm, which would be expected to yield a homogeneous Fe concentration of 2 wt.% (equivalent to control alloy CDA614) to a treatment depth of 200 µm. Electrodeposition was from a ferrous sulphate bath using a plating current density of 30 mA/cm^2. Plating thickness was controlled by coulometric analysis, and confirmed by specimen mass gain measurements.

2.2 Laser Processing

Laser treatment was carried out using a Photon Sources Turbolase T3000 continuous wave (CW) carbon dioxide (CO_2) laser located at the National Research Council, Ottawa. The laser was operated at a fixed output of 2450W at a 10.6 µm wavelength. Table I outlines the laser processing variables, and the variable ranges examined in this investigation.

TABLE I

SUMMARY OF LASER PROCESSING VARIABLES

Parameter	Range Examined
Output Power	2450 W (fixed)
Focal Height	0 - 25.4 mm
Scan Rate	21 - 127 mm/s
Scan Jog	0.127 - 0.3 mm

On the basis of results presented in Progress Reports numbered 1 - 3, it was determined that a two-stage laser treatment procedure involving an initial alloying scan, followed by a laser scan yielding compositional homogenization and rapid resolidification would be required. In addition, it was determined that a higher power density (achieved through a reduced focal height) and a more rapid scan rate than that previously utilized (i.e. Progress Reports numbered 1 - 3) would yield (1) greater homogenization of Fe in the laser treated zone as a result of more violent mixing under high power density conditions, and (2) enhanced structural refinement as a consequence of the higher cooling rates resulting from increased laser scan rates. The optimized laser treatment conditions pertaining to this report are outlined in Table II.

TABLE II

SUMMARY OF LASER TREATMENT CONDITIONS

Treatment		Scan Rate (mm/s)	Focal Height (mm)	Jog Distance (mm)
A-1	Initial Area Scan:	42.3	12.7	0.38
	Final Area Scan:	84.6	6.4	0.25
A-2	Initial Area Scan:	42.3	12.7	0.38
	Final Area Scan:	126.9	6.4	0.25
B-1	Initial Area Scan:	63.5	12.7	0.38
	Final Area Scan:	84.6	6.4	0.25
B-2	Initial Area Scan:	63.5	12.7	0.38
	Final Area Scan:	126.9	6.4	0.25
C	Initial Area Scan:	42.3	12.7	0.25
	Final Area Scan:	84.6	6.4	0.13

2.3 Corrosion and Mechanical Tests

Immersion tests were conducted to evaluate the relative corrosion behaviour of (1) Cu-7 wt.% Al, (2) Cu-7 wt.%Al-2 wt.% Fe, and (3) laser alloyed (with Fe) Cu-7 wt.% Al. Tests were conducted in 3% NaCl solutions, acidified to pH 4 by HCl additions, at 25°C (8, 24 and 72 h immersion time), and 50°C (8 and 24 h immersion time). Corrosion coupons of CuAl and CuAlFe were prepared with a standard 400 grit surface finish, and all coupons for weight loss determination were degreased in acetone prior to incorporation in the program. Corrosion susceptibility was evaluated on the basis of mass loss (±0.0001 g), and reported as (1) mass loss per unit area (mg/dm^2), and (2) corrosion rate (mils/yr).

Surface hardness of (1) Cu-7 wt.% Al, (2) Cu-7 wt.% Al-2 wt.% Fe, and (3) laser alloyed (with Fe) Cu-7 wt.% Al was evaluated using Rockwell 15T superficial hardness tests, with 12 indentations recorded per sample.

2.4 Metallography and Chemical Analysis

Laser treated specimens were analyzed in cross-section by light and electron optical metallography in order to determine (1) the depth, and (2) the microstructural characteristics of the laser treated zone. Energy dispersive X-ray microanalysis (EDX) was utilized in both the (1) standard spot analysis, and (2) elemental mapping modes in order to evaluate the chemical composition of the laser treated zone.

3. RESULTS AND DISCUSSION

3.1 Microstructural and Chemical Characteristics of the Laser Treated Surfaces

Figure 2 shows an optical micrograph of the cross-section of a laser alloyed specimen, treated under the A-1 condition (Table II). As shown in this figure, the laser treated zone extends to approximately 275 µm below the surface of the specimen. Within this zone, narrow dendrites, oriented perpendicularly to the surface (i.e. direction of solidification) are noted. These dendrites are observed to initiate at the substrate-laser treated zone interface, and tend to diminish on approaching the free surface. Within the laser treated zone, a secondary interface is noted at approximately 175 µm from the surface, with this most likely arising from the high scan rate secondary laser treatment associated with the A-1 treatment. Figure 3 (a) shows a scanning electron micrograph of an A-1 cross-section extending to ~225 µm below the free surface. Oriented microdendrites are noted at the base of the micrograph. These microdendrites dissipate on approaching the free surface, and are completely eliminated at a point ~125 µm from the surface. Figure 3 (b) shows a scanning electron micrograph of a region within 125 µm of the free surface. A cellular structure is noted with a mean cell diameter of 1.6 µm. The observed microstructures (i.e. microdendrites transforming to microcells) are indicative of rapid solidification (RS) phenomena. Further evidence for RS conditions is noted through the absence of (1) second phase particulates and (2) coarse crystallographically oriented (usually <100> in fcc alloys) crystals, in the microstructures, which would be indicative of low to moderate cooling rates. Figure 3 (c) shows elemental maps (Cu, Al, Fe) corresponding to the rapidly solidified microstructure shown in Figure 3 (a). As indicated on these maps, Cu and Al are evenly distributed; however, Fe is noted to be most highly concentrated in the melt track associated with the high scan rate final pass of the A-1 treatment (i.e. ~200 µm depth in Figure 3 (a)). Table III summarizes the determined elemental composition at various depths from the free surface (i.e. Figure 3 (a)).

TABLE III

CHEMICAL COMPOSITION AS A FUNCTION OF DEPTH DETERMINED FOR THE REGION SHOWN IN FIGURE 3 (c) (i.e. along centre of micrograph)

Depth (µm)	Concentration (Wt.%)		
	Cu	Al	Fe
12	91.9	5.6	2.5
105	93.8	4.8	1.4
210	94.9	5.0	0.1

Since the values reported in Table III correspond to the centreline of Figure 3 (a), only the 12 and 105 µm depths lie within the secondary melt track. As indicated in the elemental map (Figure 3 (c)), Fe is distributed homogeneously within this track, and on the basis of the tabulated data, at a concentration of ~1.5 - 2.5 wt.%.

Figure 4 (a) shows a scanning electron micrograph of another area on the A-1 treated specimen. Figure 4 (b) shows the elemental maps corresponding to the area shown in Figure 4 (a). The distribution is shown to be quite homogeneous to a depth of ~80 µm. Table IV lists the determined chemical composition at various depths from the free surface (i.e. Figure 4 (a)).

TABLE IV

CHEMICAL COMPOSITION AT VARIOUS DEPTHS FROM THE FREE SURFACE AS SHOWN IN FIGURE 4 (a)

Depth (µm)	Concentration (Wt.%) Cu	Al	Fe
7	89.3	6.6	4.1
38	90.3	5.5	4.2
70	89.9	5.4	4.7

As indicated in this table, a relatively uniform iron distribution is present to within 70 µm of the surface, with concentrations in the range of 4 - 4.7% observed. These values are substantially higher than those determined from the area shown in Figure 3. These variations are most likely attributable to (1) scan to scan variation in power density arising from minor variations in surface level, and (2) local variation in Fe coating thickness. These variations in composition can possibly be minimized by a reduction in jog distance, thus providing greater overlap of adjacent melt tracks, and thus a more homogeneous Fe distribution in the melt zone. The microstructures shown in both Figures 3 and 4 display RS characteristics, thus demonstrating that the A-l treatment is suitable for (1) laser alloying (Fe) and (2) surface modification.

Figure 5 shows an optical micrograph of the cross-section of a specimen treated under the A-2 condition. The laser treated zone again extends to approximately 275 µm from the free surface. Melt tracks for the final area scan (i.e. 126.9 mm/s) are not identifiable. A uniform fine scale structure is observed. Figure 6 shows scanning electron micrographs of the observed structure. A fine, slightly elongated dendritic structure is evident (Figure 6 (a)). Figure 6 (b) illustrates the microstructural differences at the melt track (i.e. laser treated zone)-base alloy interface. Figure 7 shows a cross-sectional area of an A-2 treated specimen, with the associated elemental maps (Figure 7 (b)). As demonstrated in this figure, Fe tends to be more concentrated near the base of the melt track. This is further demonstrated in Table V, which shows chemical composition at various depths from the surface of the area shown in Figure 7 (a).

TABLE V

CHEMICAL COMPOSITION AT VARIOUS DEPTHS FROM THE FREE SURFACE AS SHOWN IN FIGURE 7 (a)

Depth (µm)	Concentration (Wt.%) Cu	Al	Fe
6	90.8	5.7	3.5
48	91.5	4.8	3.7
100	89.2	4.9	5.9

The observed variations in Fe concentration can be attributed to an ineffective secondary scan, which, because of too high a scan rate, does not result in a melt zone of sufficient depth to homogenize the Fe distribution.

Figure 8 shows an optical micrograph of a cross-section of a specimen treated under the B-1 condition. The more rapid primary scan leads to a melt track of ~170 µm. The secondary melt track is also evident in this micrograph, and is observed to extend to a similar depth as that noted with the primary track. Perpendicularly (i.e. to surface) oriented microdendrites are evident at the base of the melt track. Figure 9 (a) shows a cross-sectional scanning electron micrograph of the near-surface region of a B-1 treated specimen. Fine dendrites and coarser oriented crystals are evident. Figure 9 (b) shows the corresponding elemental maps. Fe is observed to be uniformly distributed within the analyzed cross-section (Figure 9 (a)). Table VI lists the chemical composition determined at various depths from the surface of the cross-section shown in Figure 9 (a). A relatively uniform Fe concentration of ~4 - 5 wt.% is evident to a depth of ~45 µm.

TABLE VI

CHEMICAL COMPOSITION OF VARIOUS DEPTHS FOR THE SURFACE OF THE CROSS-SECTION SHOWN IN FIGURE 9 (a)

Depth (µm)	**Concentration (Wt.%)**		
	Cu	**Al**	**Fe**
2.5	89.0	5.6	5.4
22.0	91.2	4.5	4.3
41.0	90.2	4.7	5.1

Figure 10 shows an optical micrograph of the cross-section of a B-2 treated specimen. The primary melt track is observed to extend to ~125 µm; the secondary melt track is not identifiable. Figure 11 shows a scanning electron micrograph of the laser melted zone. A microdendritic microstructure is evident, with the microstructural variation between the laser-treated zone and substrate demonstrated in Figure 11 (b). Figure 12 shows a cross-sectional scanning electron micrograph of the near surface of a B-2 treated specimen (Figure 12 (a)), and the associated elemental maps (Figure 12 (b)). The distribution of Fe is observed to be non-uniform, with this likely being the result of an ineffective secondary scan. Table VII lists the chemical composition determined at various depths from the surface of the cross-section shown in Figure 12 (a).

TABLE VII

CHEMICAL COMPOSITION AT VARIOUS DEPTHS FROM THE SURFACE OF THE CROSS-SECTION SHOWN IN FIGURE 12 (c)

Depth (µm)	Concentration (Wt.%) Cu	Al	Fe
4	93.1	4.9	2.0
23	90.7	4.6	4.7
40	92.7	4.2	3.1

Table VIII summarizes the effects of laser processing treatment on the characteristics of the treated specimens. All treatments were found to result in both (1) successful surface alloying, and (2) microstructures having RS characteristics; however, the best combination of (1) treatment depth and (2) RS microstructure was achieved using the A-1 treatment. The scan rates applied in this treatment were subsequently utilized to produce specimens for the evaluation of laser treated properties; however, in an attempt to alleviate point-to-point variations in bulk surface composition (see Table VIII, A-1(1) and A-1(2)), a refined jog distance was applied in the preparation of these specimens (see Table II 'C' Treatment).

TABLE VIII

SUMMARY OF LASER TREATMENT MICROSTRUCTURES AND CHEMISTRY

Treatment		Scan Rate (mm/s) Primary	Secondary	Melt Track Depth (μm) Primary	Secondary	Alloyed Zone Depth (μm)	Fe Conc. (wt.%)	Micro-structure
A-1	(1)	42.3	84.6	275	175	~200	1.4 - 2.5	RS
	(2)	42.3	84.6	250	160	~150	4 - 5	RS
A-2		42.3	126.9	275	-(0)	~125	3.5 - 5.9	RS
B-1		63.5	84.6	170	170	~100	4.3 - 5.4	RS
B-2		63.5	126.9	125	-(0)	~60	2.0 - 4.7	RS

3.2 Mechanical Properties

Surface hardness values for (1) Cu-7 wt.% Al, (2) Cu-Al-Fe (Alloy 614), and (3) laser treated (alloyed) Cu-7 wt.% Al are reported in Table IX.

TABLE IX

SURFACE HARDNESS MEASUREMENTS

Specimen	Hardness (Rockwell 15T) Avg.	Std. Deviation
Cu-7 wt.% Al	61.3	±0.9
Cu-Al-Fe (Alloy 614)	85.7	±0.8
Laser Treated Cu-Al	69.0	±0.8

As shown in this table, point-to-point (i.e. indentation to indentation) variations in hardness are consistent for the laser treated and non-laser treated specimen (i.e. ~1 hardness unit), indicating that the surface of the laser treated specimen can be considered to be structurally and chemically homogeneous. The average hardness of the laser treated specimen is moderately higher (i.e. 12.6%) than that of the non-laser treated (and non-alloyed) Cu-7 wt.% Al alloy. This increase in hardness can be attributed to both (1) microstructural refinement, and (2) solid solution strengthening (i.e. Fe alloying) mechanisms. The substantially higher hardness associated with Alloy 614 (i.e. Cu-Al-Fe) is a result of precipitation hardening, which is a consequence of the limited solid solubility of Fe in Cu-Al alloys under conventional (i.e. equilibrium) processing. The RS conditions operative during laser treatment result in non-equilibrium concentrations of Fe in solution which precludes precipitation hardening as a strengthening mechanism.

3.3 Corrosion Behaviour

Weight loss data for (1) Cu-7 wt.% Al, (2) Cu-Al-Fe (Alloy 614), and (3) laser treated (and alloyed) Cu-Al are shown in Figure 13. Calculated, apparent corrosion rates (mils/yr) are plotted as a function of immersion time in Figures 14 (25°C) and 15 (50°C). At 25°C (Figure 14), alloy 614 (Cu-Al-Fe) shows a high initial corrosion rate, followed by a substantial decrease over the 72 h immersion period. This decrease in corrosion rate is indicative of the formation of a protective surface film. Both the laser and non-laser treated Cu-Al specimens display a negligible corrosion rate over the first 8 h immersion period. The laser treated Cu-Al specimen displays increasing corrosion rate over the remainder of the 72 h immersion period, while the non-laser treated Cu-Al specimen displays erratic behaviour whereby an increase in corrosion rate, followed by a subsequent decrease is noted. The corrosion rate data shown in Figure 14 demonstrate that the laser treated specimen can provide improved corrosion resistance over both the conventional Cu-7 wt.% Al and Cu-Al-Fe alloys during short term exposure; however, long-term immersion (e.g. 72 h) results in an equilibration of corrosion rates for these specimens. The increasing values of corrosion rate (with time) noted with the laser treated specimen are indicative of localized corrosion processes, and may be the result of the relatively 'rough' surface topography arising from laser processing. Corrosion rate data for the 50°C immersion tests are shown in Figure 15. All three specimens show decreasing corrosion rates over the 24 hour immersion period. Increasing solution temperature generally results in increasing corrosion rates, with this effect being most pronounced with the non-treated and laser treated Cu-7 wt.% Al specimens. Corrosion resistance at 50°C is observed to be in the following order: Cu-Al-Fe > Laser Treated Cu-Al > Cu-7 wt.% Al (non-laser treated).

Considerably more data need to be generated to profile corrosion rates with time so that corrosion mechanisms can be understood. The corrosion data generated here from coupon weight loss should be looked at for trends, not for detail. Thus, it appears that at 50°C the corrosion rates of CuAlFe, CuAl and laser treated CuAl are comparable, whereas at 25°C the latter material can be favourably differentiated from the other two during limited exposure to a corrosive medium. The alloyed RS surface is thus "apparently" affording more corrosion protection at this temperature over short exposure times, a phenomenon that requires further investigation, both electrochemically and metallurgically.

4. SUMMARY AND RECOMMENDATIONS

Laser processing parameters have been established for Al-bronze which yield a laser treated zone of ~200 µm depth having (1) a relatively uniform alloyed Fe concentration, and (2) a fine scale microstructure having rapidly solidified (RS) characteristics. Laser treated specimens were determined to have a surface hardness greater than a conventional Cu--7 wt.% Al. Under limited exposure at 25°C, these laser treated specimens were also determined to provide improved corrosion resistance in acidified 3% NaCl over conventional Cu-7 wt.% Al, and Alloy 614 (Cu-Al-Fe). The enhanced surface hardness and corrosion resistance observed, provides considerable promise for laser technology in providing novel Al-bronze alloys for erosion-corrosion and cavitation resistance in marine environments; however, further work will be necessary to improve the long-term performance of these materials. Further efforts in this area should focus on the (1) modification of laser processing parameters to yield "smoother" surfaces, and (2) optimization of surface chemistry (i.e. Fe concentration) to yield more substantive improvements in surface hardness and corrosion resistance.

G. Palumbo
Project Scientist
Metals & Corrosion Technologies

R Lassau
R. T. Lassau
Manager
Metals & Corrosion Technologies

Figure 1

Optical Micrograph of As-cast Cu-7 wt.% Al Showing Radial (top) and Longitudinal (bottom) Cross-sections (Magnification: 5X)

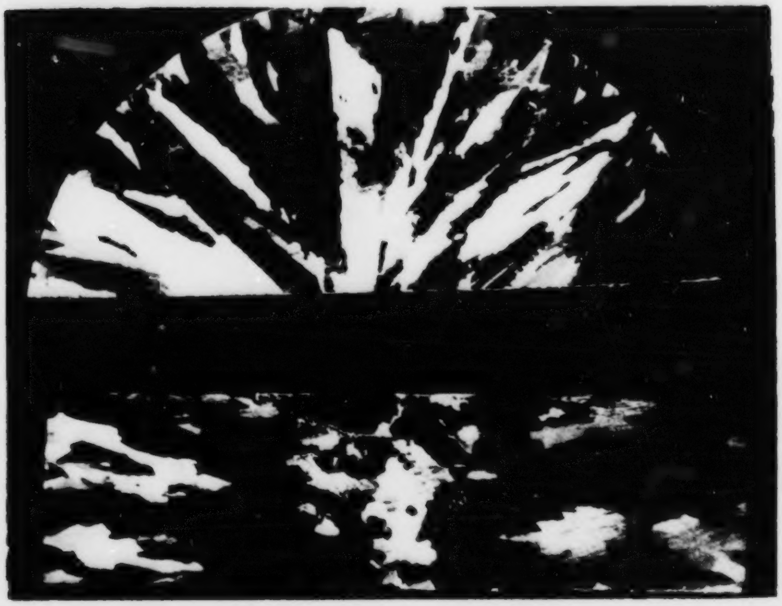

Figure 2

Cross-sectional Optical Micrograph of
an A-1 Laser Treated Specimen (Magnification: 200X)

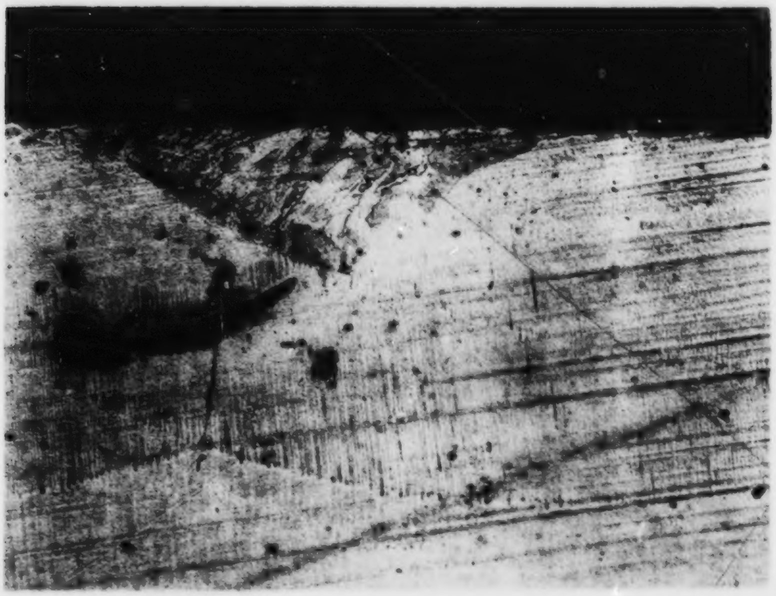

Figure 3

(a, b) Cross-sectional Scanning Electron Micrograph of an A-1 Laser Treated Specimen; (c) Elemental Maps Corresponding to Figure 3 (a)

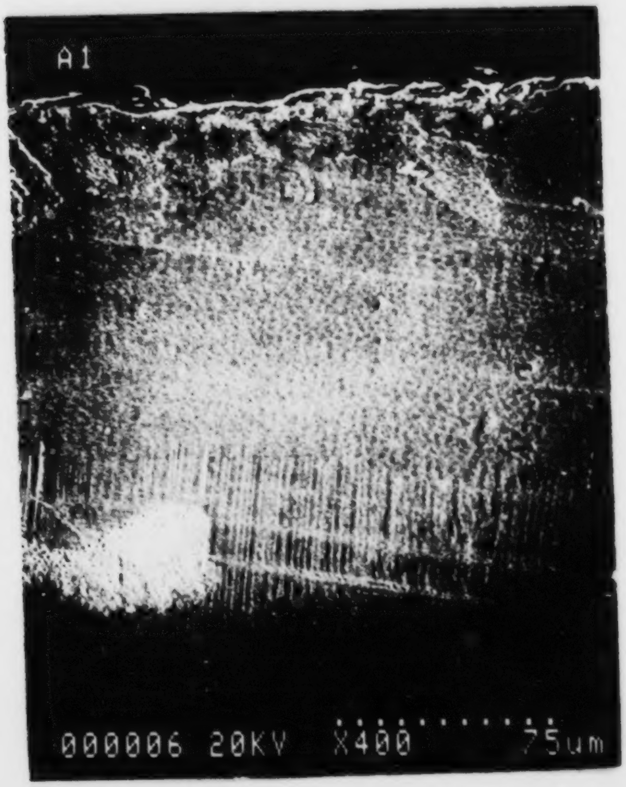
A1
000006 20KV X400 75um

3 (a)

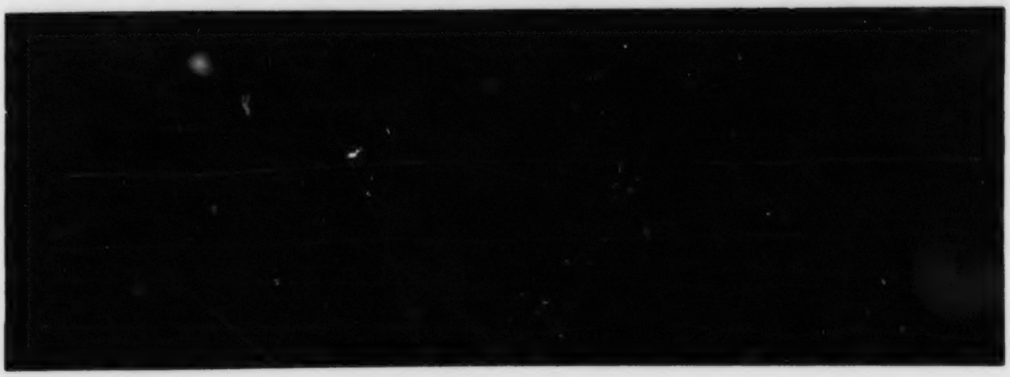

3 (c)

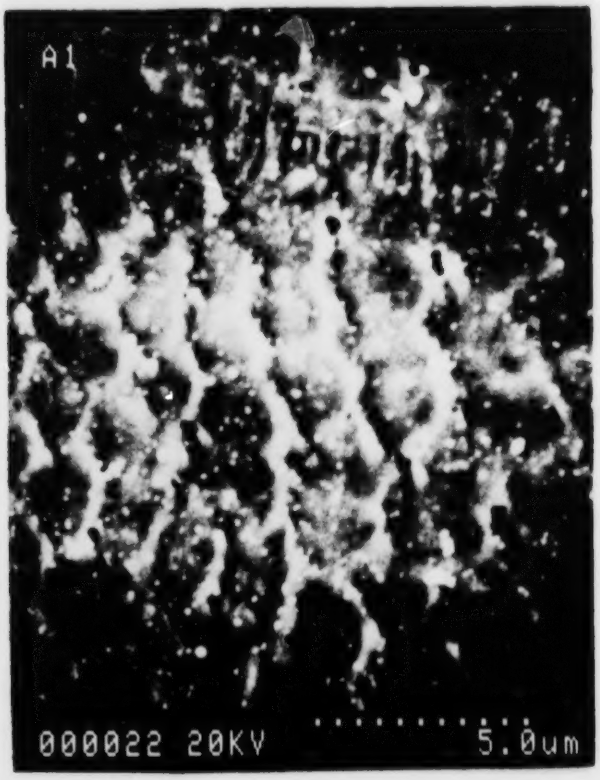
A1
000022 20KV
5.0um

3 (b)

Figure 4

(a) Cross-sectional Scanning Electron Micrograph of an

A-1 Laser Treated Specimen

(b) Corresponding Elemental Maps

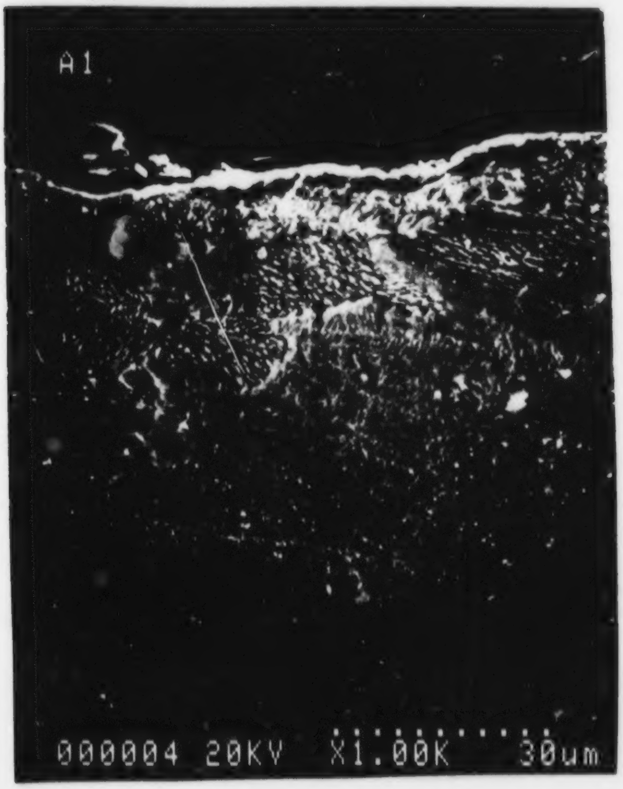
A1
000004 20KV X1.00K 30um

4 (a)

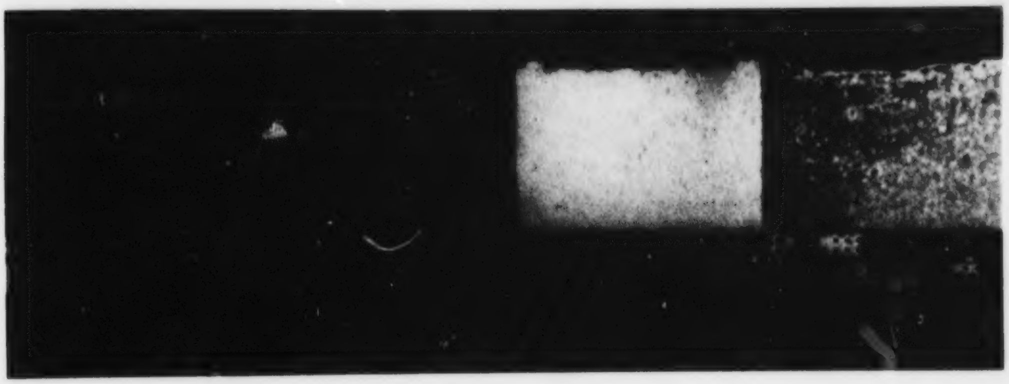

4 (b)

Figure 5

Cross-sectional Optical Micrograph of
an A-2 Laser Treated Specimen (200X)

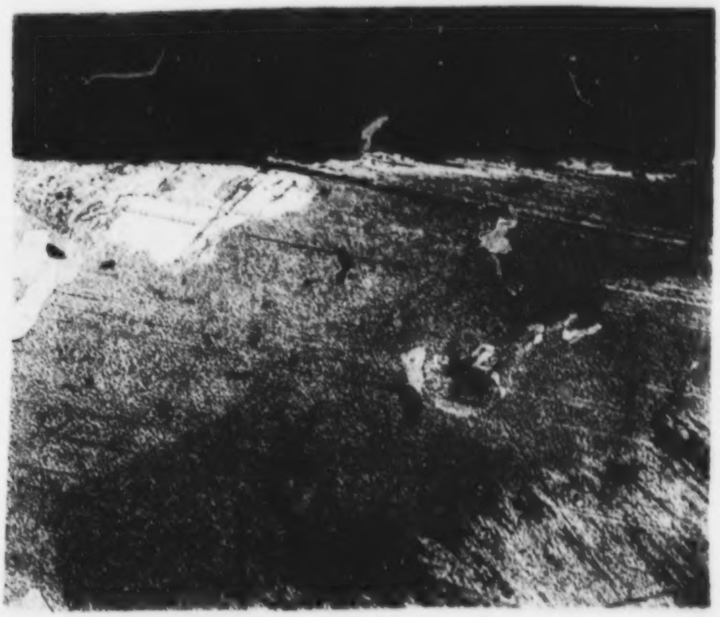

Figure 6

Cross-sectional Scanning Electron
Micrographs of A-2 Laser Treated Specimens

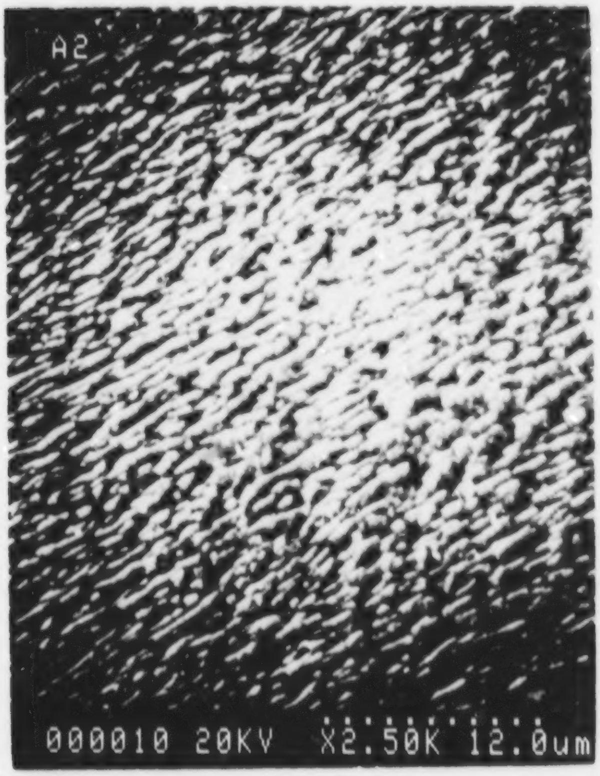
A2
000010 20KV X2.50K 12.0um

6 (a)

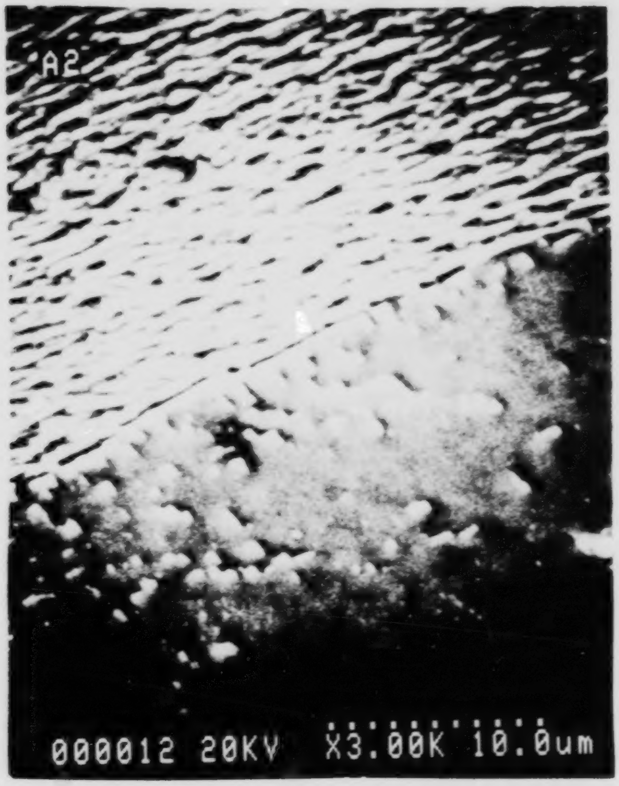
A2
000012 20KV X3.00K 10.0um

6 (b)

Figure 7

(a) Cross-sectional Scanning Electron Micrographs
of A-2 Laser Treated Specimen
(b) Corresponding Elemental Maps

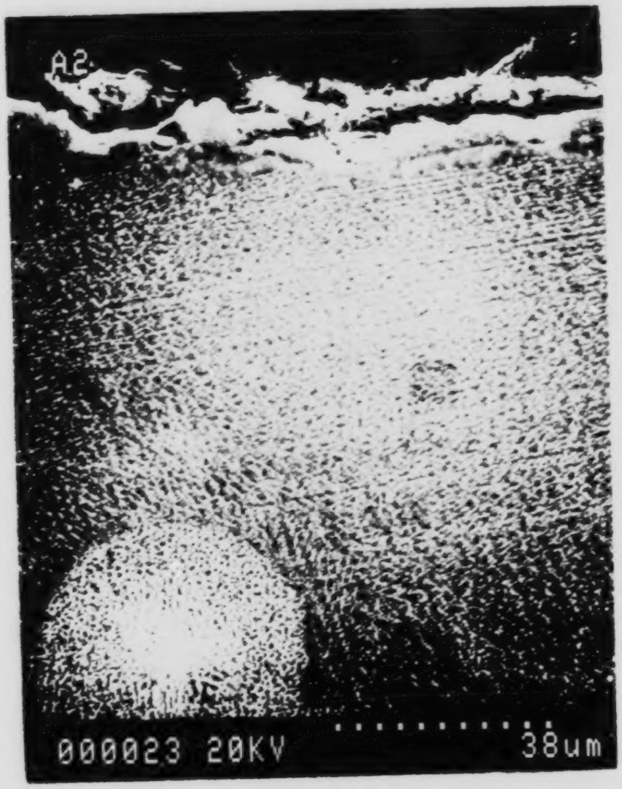

7 (a)

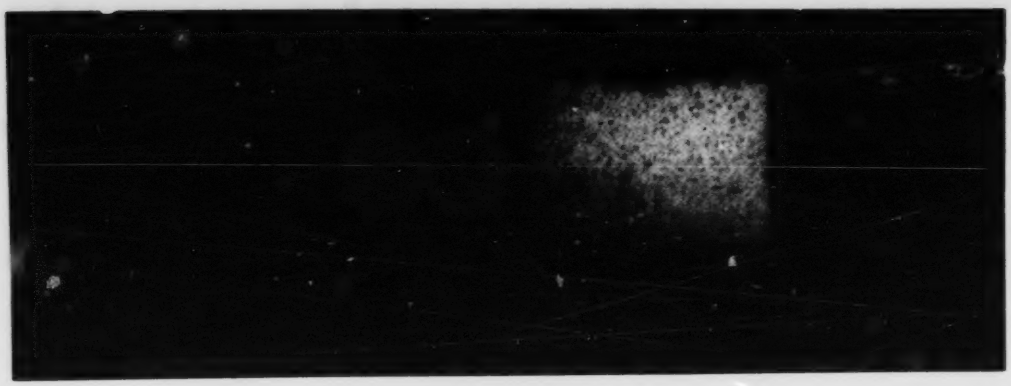

7 (b)

Figure 8

Cross-sectional Optical Micrograph of
B-1 Laser Treated Specimen (200X)

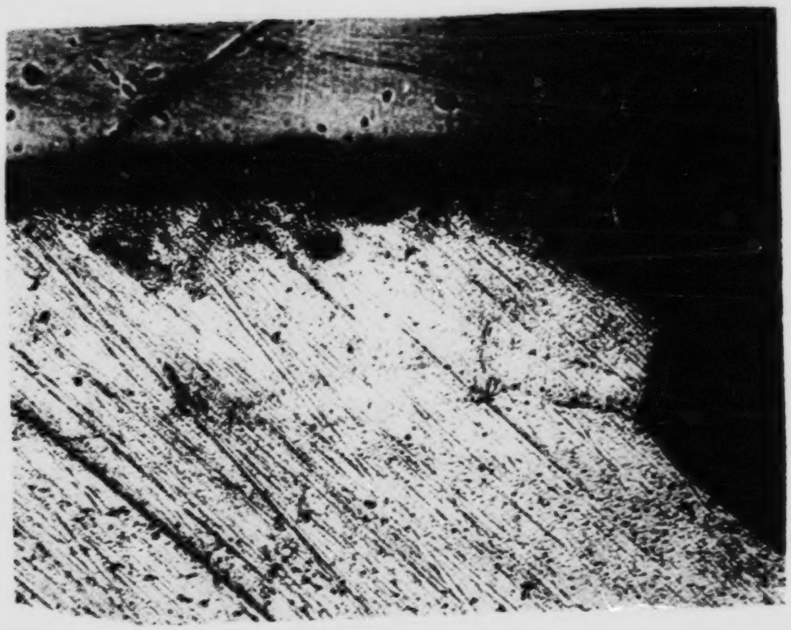

Figure 9

(a) Cross-sectional Scanning Electron Micrograph
of B-1 Laser Treated Specimen
(b) Corresponding Elemental Maps

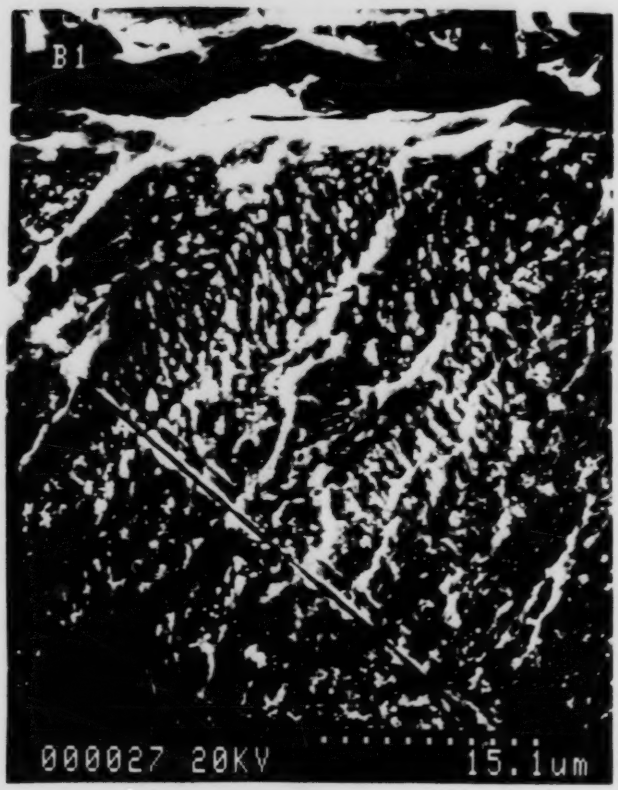
B1
000027 20KV
15.1um

9 (a)

9 (b)

Figure 10

Cross-sectional Optical Micrograph of a
B-2 Laser Treated Specimen (200X)

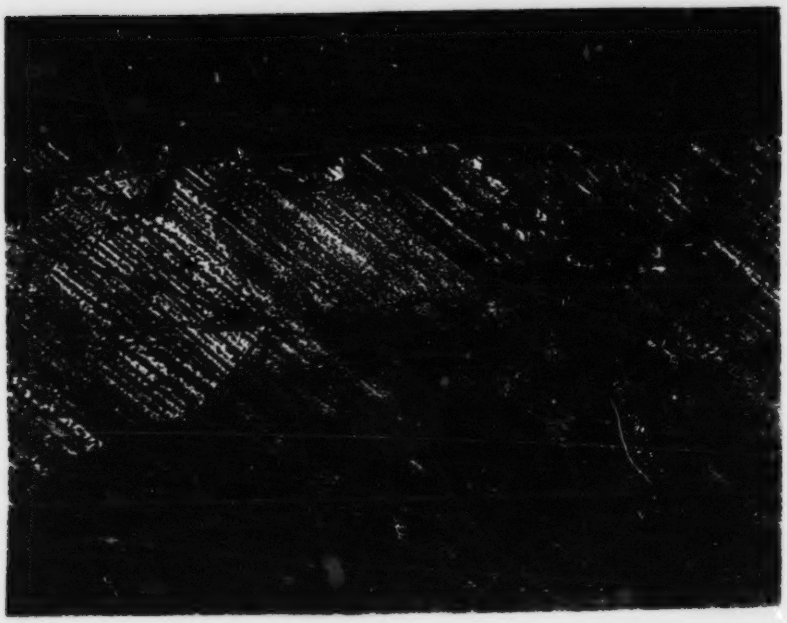

Figure 11

(a, b) Cross-sectional Scanning Electron Micrographs
of a B-2 Laser Treated Specimen

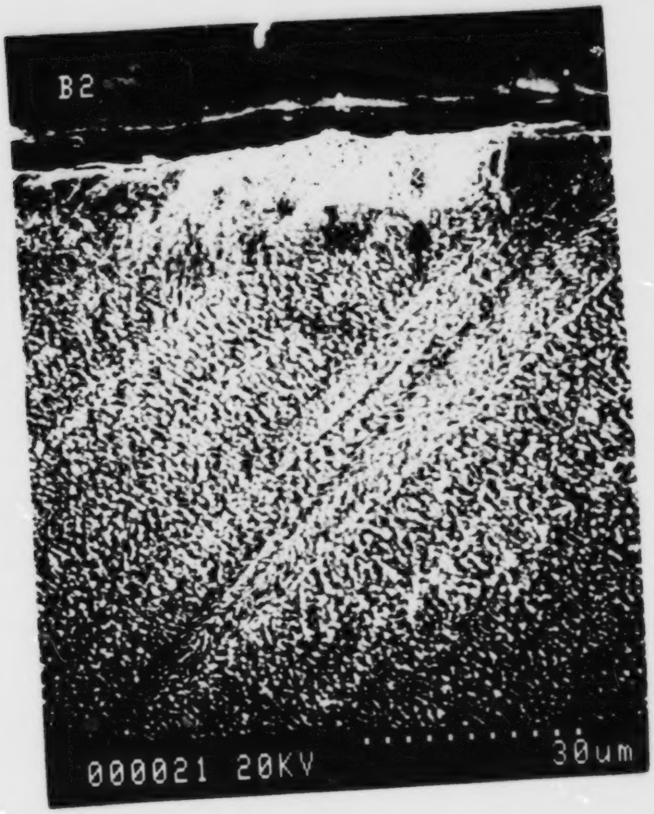
B2
000021 20KV
30um

11 (a)

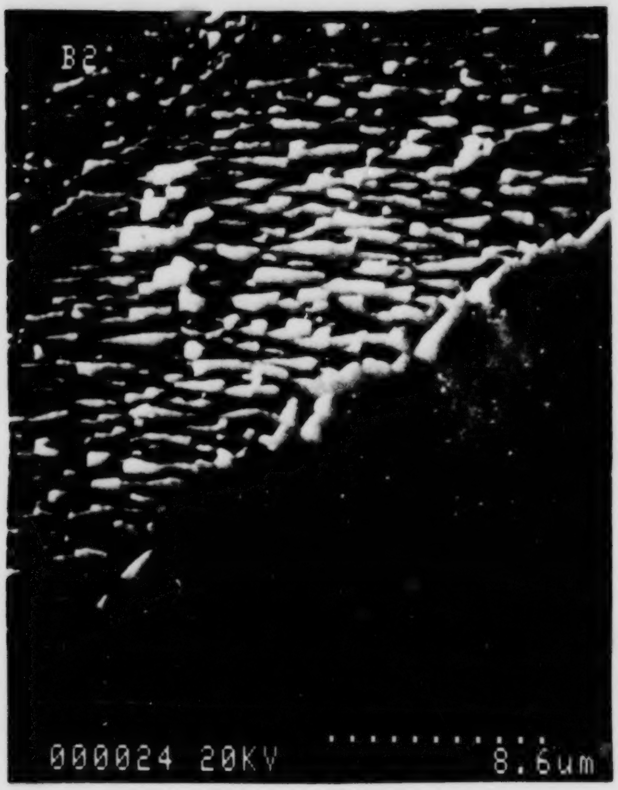
B2
000024 20KV
8.6um

11 (b)

Figure 12

(a) Cross-sectional Scanning Electron Micrograph
of a B-2 Laser Treated Specimen
(b) Corresponding Elemental Maps

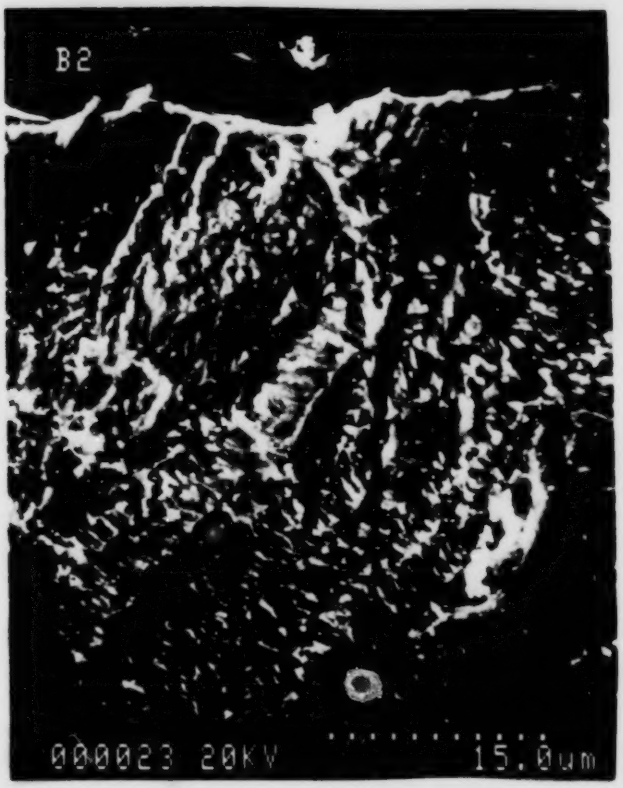
B2
000023 20KV
15.0um

12 (a)

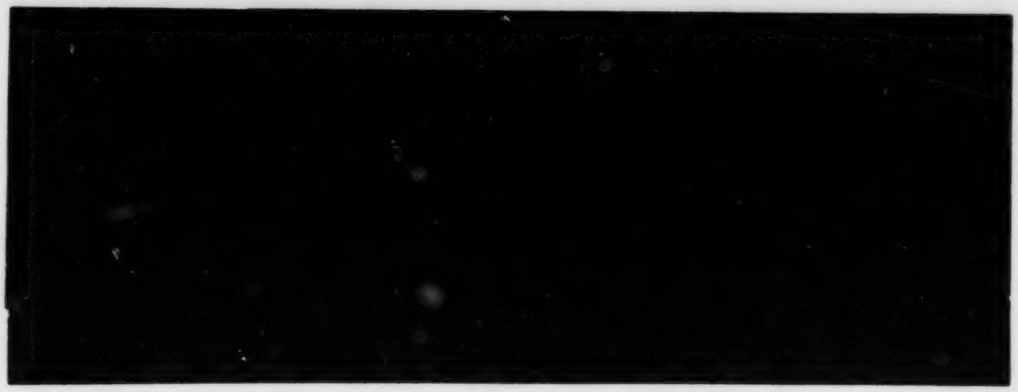

12 (b)

Figure 13

Weight Loss as a Function of Test Time in Acidified (pH = 4) 3% NaCl at 25° and 50°C

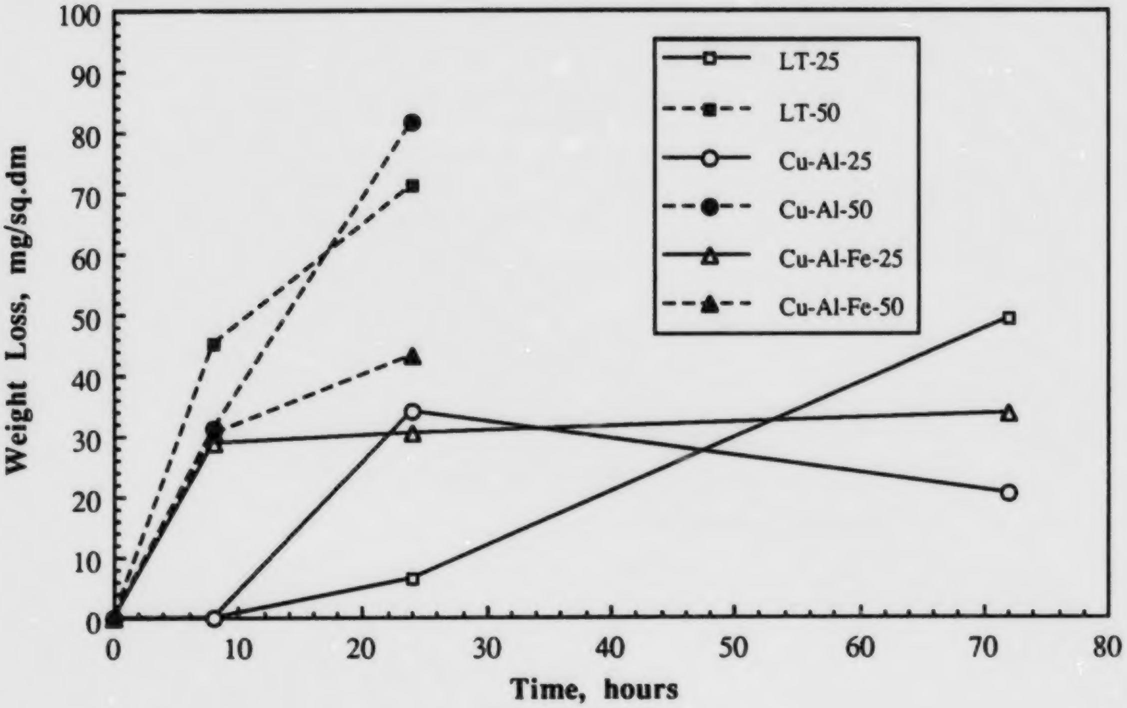

Figure 14

Apparent Corrosion Rate as a Function of Test Time in 3% NaCl (pH = 4) at 25°C

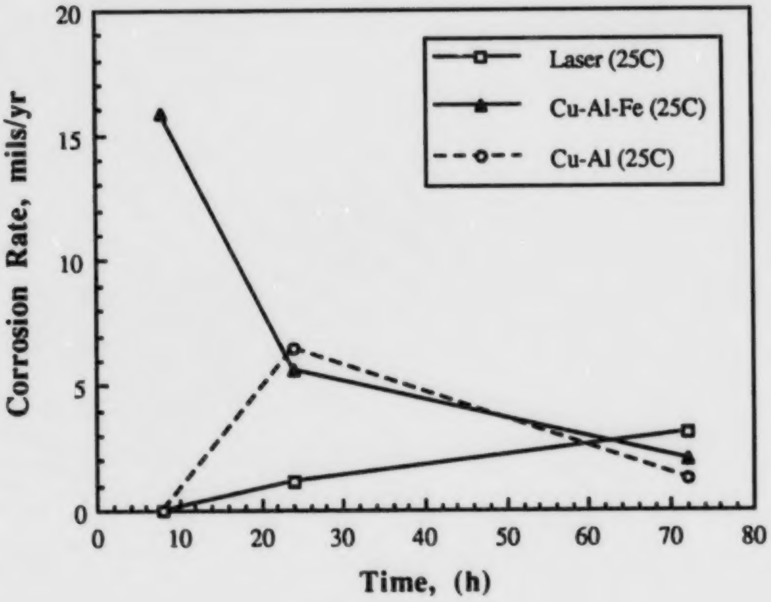

Figure 15

Apparent Corrosion Rate as a Function of Test Time in 3% NaCl (pH = 4) at 50°C

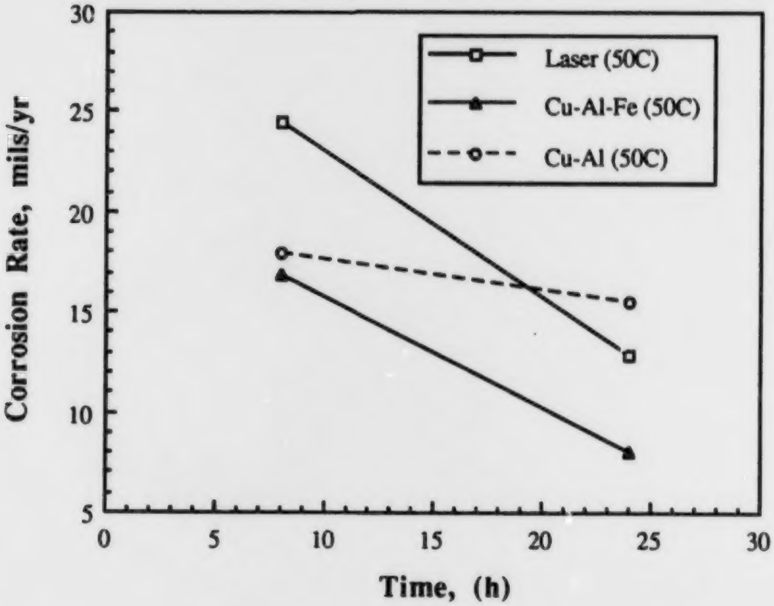

APPENDIX A

Laser Treatment of Aluminum Bronzes

Progress Report No.1
Contract No. 67-10908B

Mr. Troy Lassau
Section Manager
Metals and Corrosion Technologies Section

Submitted by:

Dr. T. Kilp
Laser Applications Section
Industrial Materials Technology Centre

August 17, 1988

ONTARIO**RESEARCH**
FOUNDATION

SHERIDAN PARK RESEARCH COMMUNITY
MISSISSAUGA, ONTARIO, CANADA, L5K 1B3
(416) 822-4111 * TELEX 06-982311

WE, THE ONTARIO RESEARCH FOUNDATION, STIPULATE THAT THIS DOCUMENT IS SUBJECT TO THE FOLLOWING TERMS AND CONDITIONS:

1. ANY PROPOSAL CONTAINED HEREIN WAS PREPARED FOR THE CONSIDERATION OF THE ADDRESSEE ONLY. ITS CONTENTS MAY NOT BE USED BY NOR DISCLOSED TO ANY OTHER PARTY WITHOUT OUR PRIOR WRITTEN CONSENT.
2. ANY TESTING, INSPECTION OR INVESTIGATION PERFORMED BY US WILL BE CONDUCTED IN ACCORDANCE WITH NORMAL PROFESSIONAL STANDARDS. NEITHER WE NOR OUR EMPLOYEES SHALL BE RESPONSIBLE FOR ANY LOSS OR DAMAGE RESULTING DIRECTLY OR INDIRECTLY FROM ANY DEFAULT, ERROR OR OMISSION.
3. ANY REPORT, PROPOSAL OR QUOTATION PREPARED BY US REFERS ONLY TO THE PARTICULAR MATERIAL, INSTRUMENT OR OTHER SUBJECT REFERRED TO IN IT. NO REPRESENTATION IS MADE THAT SIMILAR ARTICLES WILL BE OF LIKE QUALITY.
4. NO REPORT ISSUED BY US SHALL BE PUBLISHED IN WHOLE OR IN PART WITHOUT OUR PRIOR WRITTEN CONSENT.
5. OUR NAME SHALL NOT BE USED IN ANY WAY IN CONNECTION WITH THE SALE, OFFER OR ADVERTISEMENT OF ANY ARTICLE, PROCESS OR SERVICE.
6. WE RESERVE THE RIGHT NOT TO COMMENCE AND/OR CONTINUE ANY WORK UNTIL PAYMENT ARRANGEMENTS SATISFACTORY TO US ARE ESTABLISHED.

TABLE OF CONTENTS

Page

1. INTRODUCTION 1

2. EXPERIMENTAL 1

3. RESULTS 2

3.1 Ternary Aluminum Bronze Coupons 614 to 645 2

3.2 Iron Coated Binary Aluminum Bronze Coupons 10

3.3 Comparison to Literature Results 13

4. CONCLUSIONS 13

1. INTRODUCTION

This progress report outlines the details of initial studies of the laser treatment of aluminum bronze alloys. The work to be described here was aimed at establishing fundamental laser processing parameters which would subsequently be used to produce coupons for testing and evaluation. Two types of coupons were treated consisting of ternary alloys as well as of binary alloys having a thin layer of iron deposited onto one flat surface.

2. EXPERIMENTAL

Coupons having approximate dimensions of 2.5 cm x 2.5 cm x 0.5 cm were received from B. Elliott. These consisted of a ternary aluminum bronze alloy. In addition, binary aluminum bronze coupons having a thin layer of iron deposited on one flat face were received. No additional energy absorbing coatings, such as black paint or graphite, were used.

Laser treatment was carried out using a Photon Sources Turbolase T3000 continuous wave (CW) carbon dioxide (CO_2) laser. The laser was operated at a fixed output of 2450 W at 10.6 μm and TEM_{00} mode throughout these studies. It was not possible to vary the output power of this laser.

Figure 1 is a schematic representation of the optical parameters available. The horizontal laser beam emerging from the laser was reflected downwards through 90°. It was then passed through a water cooled focussing lens having a 5 inch focal length.

Emerging from the lens, the laser beam is brought to a focal point at a height HF (Figure 1) above the top surface of the substrate (aluminum bronze coupon). Beyond this point, the beam becomes divergent.

Varying the height of the focal point above the substrate, therefore, changes the beam diameter impinging upon the coupon. For a constant laser output power, this results in variations in the energy density delivered to the workpiece surface.

The coupons were mounted on a Coherent Lasertrac CNC motion table. In all experiments, the samples to be exposed were moved through the stationary laser beam using the motion table. A stream of Argon cover gas, flowing co-axially with the laser beam was used in all exposures.

Following exposure, the coupons were photographed. They were then cross-sectioned in a direction perpendicular to the direction of laser beam scanning. The cross-sections were embedded in an epoxy mount, polished and finally etched to bring out grain details for microscopic examination.

3. RESULTS AND DISCUSSION

3.1 Ternary Aluminum Bronze Coupons 614 to 645

Laser treatment of this alloy was intended to provide a link between the current effort to develop novel aluminum bronzes and data already available in the published literature. It was not intended to duplicate previous work. Rather, it was of interest to evaluate the effects of using more powerful lasers in terms of depth of treatment and maximum surface area coverage per unit time. These have obvious product quality and process economics implications.

In Table I (and subsequent tables), Rate refers to the traverse speed of the laser beam across the coupon surface. HF (see Figure 1) refers to the height of the laser beam focal point above the coupon's upper surface. Spot size is the diameter of the laser beam as it impinges upon the coupon. Increasing HF will increase the spot size (Figure 1) resulting in reduced power densities (W/cm^2) at the coupon surface.

The energy density through a cross-section of a laser beam operating in the TEMoo mode is not uniform. A typical profile would be nearly Gaussian in shape with peak energy densities at or very near the centre of the beam. Since there is generally a minimum energy density requirement for effecting a desired change in the substrate, the edges of the beam are often ineffective for this purpose.

The result is that the effective size of the laser beam is often less than the actual beam size impinging upon the workpiece surface. In Table I and subsequent tables, the effective beam size was measured from the width of the melt tracks obtained from any given set of experimental parameters.

Dwell time is defined as D_{eff}/V where D_{eff} is the effective spot size and V is the rate of traverse of the beam across the sample surface. Treatment depth refers to the depth to which visible changes in microstructure were effected in the metal coupons.

Coupon 614-1

Figure 2 depicts ternary alloy Coupon 614-1. Eight laser tracks were laid on this coupon with the conditions for each listed in Table I. Only five scans resulted in surface melting and are thus visible in Figure 2.

In Figure 2, tracks 1 to 3 were laid down with the beam focal point nominally on the surface of the coupon. Figure 3 shows the resultant melt track at the start and finish of scan #1. The track width is quite uniform at 0.55 mm along its entire length. This uniformity is general to all of the exposures carried out here.

Figure 4 shows the cross-section of the melt tracks 1 to 3 from Figure 2. Treatment depths, measured from the photographs are listed in Table I. As expected, the maximum depth of the melt tracks decrease from 160 μm to 120 μm as processing rates increase from 21.2 mm/s to 46.6 mm/s.

Increasing the height of the focal point (HF) to 25.4 mm above the coupon (exposures 4 and 5, Table I) resulted in heat treatment only. No surface melting was observed.

For tracks #6 and #7 in Figure 2, HF was dropped to 12.7 mm and at 21.2 mm/s and 46.6 mm/s scan rates, surface melting was observed. Although the tracks are highly visible in Figure 2, microscopic examination (Figure 5) indicated they were very shallow.

Exposure No.8 (HF of 19.1 mm, rate of 21.2 mm/s) again resulted in only surface heat treatment and no melting.

The results for coupon 614-1 are considered to be erroneous. For example, with a total beam power of 2450 W concentrated on a spot size of 0.28 mm (exposures 1 to 3 in Table I), the resultant melt tracks were expected to be much deeper than shown in Figure 3. Similarly, very thin (less than 10 μm surface melting obtained with the conditions used for exposures 6 and 7 (Table I) was unexpected.

Periodic checks of the laser power levels indicated that reduced power was not the cause of the above behaviour. As a result, the laser optical parameters were re-set with particular attention given to the exact position of the focal point of the beam. The above results are only given here for sake of reporting completeness.

Coupon 614-2

Following re-setting of the optical parameters, coupon 614-2 was treated as outlined in Table II. The results are shown in Figure 6.

With HF values of either 6.4 mm or 12.7 mm and a traverse speed of 21.2 mm/s, massive melt tracks were obtained. These were expected in consideration of the experimental parameters and confirm the unreliability of the results obtained with coupon 614-1.

These results confirm that any problem that might have existed with coupon 614-1 was eliminated. The magnitude of the effects generated upon coupon 614-2 is too high to be of direct interest to the current programme objectives. As a result, no further discussion of these exposures will be made here.

Coupon 614-3

Nine separate exposures, with conditions as listed in Table III, were carried out on this coupon. Figure 7 illustrates the results.

For track #1, the basic parameters were kept as in coupon 614-2 but the traverse speed was tripled from 21.2 mm/s to 63.5 mm/s. As seen from Figure 7, massive melting still resulted.

Figure 8 shows the cross-section of track #1 (as well as those of tracks #8 and #9). The track has the well-known "champagne glass" shape with width and depth both being about 1400 µm. The shape of the cross-section indicates that the power densities and traverse speeds used here were more appropriate for cutting or welding than surface melting.

For exposures 2, 3 and 4, the value of HF was increased to 12.7 mm and then kept constant. The variable in this sequence was the traverse rate, which was dropped from 63.5 mm/s to 42.3 mm/s to 21.2 mm/s (Table III). A closer view of track #2 (beginning and end) is shown in Figure 9. The latter shows surface cracking in the melt track which appears tp correlate with shallow treatment depths (50 µm or less) resulting from lower power densities and/or high traverse rates (low dwell times).

Figure 10 shows the cross-sections of the melt tracks 2, 3 and 4. Consistent with a decreasing traverse rate, the melt track depths increase from 40 µm to 60 µm to 80 µm (Table III). The track cross-section also becomes more clearly defined.

For tracks 5, 6 and 7, HF was dropped to 9.5 mm and traverse rates went from 21.2 mm/s to 42.3 mm/s to 63.5 mm/s, respectively.

Cross-section are shown in Figure 11 and melt depths range from 120 µm for track #5 to 90 µm for track #7 (Table III).

For track #8, HF was dropped to 6.4 mm from the 9.5 mm used to produce track #7. Traverse rate was kept at 63.5 mm/s as for track #7. This change resulted in a massive melt track (Figure 7) as opposed to the controlled modification resulting from the conditions as in exposure #7.

It is noted that the process parameters for track #8 were identical to those for track #1. This confirms that the abrupt change in melt behaviour was not due to some experimental aberration. Additional confirmation was obtained from exposure #9 in which HF was dropped to 3.2 mm and similar results were noted as for exposures #1 and #8. Cross-sections of all three exposures are shown in Figure 8.

The sequence of tests carried out on coupon 614-3 strongly suggests that for a given traverse rate, there exists a power density level threshold above which the melting process becomes violent and uncontrollable. From exposures #1 (or #8) and #7, this threshold lies somewhere between 1.48 x 10^4 W/mm^2 and 0.76 x 10^4 W/mm^2 for a processing rate of 63.5 mm/s.

— but power input depends [illegible]

Coupon 614-4

This coupon represents the initial attempts at effecting surface coverage as opposed to single scans. On the basis of the results obtained from coupon 614-3 a value of 9.5 mm was chosen for HF as well as a processing rate of 21.2 mm/s (equivalent to single scan #5 in Table III).

The coupon was jogged 0.30 mm following each scan, resulting in approximately a 50% overlap between successive scans. Table IV lists additional information and the coupon itself is shown in Figure 12. Two exposed areas, #1 and #2 are seen clearly.

Exposure #1 consisted of 20 successive scans, followed by a brief pause. A further 20 scans were then made to complete the exposure. The first five tracks of the second set of 20 scans overlapped the last five tracks of the first set.

It can be seen in Figure 12 that a considerable amount of surface break-up exists in the region corresponding to the second set of 20 scans. Figure 13 shows more details of this feature. Figure 13A depicts the surface in the clean track portion of exposure #1 (see Figure 12). Figure 13B shows the transition between this clean track portion and the onset of the surface damaged portion.

Cross-sectional views are shown in Figure 14. At clean track areas A and B (see Figure 12), treatment depth is quite uniform at about 110 μm. In the surface damaged area (location C in Figure 12), treatment depth drops to only about 50 μm. This strongly suggests reduced laser power during the completion of exposure #1.

Exposure #2 on coupon 614-4 used identical parameters as for exposure #1. However, in this case the area was scanned twice in order to assess whether greater homogeneity could be achieved in the RST layer.

As seen from Figure 12 and in more detail in Figure 15, a considerable degree of surface cracking exists in this area. Figure 16 provides a cross-sectional view where the depth of treatment is seen to be quite uniform at about 120 μm from beginning to end of scanning.

It is strongly suspected that the cause of this surface cracking was reduced laser power levels. It is recalled that low power densities leading to very shallow treatment depths (50 µm or less) produced surface defects (see Figure 9 and discussion for coupon 614-3). From Figure 14, low powers are inferred from the shallow treatment depths for the damaged area of exposure #1. This area was covered after a brief pause following the initial exposure of 20 scans.

Similarly, for coupon 614-4, area #2, there was a brief pause prior to scanning the area a second time. It is suspected that the laser did not come back up to full power following each of these two brief interruptions. Either scanning entire areas with no interruptions or allowing a longer rest period for the laser following a pause would eliminate this problem.

Coupon 614-5

Area scans were again carried out on this specimen with all laser parameters maintained as for coupon 614-4 except traverse rate. Exposures 1A and 1B (Table V) were carried out on the same area and resulted in simple heat treatment only (Figure 17). Therefore, increasing traverse rate from 21.2 mm/s to 42.3 mm/s and 31.8 mm/s here did not lead to surface melting.

These results are, again, quite unexpected and are suspected to be erroneous. It will be recalled from Table III for coupon 614-3, that HF values of 9.5 mm and traverse rates of up to 63.5 mm/s (exposures #5 to #7 in Table III) resulted in surface melting ranging in depth from 90 µm to 120 µm. The above results of scans 1A and 1B on coupon 614-5 are completely inconsistent with these earlier results.

For area #2 on coupon 614-5, the traverse rate was dropped to 25.4 mm/s, still slightly higher than those used on coupon 614-4 (Table IV). Surface melting was observed (Figure 17) but again surface cracking is noted. Figure 18 shows the cross-section through this area and again it is seen that effective treatment depths are about 120 µm in the clean track area and under 50 µm in the surface defect track area.

These results, in conjunction with those from other coupons discussed above strongly suggest periodic instabilities in total laser power. Mode instability is not considered likely here in that total treatment depths should not drop off so drastically in the surface cracked areas.

3.2 Iron Coated Binary Aluminum Bronze Coupons

These coupons consisted of binary aluminum bronze having a thin layer of iron deposited on one flat face. They were labelled 610-1, 610-3 and 610-4.

It is noted that the iron coating was not entirely acceptable. It was loose and friable, showing virtually no adhesion to the substrate. This resulted in a tendency for the iron to blow off the coupon when subjected to the combination of thermal shock from the laser beam and the co-axial stream of argon cover gas.

Further, the coating was black in appearance, suggesting the iron was heavily oxidized. It is not expected that alloying in iron oxides as opposed to elemental iron would lead to equivalent RST surfaces on the binary alloy coupons.

As the coupons were available, some exposures were carried out. However, due to the above concerns, no detailed analysis of the results, such as distribution of iron alloyed into the coupons, was carried out.

Coupon 610-4

Two exposures were made on this coupon as shown in Figure 19. Conditions, listed in Table VI were set equivalent to those producing melt depths of about 120 μm in the ternary alloys discussed above.

Coupon 610-4 had a very poor iron coating which exhibited considerable roughness and ridging and very poor adhesion to the substrate. As can be seen from Figure 19, most of the coating blew off as the laser beam hit the coupon.

Figure 20 illustrates the melt track cross-section on coupon 610-4. It is noted (see Table VI) that the melt track widths are considerably greater than the beam spot size. Further, melt depths are 270 μm and 320 μm, respectively, for tracks #1 and #2. This is much greater than melt depths achieved with the ternary coupons using the same exposure parameters.

These differences are attributable to the iron coating on the binary coupon. The black coating allows much more efficient coupling of the laser beam into the surface of the coupon due to reduced reflectivity. This leads to greater melt depths and widths compared to the highly reflective ternary coupons.

Coupon 610-3

Two area scans were carried out under the conditions listed in Table VI. The samples were jogged 0.30 mm between successive scans. However, because of the much wider melt tracks in these samples, this resulted in about an 80% overlap in successive scans. Overlap for the ternary coupons above was about 50% it will be recalled.

Figures 22 and 23 illustrate cross-sections in various locations (as indicated on Figure 21) of the laser treated areas. As expected, the lower traverse rates in exposure #2 result in deeper melt zones than in exposure #1 (320 µm and 260 µm, respectively).

More interesting, perhaps, is the observation from Figures 22 and 23 that there appears to be a greater degree of microstructural order at the bottom of the melt zones than at the top (near the coupon surfaces). This ordered appearance extends for a distance of about 120 µm to 150 µm, roughly equal to effective treatment depths obtained with the ternary coupons discussed above.

This observation suggests there might be a limit to the depth of effective treatment. The ordered structures at the bottom of the melt zone are likely formed due to more rapid cooling rates as a result of proximity to the heat sink (the underlying bulk of the coupon).

Coupon 610-1

A single large area scan was carried out on this coupon as shown in Figure 24. Optical parameters were kept identical to those used for coupon 610-3 (Table VI) but the traverse rate was increased to 42.3 mm/s.

Figure 25 shows cross-sectional views from treated areas as indicated in Figure 24. These correspond to beginning, mid-point and end of treatment. Depth of treatment appears to slowly increase from 200 µm to 230 µm to 250 µm as scanning continued. This is ascribable to warming of the coupon during treatment, allowing progressively more effective coupling of the laser beam into its surface.

3.3 Comparison to Literature Results

Studies on laser treatment of ternary aluminum bronzes have been carried out be C.W. Draper et al. (Corrosion, 36, 405 (1980)). Table VII lists a short comparison of typical exposure parameters used by Draper et al. with those used in the current study.

The laser power used in this study was considerably higher than that used by Draper et al. leading, as expected, to much greater total spot and effective spot sizes. These coupled with much lower traverse rates led to significantly greater dwell times (by three orders of magnitude) in the current study. The result, however, is optimum depths of 120 to 150 µm for this work, as compared to about 10 µm in the earlier studies.

4. CONCLUSIONS

Conclusions which might be drawn from the results obtained to date are as follows:

1. For treatment of ternary coupons, a distance of 9.5 mm for the height of the focal point above the coupons and a traverse rate of 20-25 mm/s would appear optimum.

2. The above conditions lead to effective treatment depths of about 120 μm to 160 μm. This should provide interesting comparative studies to those already in the published literature where treatment depths were of the order of 10 μm.

3. In future studies, it will be essential to monitor laser power closely in order to ensure no fluctuations occur. It is suspected that such fluctuations have led to some erratic results in the study to date.

4. The results with the iron coated binary alloy coupons outlined here are not useful for the determination of optimum processing parameters. This is due to the inadequacies of the iron coating. New methods of applying the coating are required and preliminary evaluations will have to be repeated.

T. Kilp

T. Kilp, Ph.D.
Section Manager
Laser Applications

J. Leidner

J. Leidner
Centre Manager
Industrial Materials Technology

TABLE I

Exposure Conditions For Coupon 614-1

Exposure Number	Rate (mm/s)	H F (mm)	Spot Size (mm)	Effective Size (mm)	Dwell Time (ms)	Treatment Depth(μm)
1	21.2	0	0.28	0.55	26	160
2	33.9	0	0.28	0.51	15	130
3	46.6	0	0.28	0.51	11	120
4	21.2	25.4	1.65	--	--	--
5	12.7	25.4	1.65	--	--	--
6	21.2	12.7	0.86	0.39	18	--
7	46.6	12.7	0.86	0.45	10	--
8	21.2	19.1	1.24	--	--	--

TABLE II

Exposure Conditions For Coupon 614-2

Exposure Number	Rate (mm/s)	H F (mm)	Spot Size (mm)	Effective Size (mm)	Dwell Time (ms)	Treatment Depth(μm)
1	21.2	6.4	0.46	--	--	--
2	21.2	12.7	0.86	--	--	--
3	21.2	6.4	0.46	--	--	--

TABLE III

Exposure Conditions For Coupon 614-3

Exposure Number	Rate (mm/s)	H F (mm)	Spot Size (mm)	Effective Size (mm)	Dwell Time (ms)	Treatment Depth(μm)
1	63.5	6.4	0.46	1.40	22	1440
2	63.5	12.7	0.86	0.24	4	40
3	42.3	12.7	0.86	0.29	7	60
4	21.2	12.7	0.86	0.34	16	80
5	21.2	9.5	0.64	0.54	25	120
6	42.3	9.5	0.64	0.45	11	100
7	63.5	9.5	0.64	0.38	6	90
8	63.5	6.4	0.46	1.30	20	1200
9	63.5	3.2	0.33	1.70	27	1700

TABLE IV

Exposure Conditions For Coupon 614-4*

Exposure Number	Rate (mm/s)	H F (mm)	Spot Size (mm)	Effective Size (mm)	Dwell Time (ms)	Treatment Depth(μm)
1	21.2	9.5	0.64	0.54	25	110
2**	21.2	9.5	0.64	0.54	25	120

* Sampled jogged 0.30 mm between scans resulting in approximate overlap of 50% between successive scans.

** Area was scanned twice using these conditions

TABLE V

Exposure Conditions For Coupon 614-5

Exposure Number	Rate (mm/s)	H F (mm)	Spot Size (mm)	Effective Size (mm)	Dwell Time (ms)	Treatment Depth(μm)
1A	42.3	9.5	0.64	--	--	--
2B	31.8	9.5	0.64	--	--	--
3	25.4	9.5	0.64	0.63	25	50 - 120

TABLE VI

Exposure Conditions For Fe Coated Binary Coupons

Coupon	Exposure Number	Rate (mm/s)	H F (mm)	Spot Size (mm)	Effective Size (mm)	Dwell Time(ms)	Treatment Depth(μm)
610-4	1	21.2	9.5	0.64	1.04	49	270
	2	12.7	9.5	0.64	1.32	104	320
610-3*	1	21.2	9.5	0.64	1.04	49	260
	2	12.7	9.5	0.64	1.32	104	320
610-1*	1	42.3	9.5	0.64	0.72	17	230

* Coupons were jogged 0.30 mm between successive line scans

TABLE VII

Comparison of Laser Treatment Parameters

Parameter	Draper et al.*	This Study
Laser Power (W)	400 - 500	2450
Spot Size (μm)	100 - 150	280 - 1650
Effective Size (μm)	50	290 - 1700
Rate (mm/s)	2000 - 3000	21 - 63
Dwell Time (μs)	25	6000 - 26000
Treatment Depths (μm)	10	30 - 1700

* C.W. Draper, R.E. Woods and L.S. Meyer; Corrosion, 36, 405 (1980)

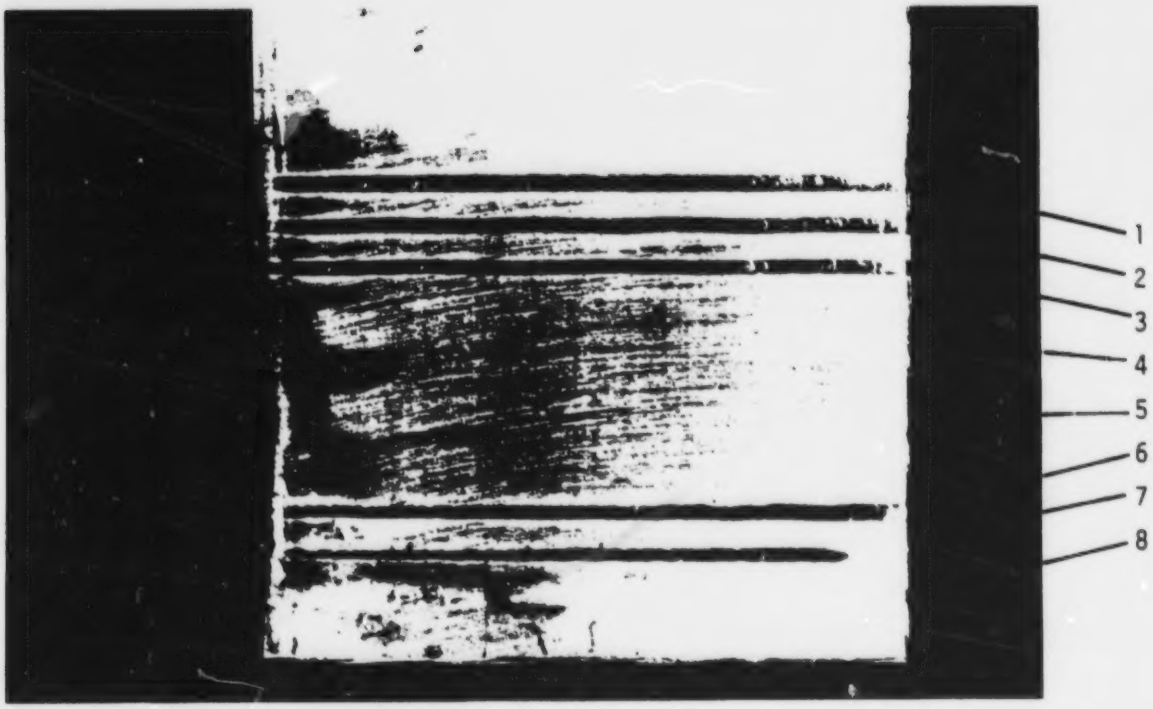

Figure 2: View of ternary alloy coupon 614-1 after laser treatment.

Figure 3: Detailed view of start (A) and finish (B) of melt track #1 on coupon 614-1 (X67).

Start

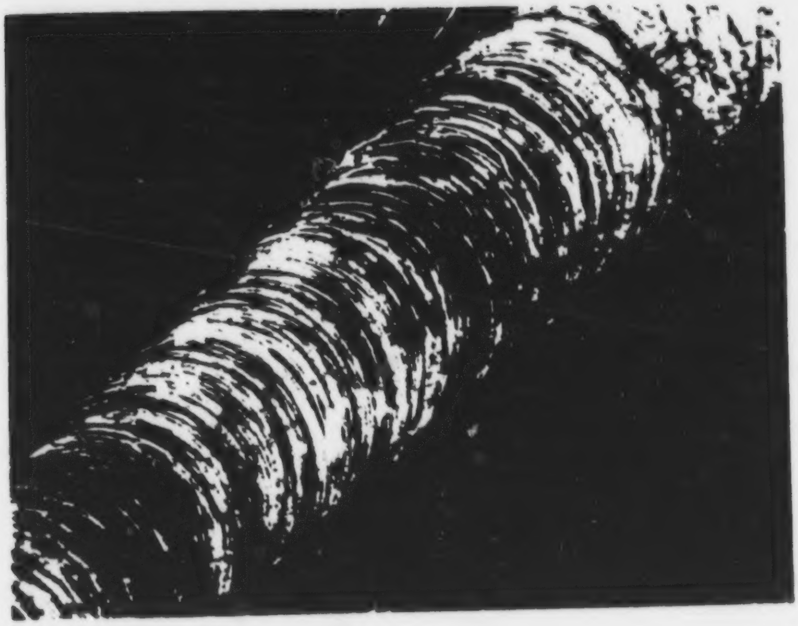

End

Figure 4: Cross-sectional views o
melt tracks #1, #2 and
on coupon 614-1 (X100).

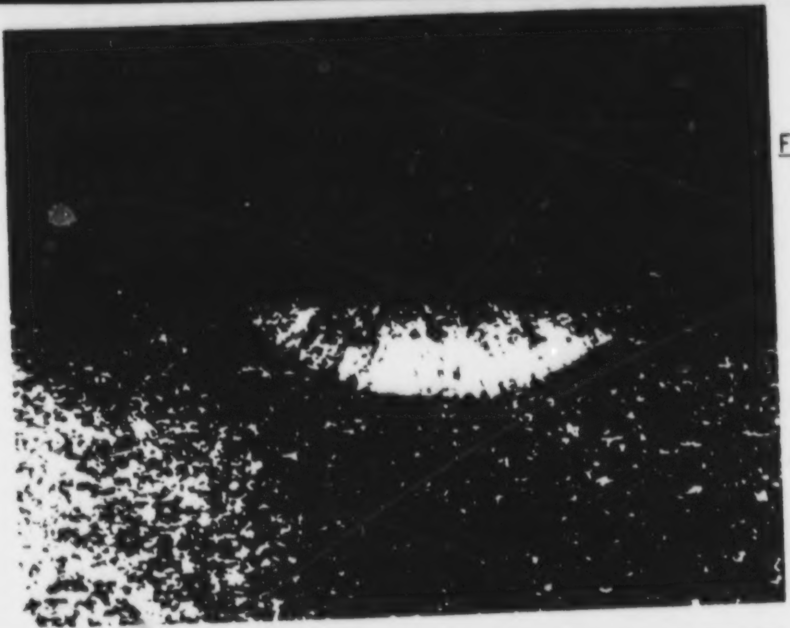

Track #1

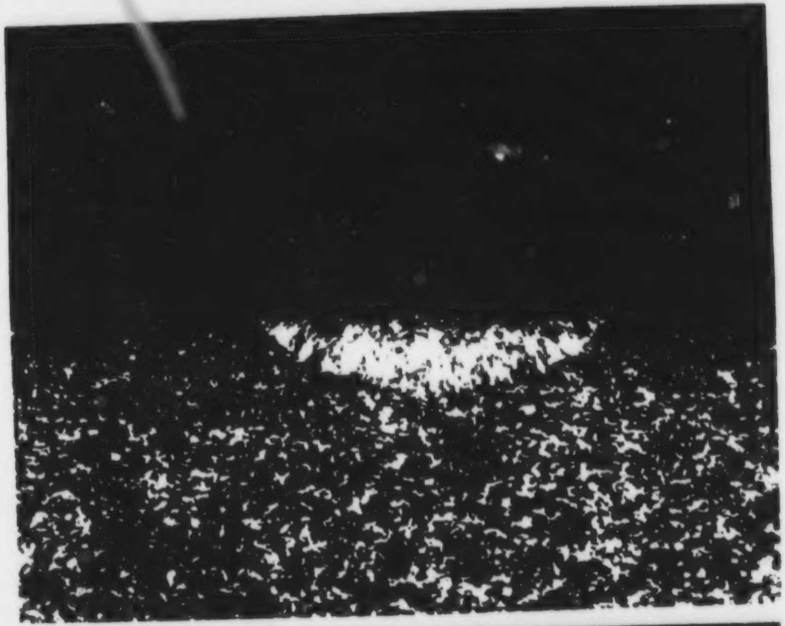

Track #2

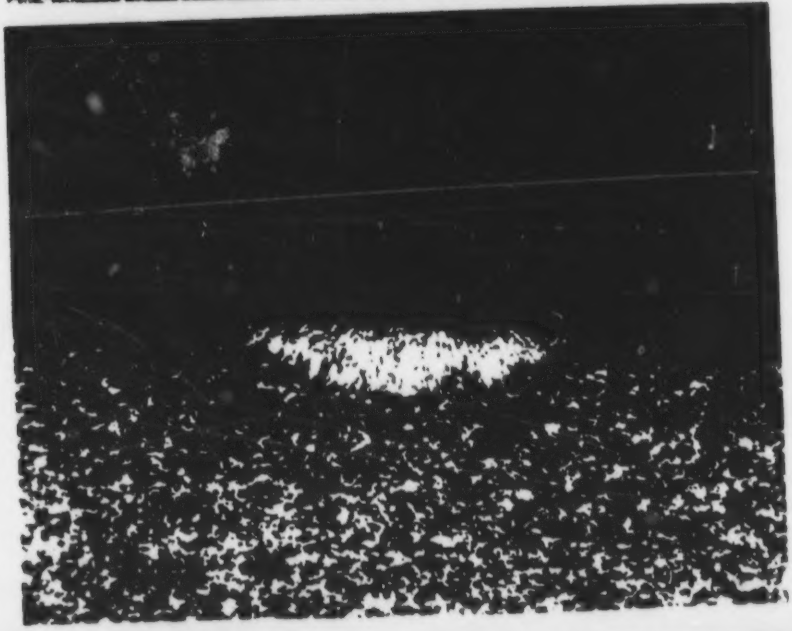

Track #3

Figure 5: Detailed view of start (A) and finish (B) of melt track #6 on coupon 614-1 (X67).

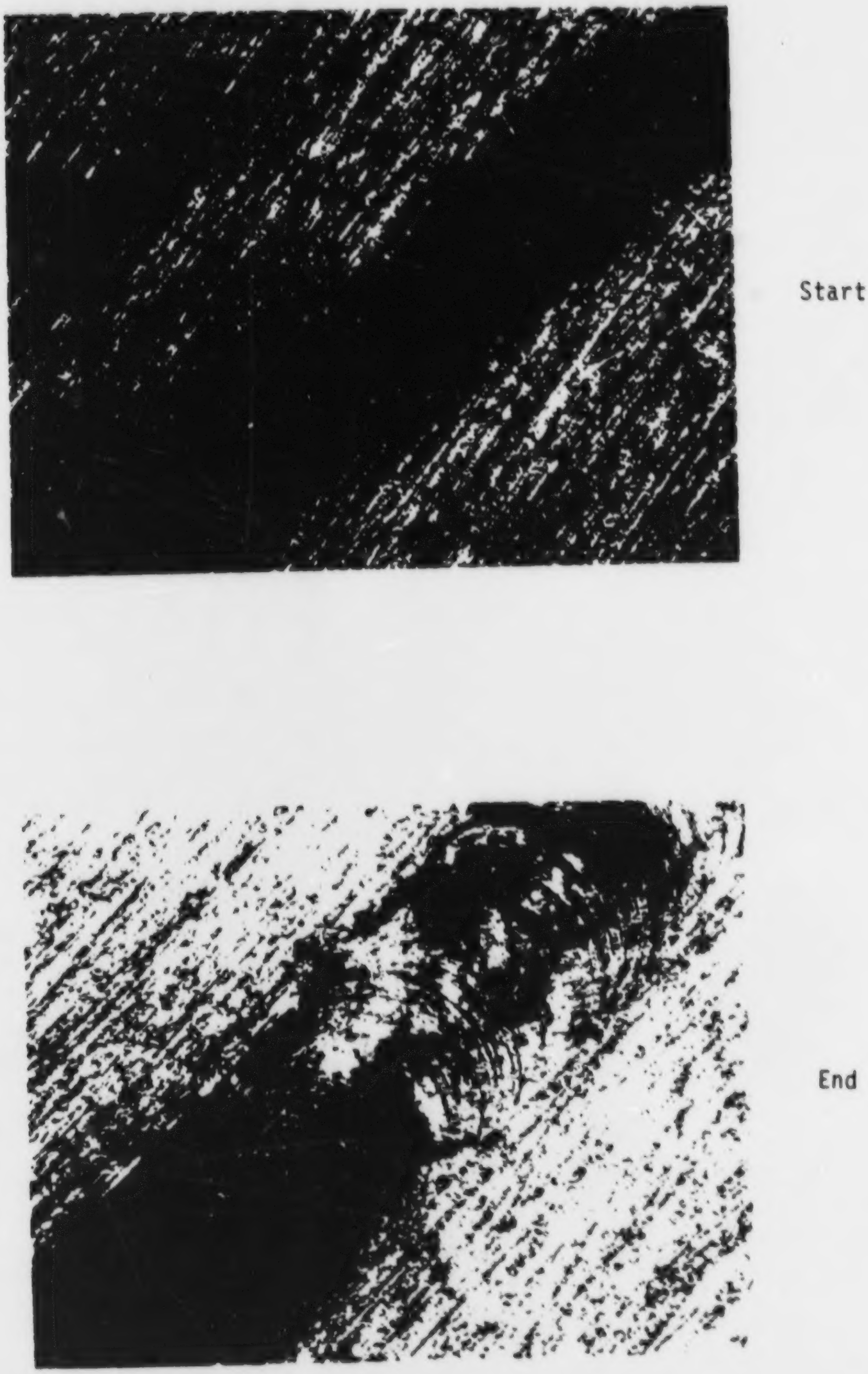

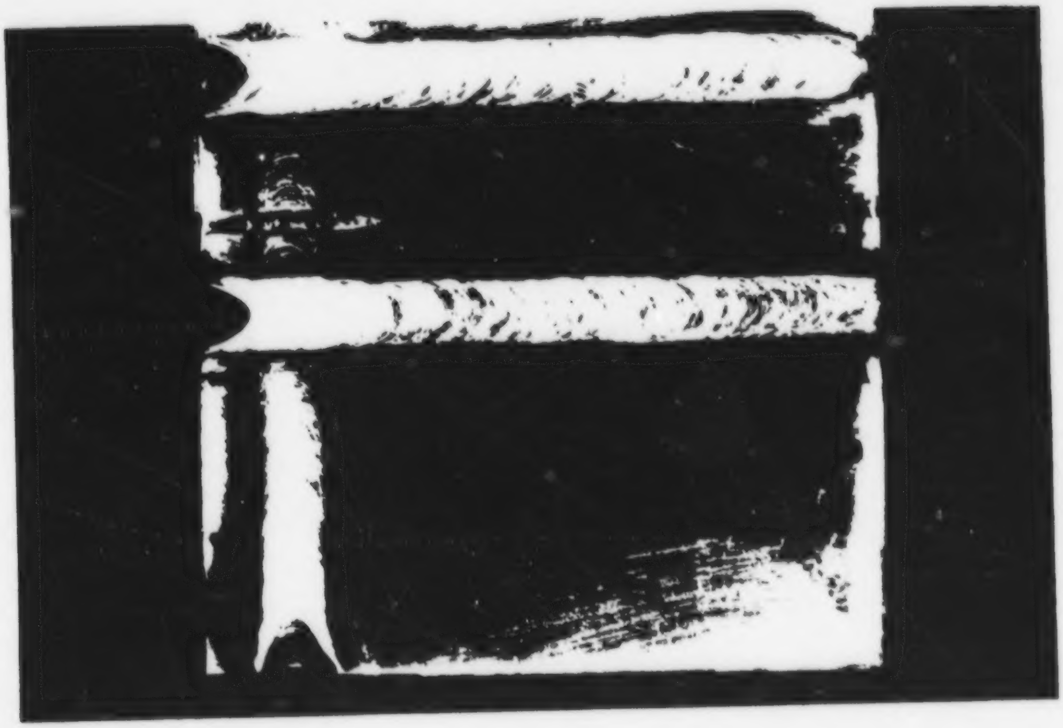

Figure 6: View of ternary alloy coupon 614-2 after laser treatment.

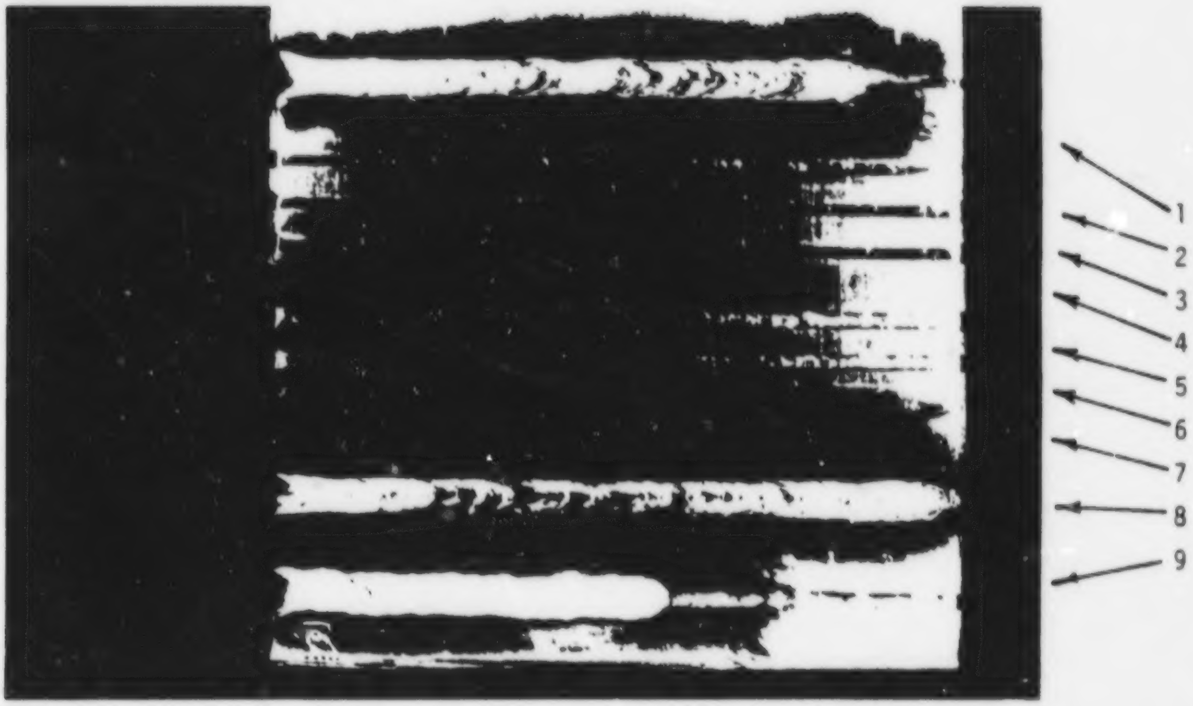

Figure 7: View of ternary alloy coupon 614-3 after laser treatment.

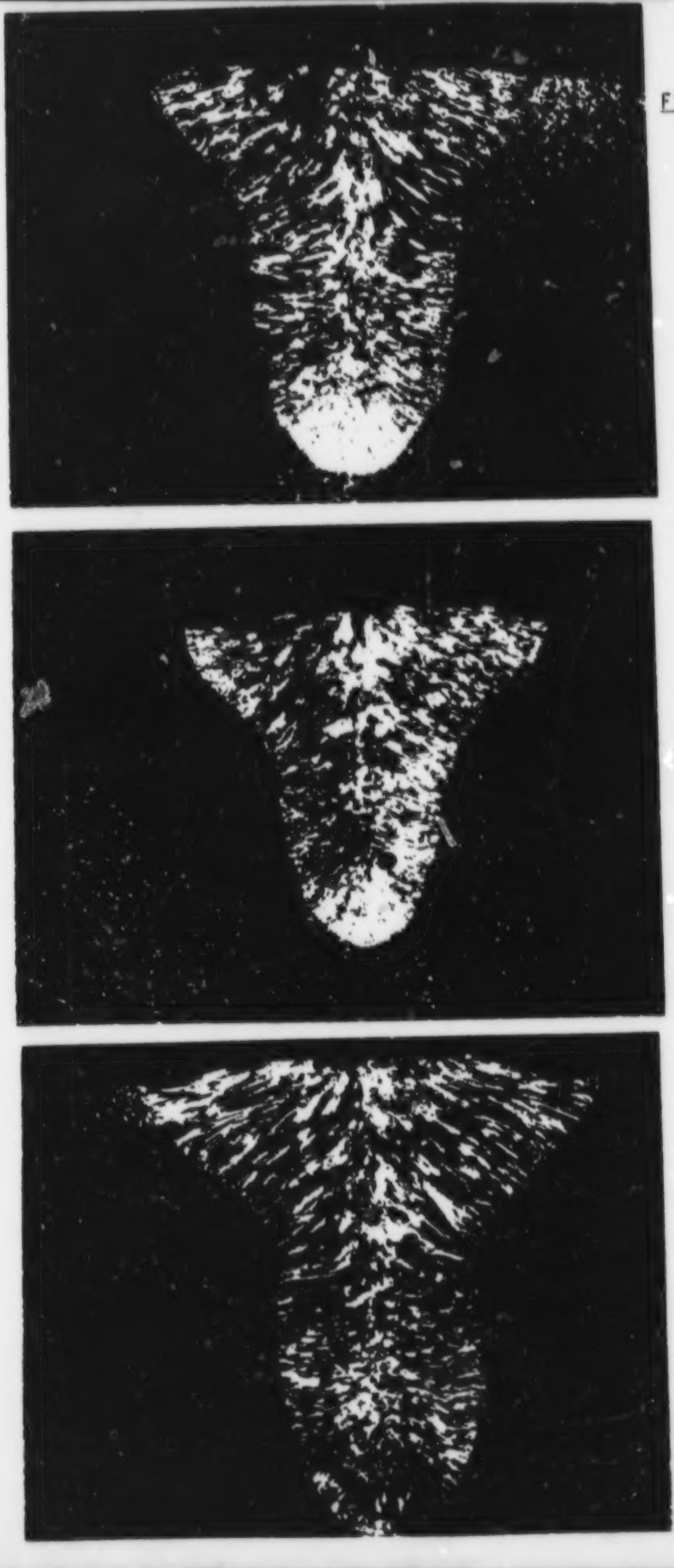

Figure 8: Cross-sectional views of melt traces #1, #8 and #9 on coupon 614-3 (X50).

Track #1

Track #8

Track #9

Figure 9: Detailed view of start (A) and finish (B) of melt track #2 on coupon 614-3 (X67).

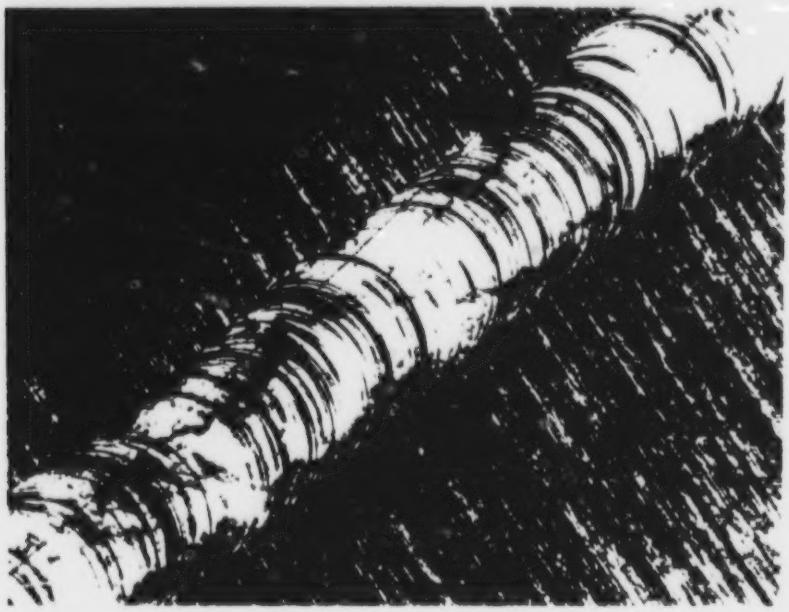

Start

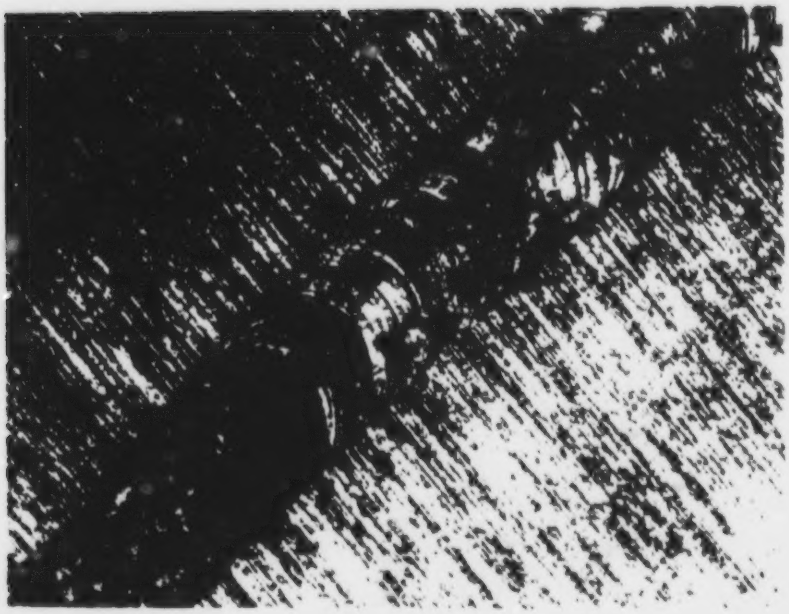

End

Figure 10: Cross-sectional views of melt tracks #2, #3 and #4 on coupon 614-3 (X100).

Track #2

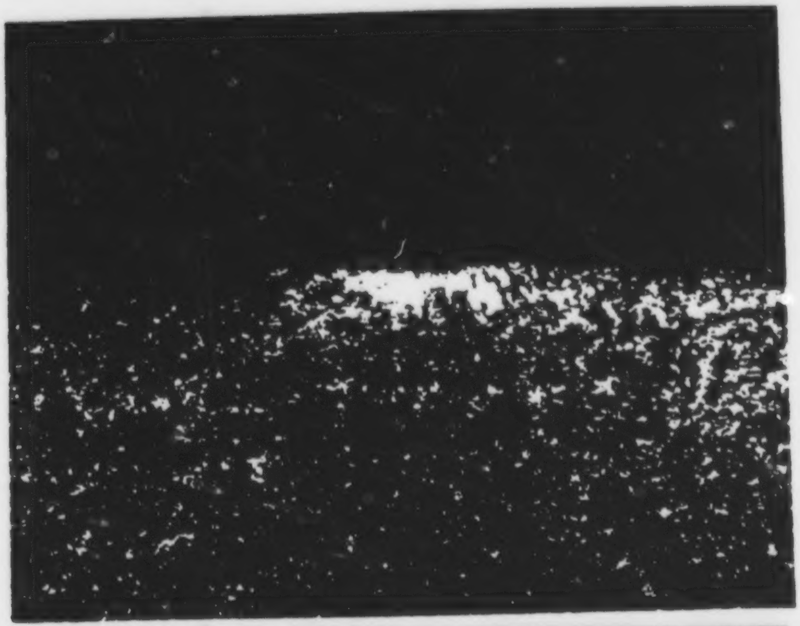

Track #3

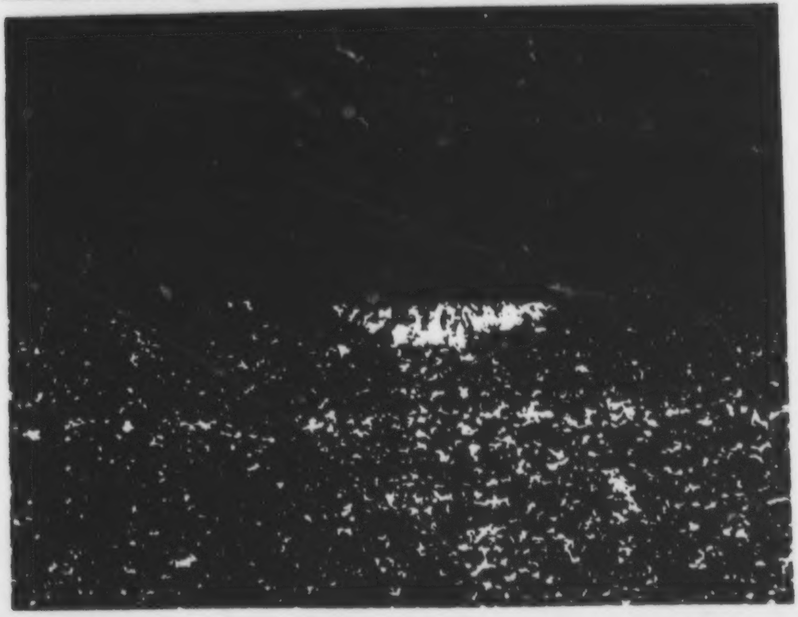

Track #4

Figure 11: Cross-sectional views melt tracks #5, #6 and on coupon 614-3 (X100)

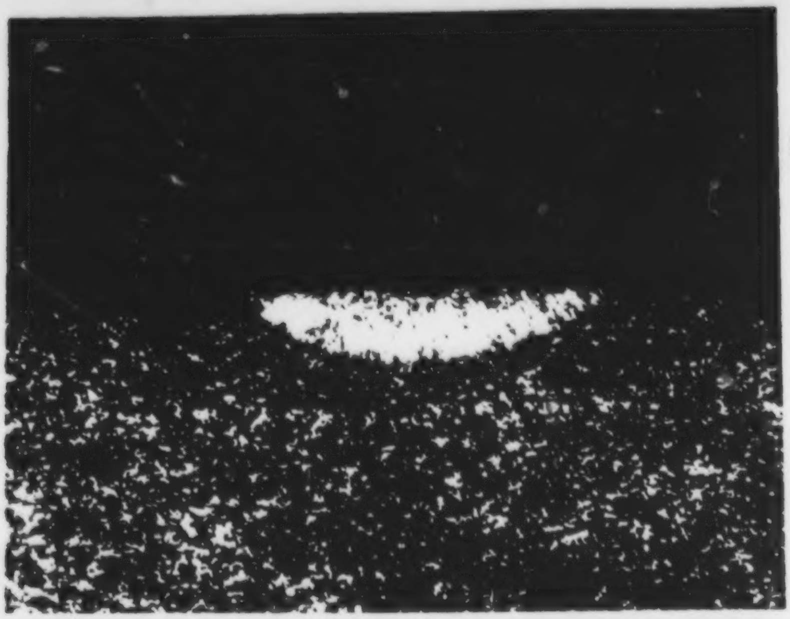

Track #5

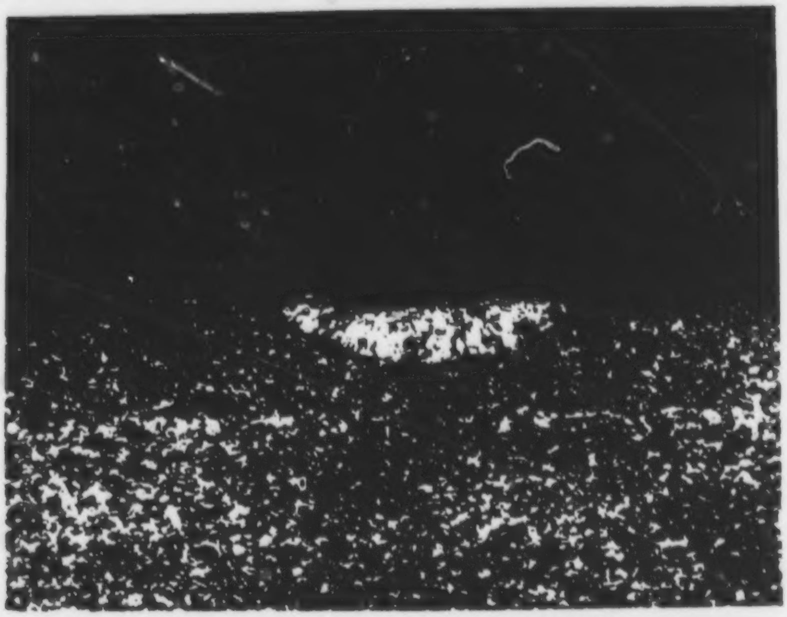

Track #6

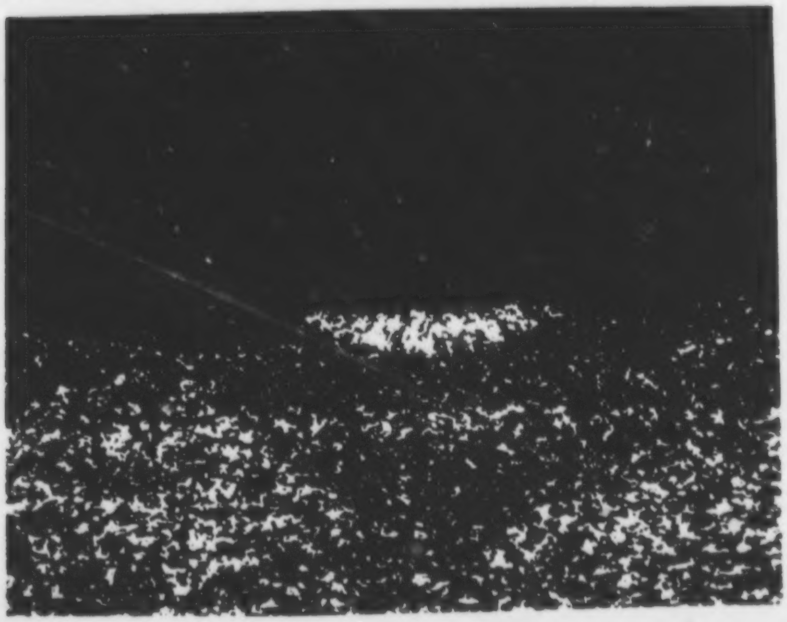

Track #7

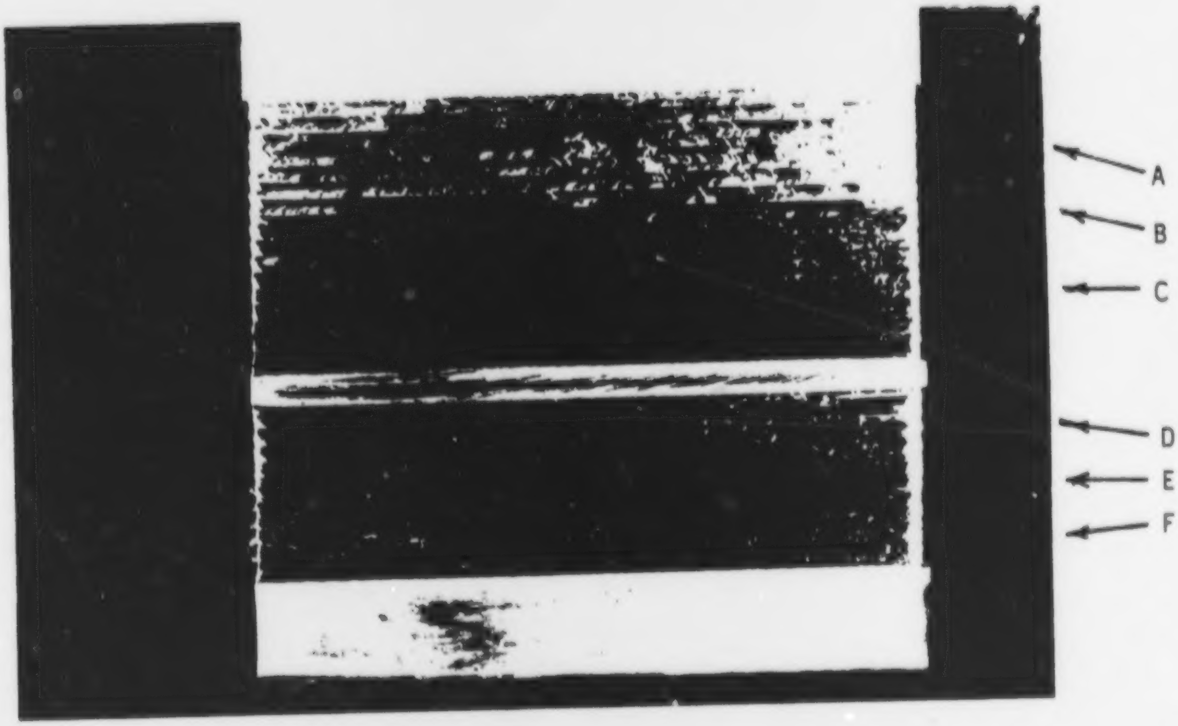

Figure 12: View of ternary alloy coupon 614-4 after laser treatment.

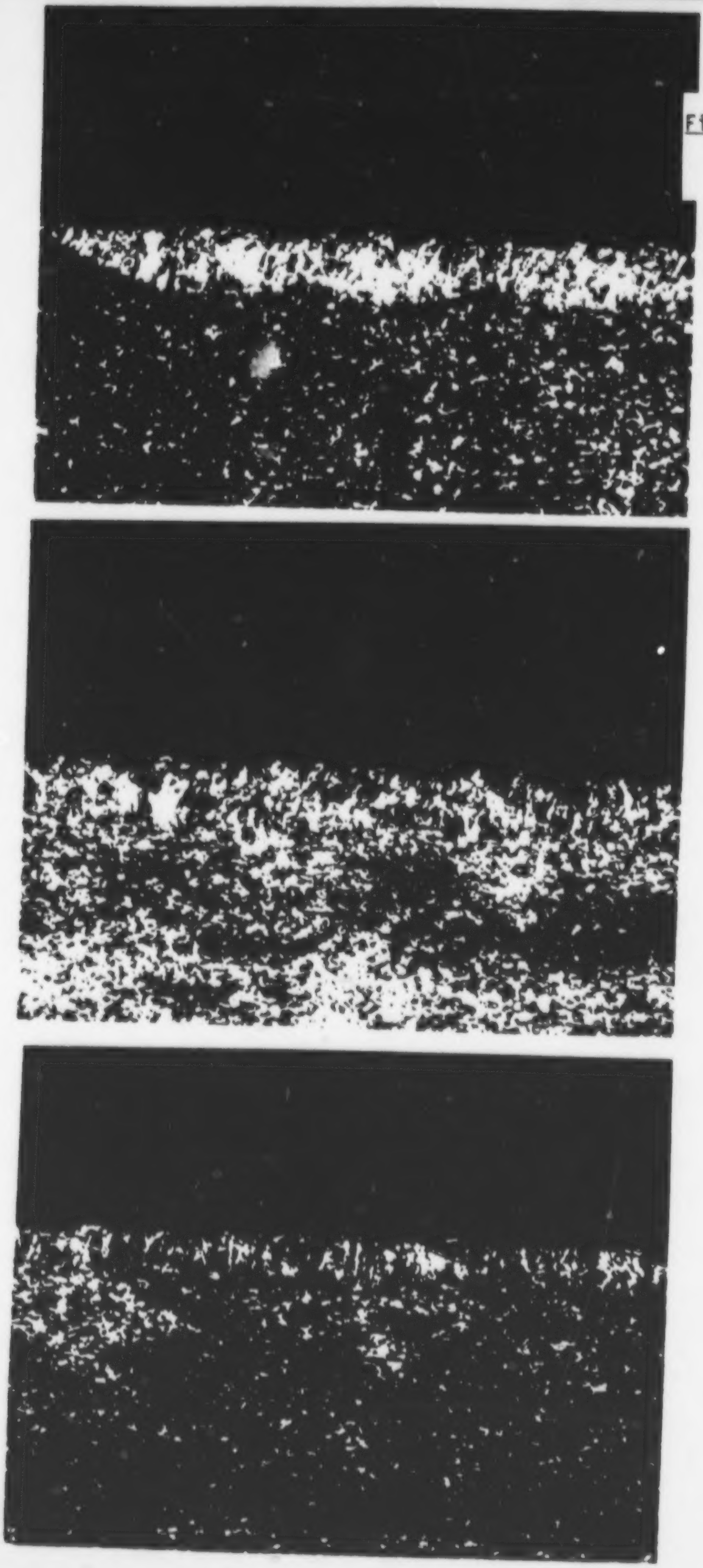

Figure 14: Cross-sectional views melt areas A, B and C on coupon 614-4 (X100)

Area A

Area B

Area C

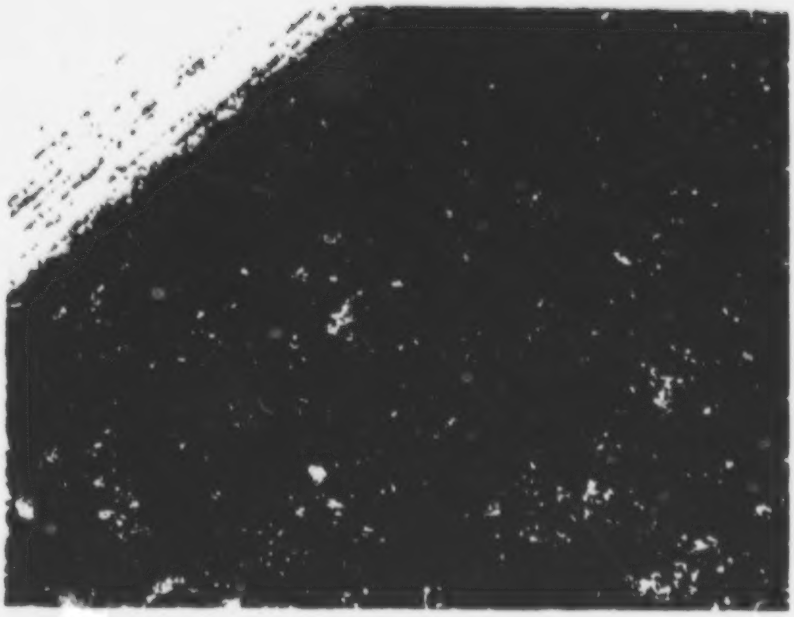

Figure 15: Detailed view of surface in area #2 on coupon 614-4 (X67).

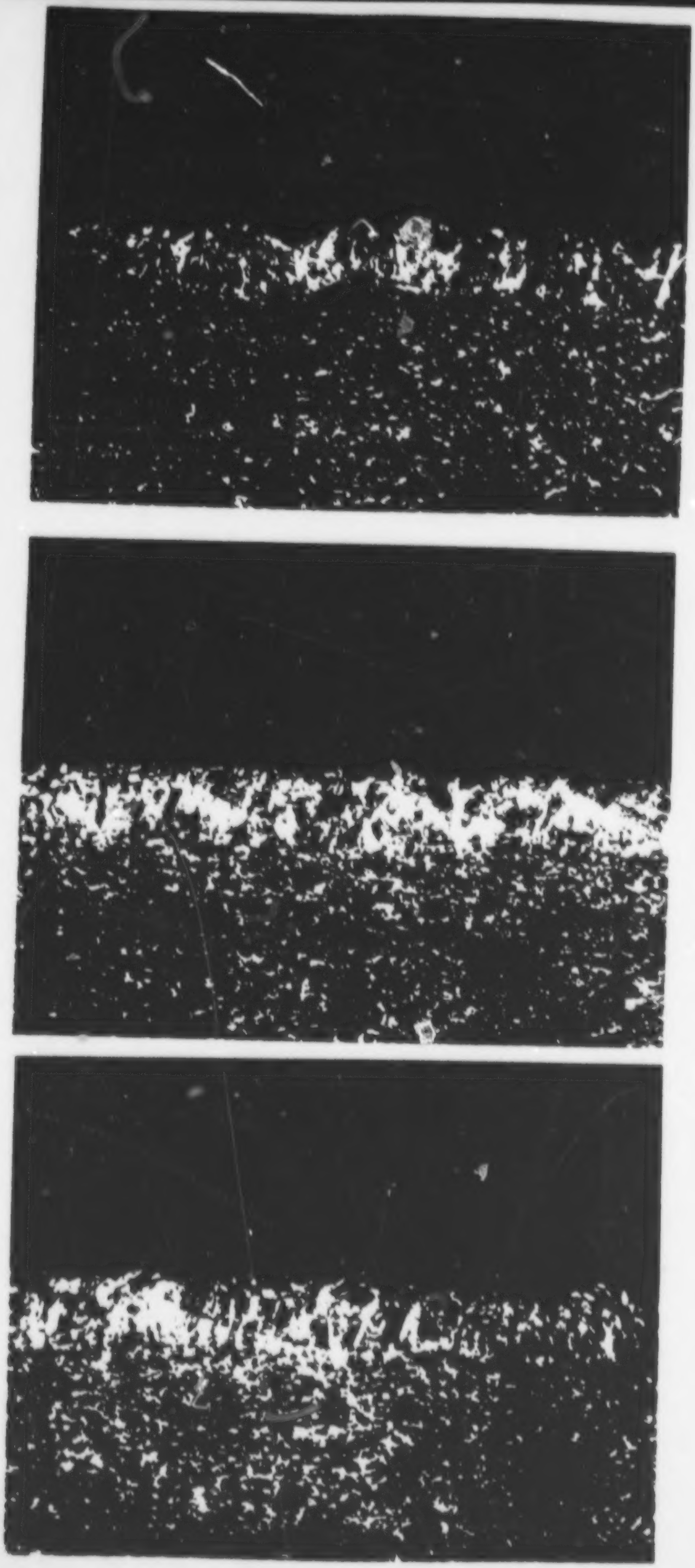

Figure 16: Cross-sectional views of melt areas D, E and F on coupon 614-4 (X100).

Area D

Area E

Area F

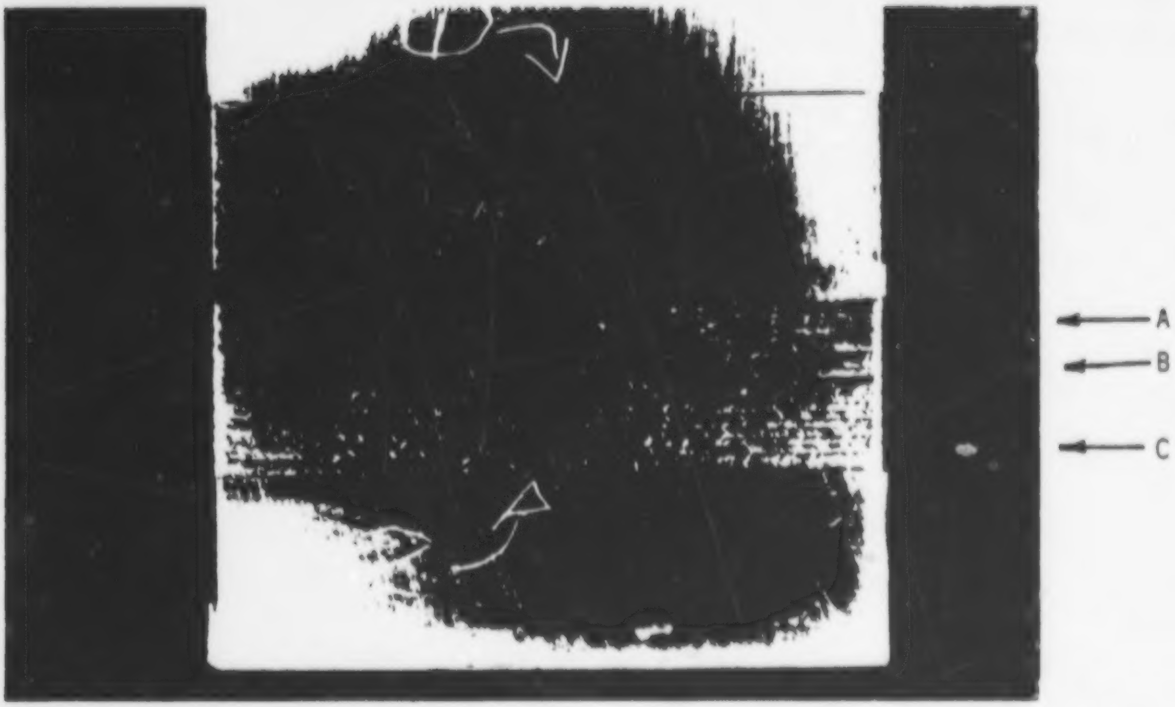

Figure 17: View of ternary alloy coupon 614-5 after laser treatment.

Figure 13: Detailed view of clean (A) track area and onset of surface cracking (B) for area #1 on coupon 614-4 (X67).

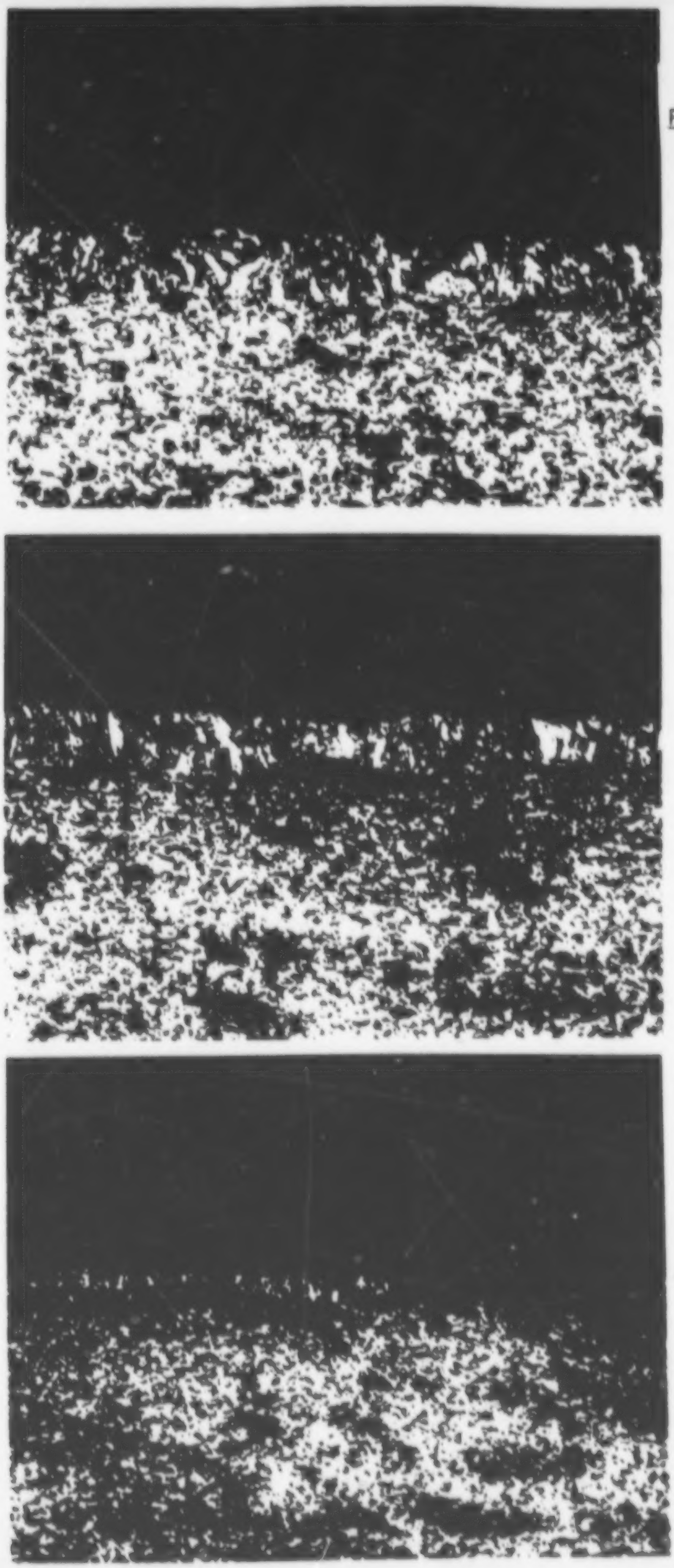

Figure 18: Cross-sectional views o
melt areas A, B and C
on coupon 614-5 (X100).

Area C

Area B

Area A

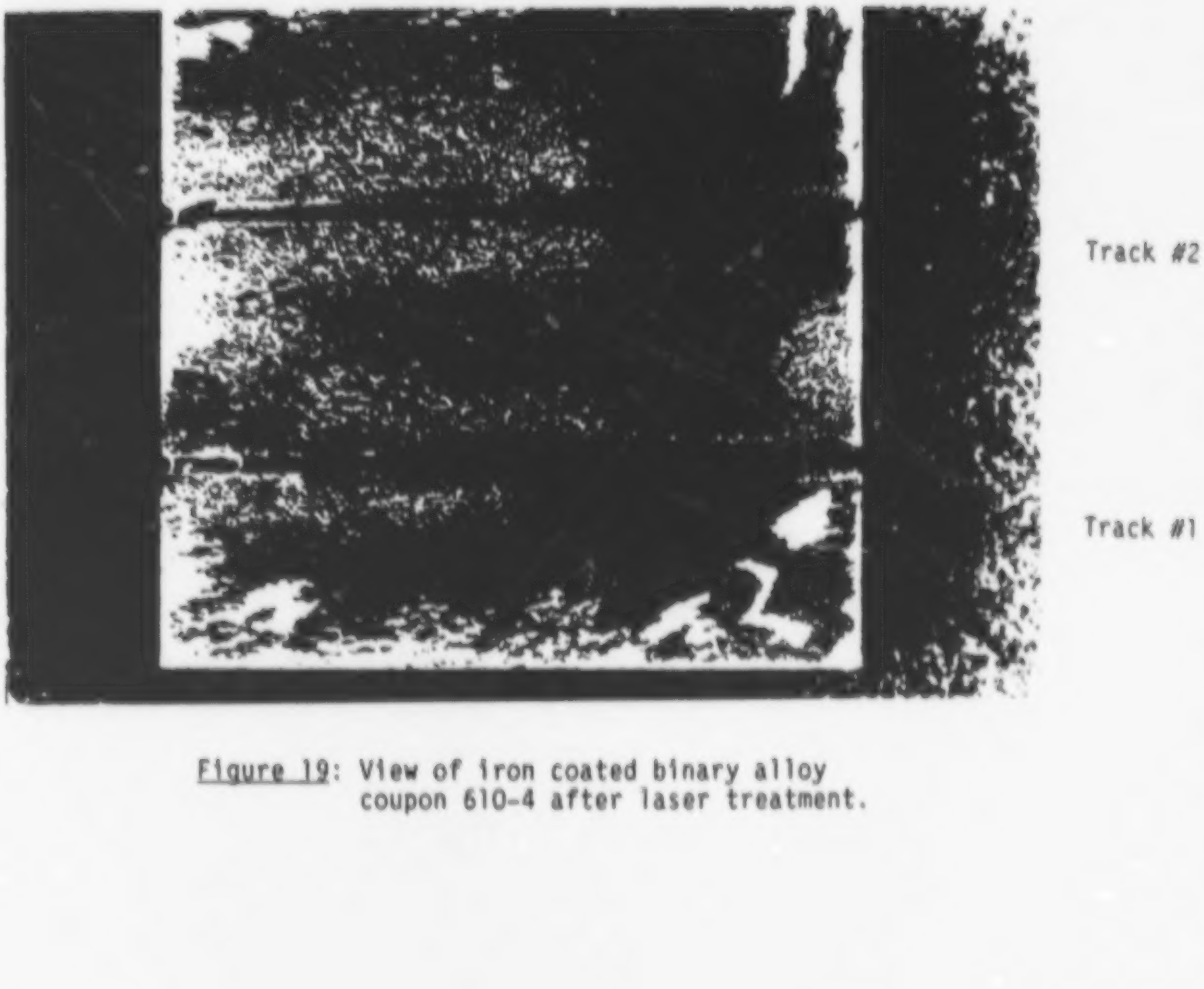
Track #2
Track #1

Figure 19: View of iron coated binary alloy coupon 610-4 after laser treatment.

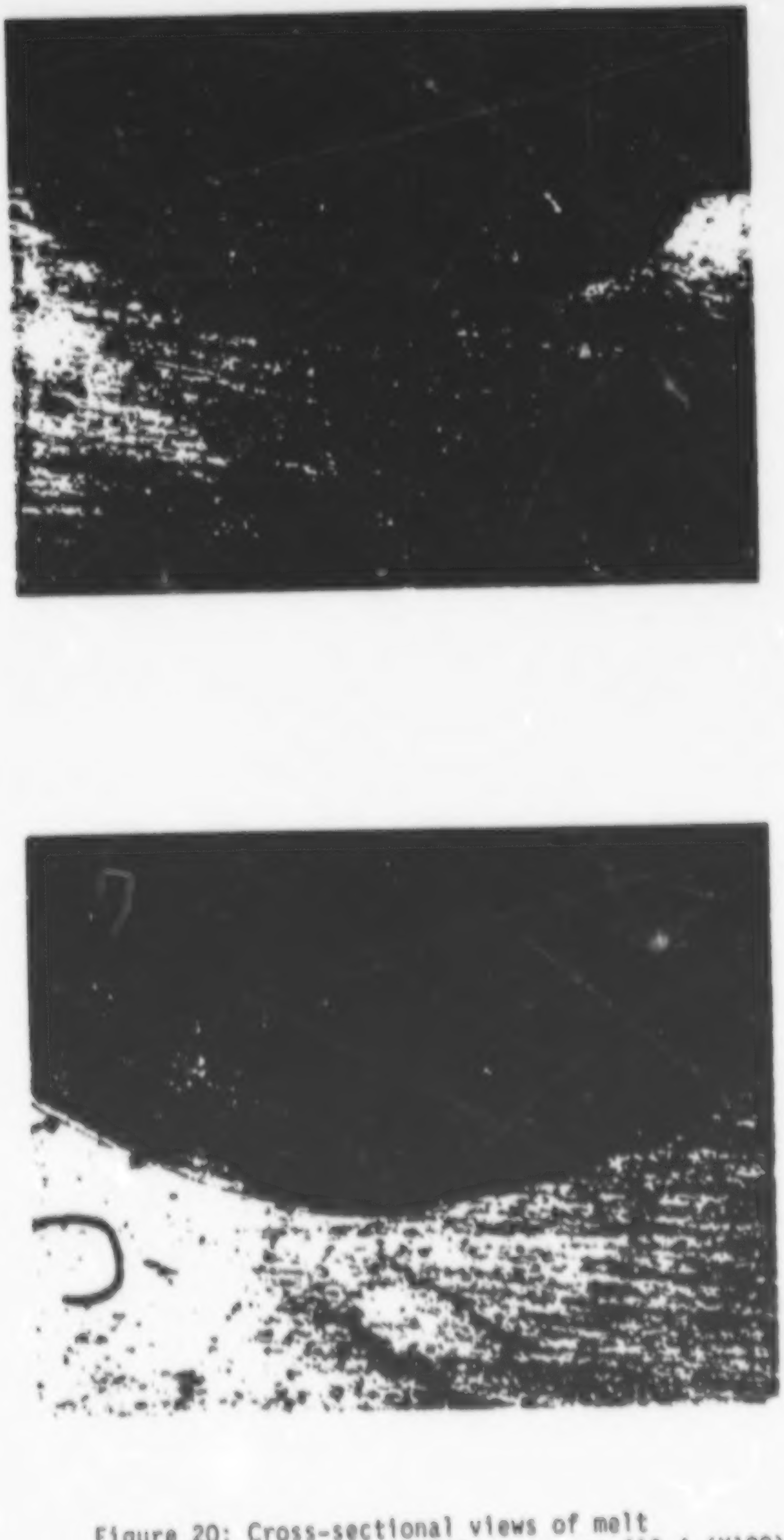

Track #1

Track #2

Figure 20: Cross-sectional views of melt tracks #1 and #2 on coupon 610-4 (X100).

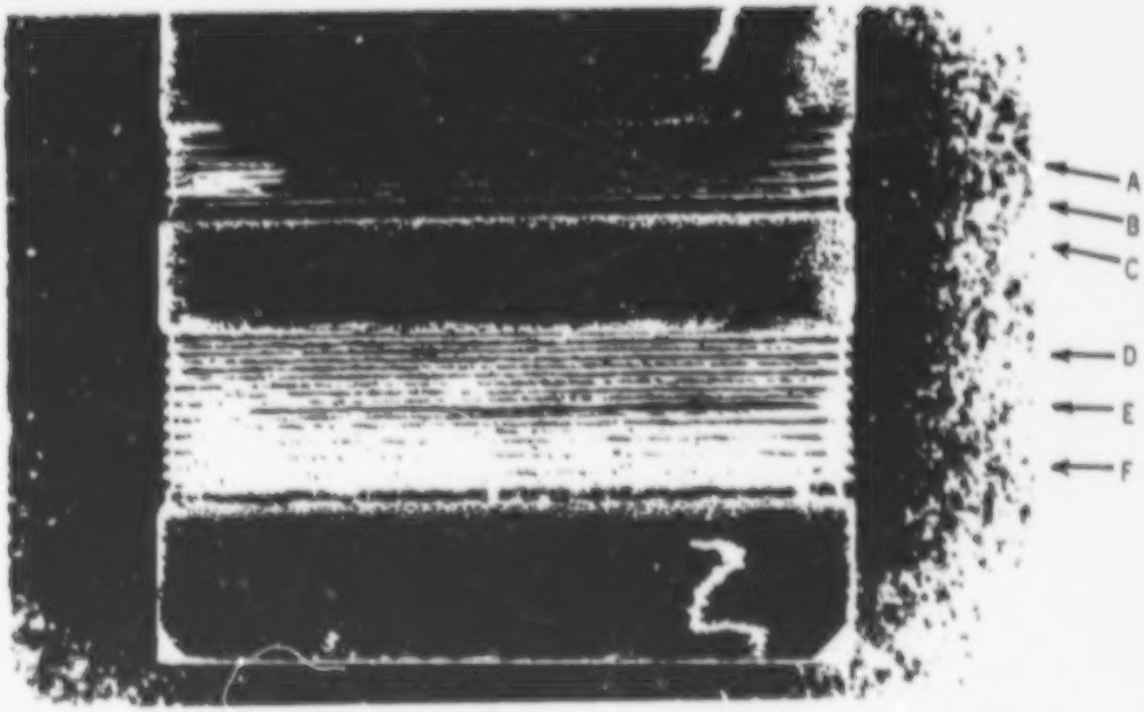

Figure 21: View of iron coated binary alloy coupon 610-3 after laser treatment.

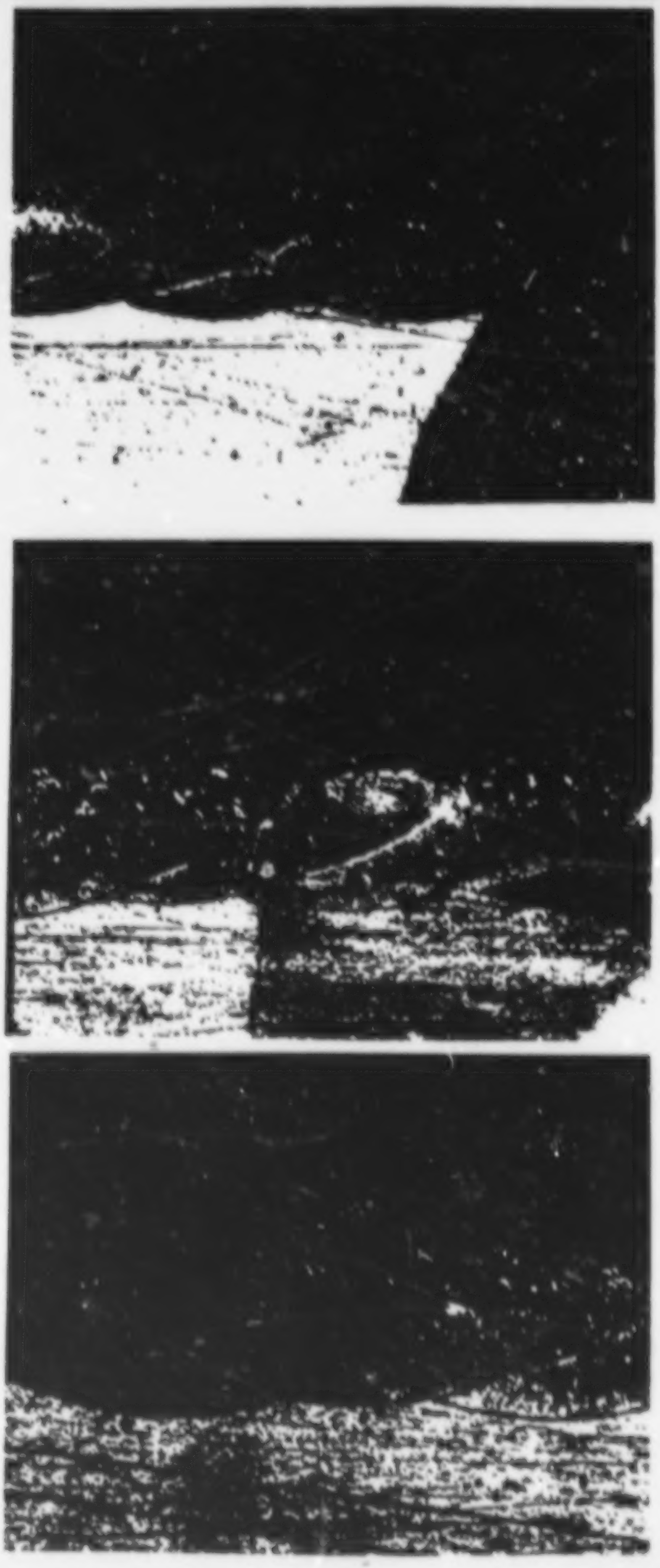

Figure 22: Cross-sectional view of melt areas A, B and C on coupon 610-3 (X100).

Area A

Area B

Area C

Figure 23: Cross-sectional view o
melt areas D, E and F
on coupon 610-3 (X100)

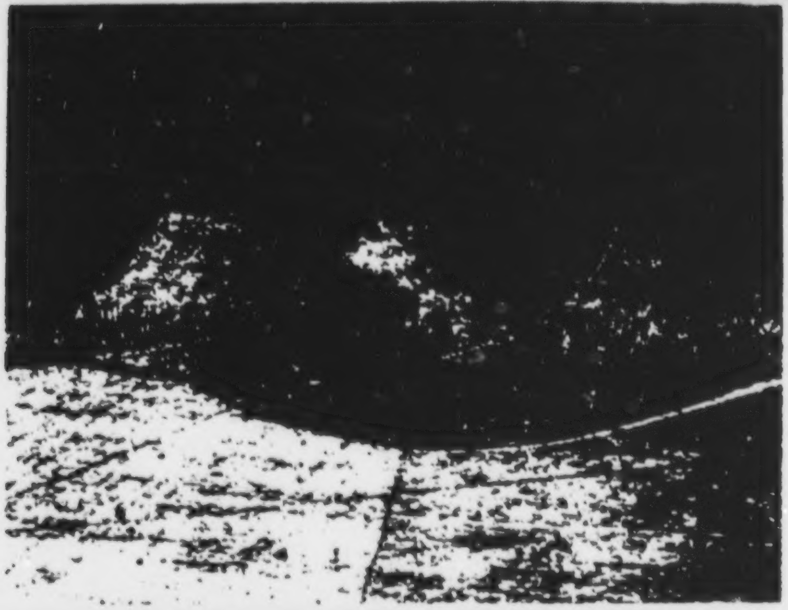

Area D

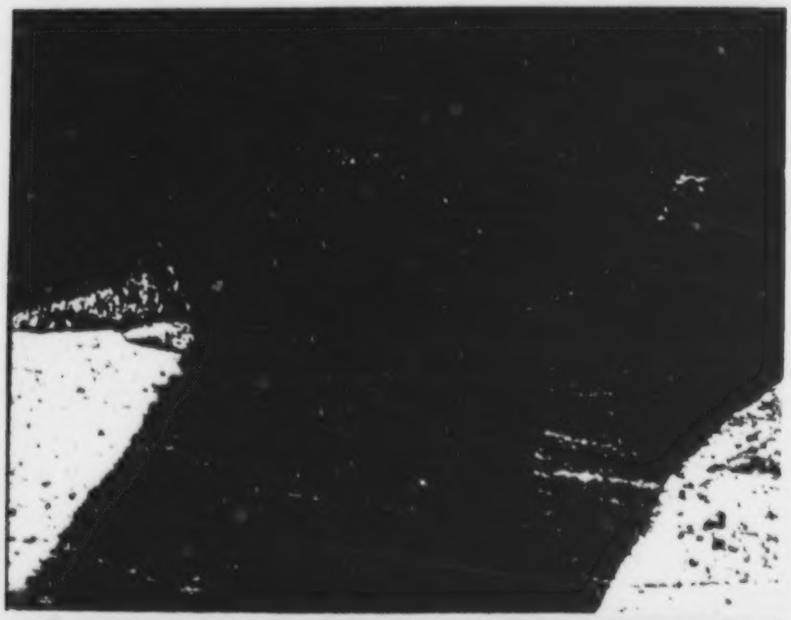

Area E

Area F

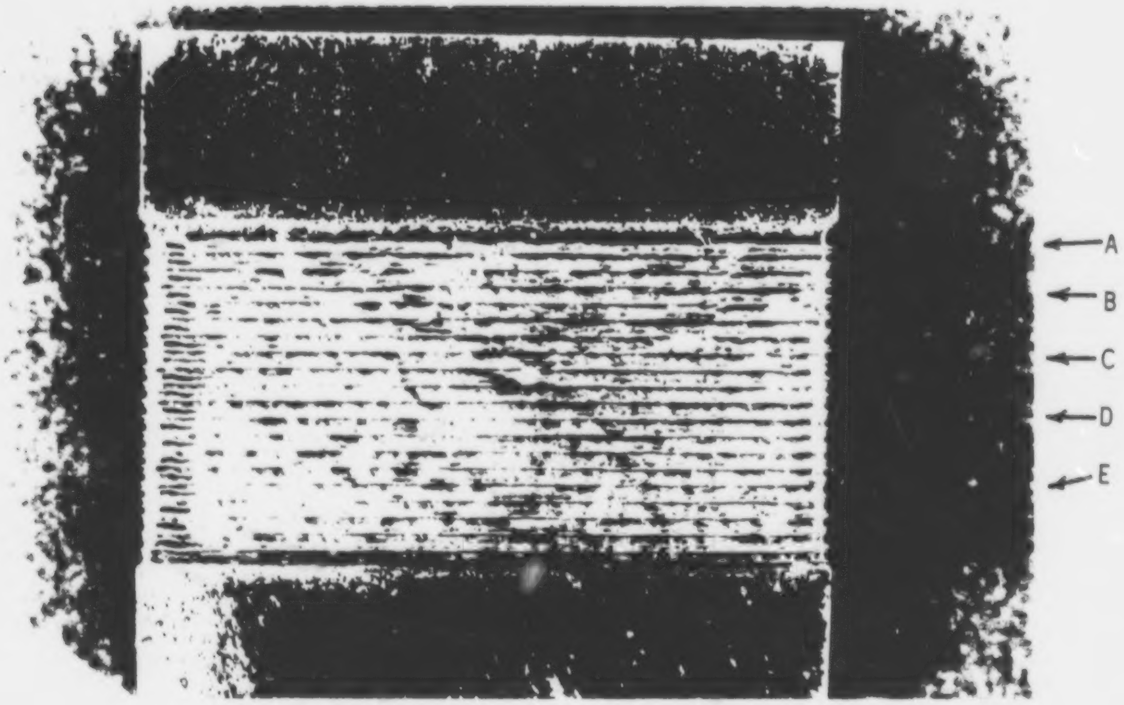

Figure 24: View of iron coated binary alloy coupon 610-1 after laser treatment

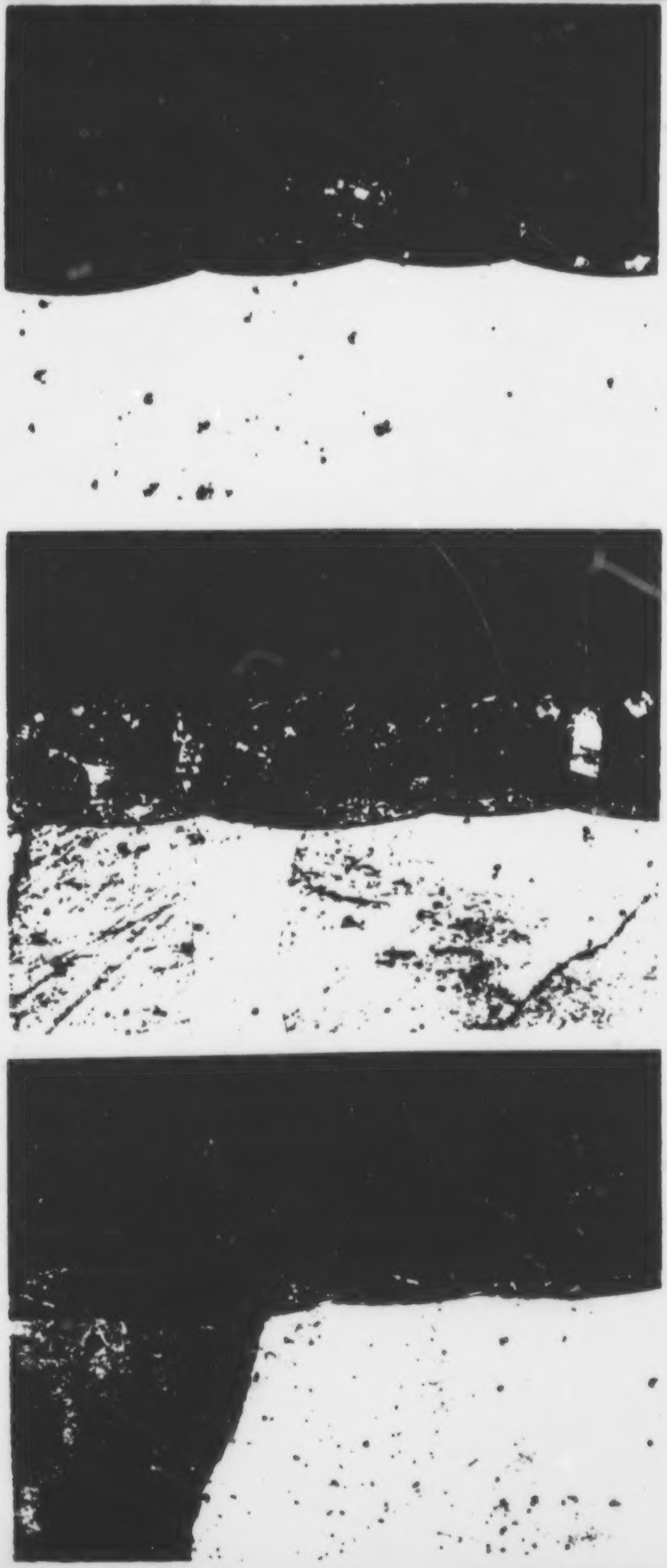

Figure 25: Cross-sectional views of melt areas A, C and E on coupon 610-3 (X100).

Area A

Area C

Area E

APPENDIX B

Laser Treatment of Aluminum Bronzes

Progress Report No. 2
Contract No. 67-10908B

Mr. Troy Lassau
Section Manager
Metals and Corrosion Technologies Section

Submitted by:

Dr. T. Kilp
Laser Applications Section
Industrial Materials Technology Centre

January 5, 1989

ORTECH
INTERNATIONAL
2395 Speakman Drive
Mississauga, Ontario L5K 1B3
(416) 822-4111 (800) 268-5390
Telefax (416) 823-1446

ORTECH Corporation

60 Years of Service to Industry

Terms and conditions on reverse.

TABLE OF CONTENTS

PAGE

1. INTRODUCTION 1

2. EXPERIMENTAL 1

3. RESULTS AND DISCUSSION 2
   3.1 Coupon 610-6
   3.2 Coupon 610-7
   3.3 Coupon 610-8

4. CONCLUSIONS 6

5. FUTURE WORK 6

Laser Treatment of Aluminum Bronzes
Progress Report No. 2

1. INTRODUCTION

In Progress Report No. 1, details of attempts to surface alloy iron into coupons of binary aluminum bronzes were outlined. Results were considered to be unsatisfactory because of the very poor quality of the iron coating on the coupons prior to exposure to the laser.

As a result, the methodology of the application of the iron coating was altered. Electrodeposition, as opposed to the previous vapour deposition techniques was used. This progress report outlines the results of initial attempts to alloy iron into the coupons.

2. EXPERIMENTAL

Three (3) binary aluminum bronze coupons having a thin surface layer, nominally 9 to 10 μ thick, of iron deposited upon them were received from B. Elliott of ORTECH. These were labelled 610-6, 610-7 and 610-8.

As with the work detailed in Progress Report No. 1, laser treatment of the coupons was carried out using a Photon Sources Turbolase T3000 continuous wave (CW) carbon dioxide (CO_2) located at the National Research Council of Canada, Ottawa.

Experimental details were as outlined in Progress Report No. 1, the exception being that the laser was operated at 2200 W for Coupon 610-6 and at 2250 W for the other two coupons. These represent the maximum power available from the laser on the particular day the studies were carried out.

A series of single line scans were carried out on Coupon 610-6 to establish reasonable processing parameters. This coupon was edge machined and polished at NRC for rapid evaluation of treatment depths as a function of process conditions.

Using the results from Coupon 610-6, Coupons 610-7 and 610-8 were laser treated by area scanning. Each of these coupons has two areas. Areas (1) represent treatment by single time coverage consisting of a series of overlapping line scans. Areas (2) represent double surface coverage, carried out to evaluate whether greater substrate homogeneity could be achieved this way.

Exposure conditions are detailed in Tables I and II

3. RESULTS AND DISCUSSION

3.1 Coupon 610-6

A series of single line scans were carried out on this coupon to establish initial optimum process parameters. Only Track #5 consisted of two successive, overlapping scans.

Process details are shown in Table I. It can be seen that the height of the laser beam focal point (HF) above the top surface of the substrate (coupon) was fixed at 12.7 mm throughout. This is larger than the optimum HF values for binary and ternary aluminum bronzes established previously (Progress Report No. 1, August 17, 1988). The larger value for HF here was chosen in anticipation of the much higher percent absorption of the laser beam by the iron coatings.

Again from Table I, the general trend in processing parameters on Coupon 610-6 is a reduction in the traverse rate. As seen, this yields a correspondingly greater coupon treatment depth, from about 30 µ in Track #1 to about 320 µ in Track #6.

Figure #1 shows the surface features of each of Tracks #1 to #6 on Coupon 610-6. Again, not unexpectedly, the trend is towards wider tracks (Effective Size in Table I) as processing rates decrease.

Figure 1 also shows some highly unusual features. In Progress Report No. 1 (August 17, 1988), typical laser tracks on binary and ternary aluminum bronzes were seen to consist of a series of clearly defined overlapping circular swirls. These are absent in the tracks shown in Figure 1 for Coupon 610-6. Rather, the surfaces of the tracks appear to consist of a series of long, needle-like crystals. It is beyond the expertise of the writer to assess the metallurgical significance of this feature.

Figure 2 shows cross-sectional details of each of Tracks #1 to #6 on Coupon 610-6. For Tracks #1 to #3, optical microscopy shows only the expected deepening and broadening of the laser track as processing rates decrease.

For Tracks #4, 5 and 6, the cross-sections begin to show the development of a considerable amount of inhomogeneity in the subsurface structure.

Dark surface patches and subsurface modules begin to be highly noticeable. Figure 3 shows an SEM micrograph of a swirl located on Track #5 of Coupon 610-6 (to the left of the photograph of Track #5 in Figure 2).

As seen more clearly in Figure 3, the swirl appears to be a porous, almost cellular structure extending down about 100 µm from the surface. Very small pits are also noticeable in the bulk metal surrounding the swirl. SEM/EDXA analysis of Areas A, B and C as indicated in Figure 3 yield 4%, 0.4% and 0% of iron, respectively (Table III).

The origin of these swirls is not understood at this time. The porous structure suggests volatilization, possibly of organic contaminants trapped in the interface between the binary aluminum bronze substrate at the iron coating. It could also represent localized non-homogeneities in the iron coating which absorb the laser beam more efficiently than the bulk coating. This increased absorbance could lead to higher localized temperature and hence some volatilization of the iron itself.

3.2 Coupon 610-7

Exposure conditions for Coupon 610-7 are listed in Table II. Area (1) represents single coverage using a series of overlapping line scans. Approximately 50% overlap (see Figures 5 and 6) was achieved between successive line scans.

Area (2) represents surface treatment using identical conditions as for Area (1) but this portion of the coupon was covered twice. The second scan represented an attempt to achieve a higher degree of homogeneity in the treated layer.

Figure 4 shows surface photographs of Areas (1) and (2) on Coupon 610-7. Again, the crystalline features already noted for Coupon 610-6 above are seen. The individual laser scans in Area (2) which was doubly treated are, as expected, much less clearly distinguished than those in Area (1).

Figures 5 and 6 represent cross-sectional details of Areas (1) and (2), respectively on Coupon 610-7. Non-homogeneities in the laser treated surface areas are again clearly noticeable. These are, however, slightly decreased in the doubly scanned area (Figure 6) as compared to the singly scanned area (Figure 5).

Table III lists SEM/EDXA analysis for iron in the locations as indicated in Figure 5 and 6. As suspected, the darker features in these figures are slightly higher in iron content than are the lighter areas.

It is noted that iron levels ranged from a maximum of about 9 to 12% (w/w) to about 0% (w/w) at approximately one half the laser affected depth. In consideration of the original state of the iron (as a thin layer of 100% (w/w) of the element on the outer surface of the coupon), these values clearly indicate a considerable degree of homogenization has been obtained. It is expected that changes in the process parameters could achieve virtually complete homogenization of the iron into the substrate.

3.3 Coupon 610-8

This coupon was treated identically to Coupon 610-7 except that a slightly higher traverse rate of 52.9 mm/s (Table II) was used. Figure 7 shows surface details very similar to those already discussed for Coupons 610-6 and 610-7.

Figure 8 illustrates the cross-sectional details of Coupon 610-8 in the single laser coverage area. Identical features as already seen in Coupon 610-7 are noted. Table III lists SEM/EDXA analytical results for iron levels in the sites marked in Figure 8.

4. CONCLUSION

Based upon the above, the following conclusions can be drawn:

- Electrodeposition of the iron coating on the coupons is highly preferable to the previously used (Progress Report No. 1) vapour deposition techniques.
- in view of the initial condition of a 100% (w/w) iron coating on the binary aluminum bronze alloy coupons, a considerable degree of homogenization was achieved by laser scanning
- complete, or nearly complete homogenization of the iron should be achievable by changes in processing parameters.

5. FUTURE WORK

An additional set of iron-coated, binary alloy coupons have been received from B. Elliott of ORTECH International. These will be treated at NRC using process changes as suggested by the results outlined above. It is expected that success will be most likely achieved by:

- using an initial surface scan at low power densities and high traverse rates to achieve a preliminary mixing of the iron into a shallow surface layer of the coupons
- using a subsequent surface scan at much higher power densities and low traverse rates to achieve homogenization of the iron throughout the treated surface layer.

It is noted that at the time of this writing, the laser at NRC is non-functional. The next series of exposures will be carried out as soon as possible following regaining of a functional status for the laser.

M. Hoffbauer
M. M. Hoffbauer
Project Scientist

T. Kilp
T. Kilp, Ph.D.
Section Manager

TABLE I

EXPOSURE CONDITIONS FOR COUPON 610-6

Exposure Number	Rate (mm/s)	HF* (mm)	Spot Size (mm)	Effective Size (mm)	Dwell Time(ms)	Treatment Depth(μm)
1	84.6	12.7	0.86	--	--	30
2	84.6	12.7	0.86	0.65	7.7	70
3	63.5	12.7	0.86	0.90	14.1	70
4	42.3	12.7	0.86	1.02	24.1	200
5**	42.3	12.7	0.86	1.30	24.1	300
6	31.8	12.7	0.86	1.21	38.1	320

* Height of beam focal point above top surface of coupon

** Track covered by two successive scans

TABLE II

EXPOSURE CONDITIONS FOR COUPON 610-7 AND 610-8

Exposure Number	Rate (mm/s)	HF* (mm)	Spot Size (mm)	Effective Size (mm)	Dwell Time(ms)	Treatment Depth(μm)
610-7(1)**	42.3	12.7	0.86	1.02	24.1	240-420μ***
610-7(2)**	42.3	12.7	0.86	1.02	24.1	300-430μ
610-8(1)**	52.9	12.7	0.86	--	--	100-400μ
610-8(2)**	52.9	12.7	0.86	--	--	300-400μ

* Height of beam focal point above top surface of coupons

** Numbers in brackets represent areas on coupon; Areas (1) were scanned once using 0.64 mm jog between successive line scans resulting in about 50% overlap; Areas (2) same as Areas (1) but areas was scanned twice.

*** From start of Area scan to end of Area scan

TABLE III

PERCENT IRON FROM SEM-EDXA ANALYSIS

Coupon	Area	Site in* Area	Percent Iron
610-6	6	A	4
		B	0.4
		C	0
610-7	1	A	9
		B	5
		C	1
		D	0
		E	0
610-7	2	A	8
		B	12
		C	1
		D	0
		E	3
		F	4
610-8	1	A	3
		B	9
		C	0
		D	5

* See Figures 3, 5, 6 and 8 for precise locations taken for EDXA analysis

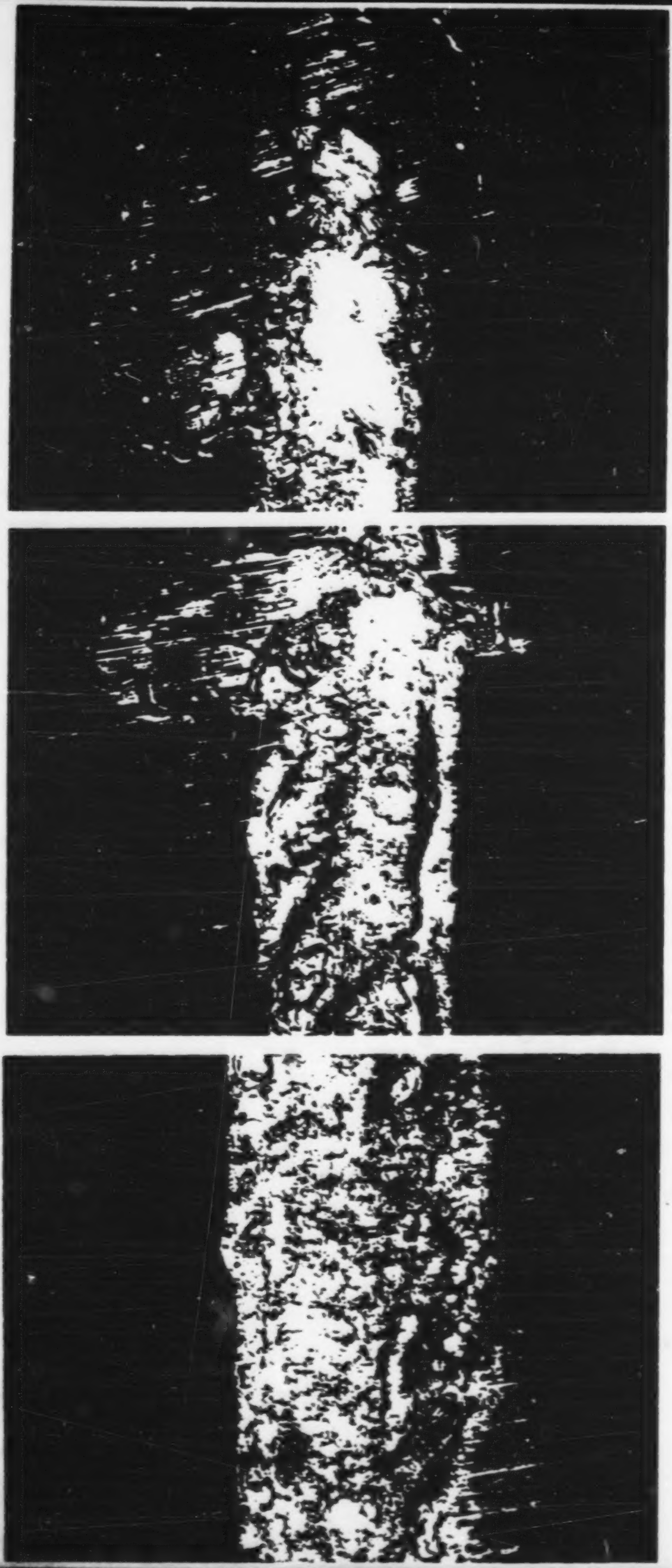

Figure 1
Coupon 610-6
Surface Views

Track #1 (X54)

Track #2 (X54)

Track #3 (X54)

Figure 1 (cont'd)

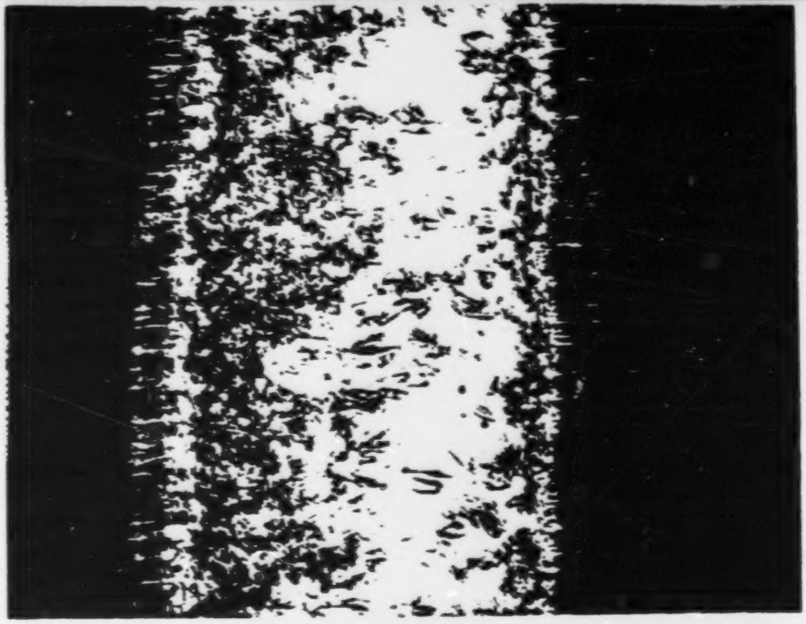

Track #4 (X54)

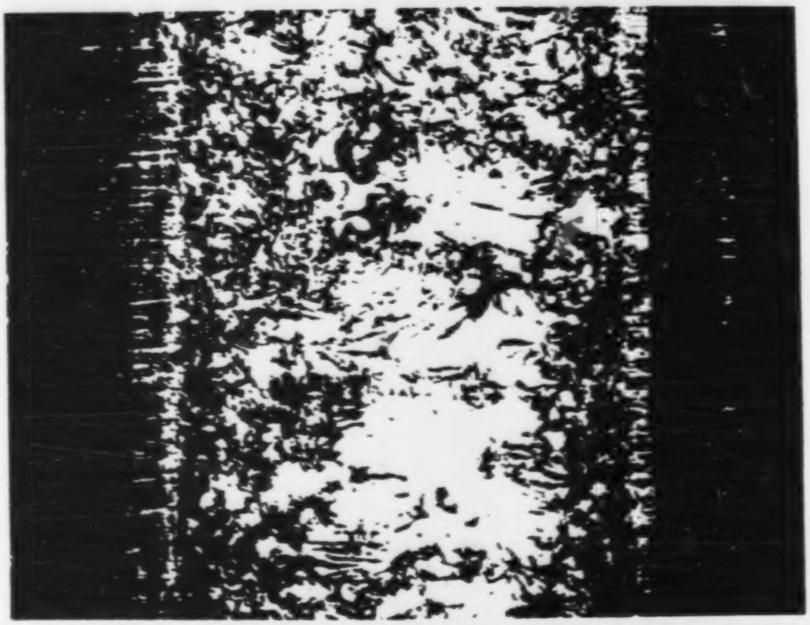

Track #5 (X54)

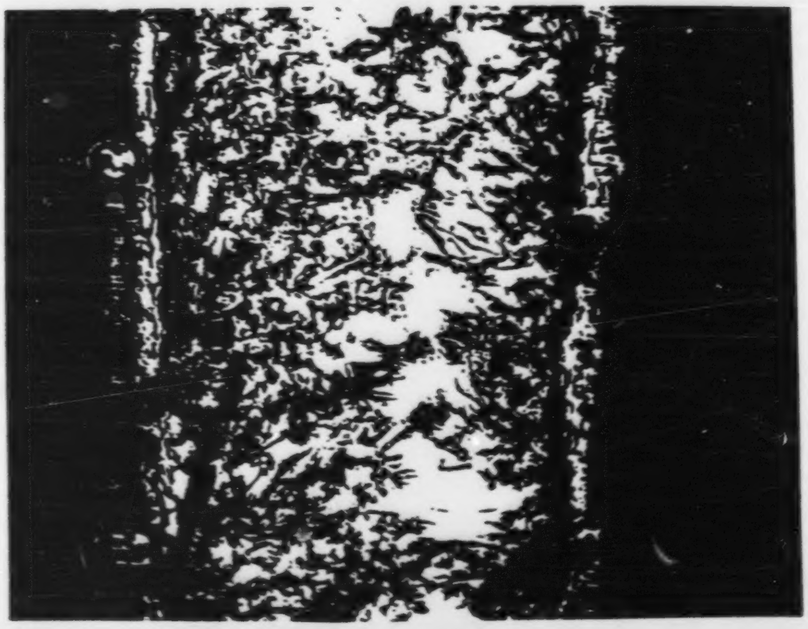

Track #6 (X54)

Figure 2
Coupon 610-6
Cross-sections

Track #1 (X100)

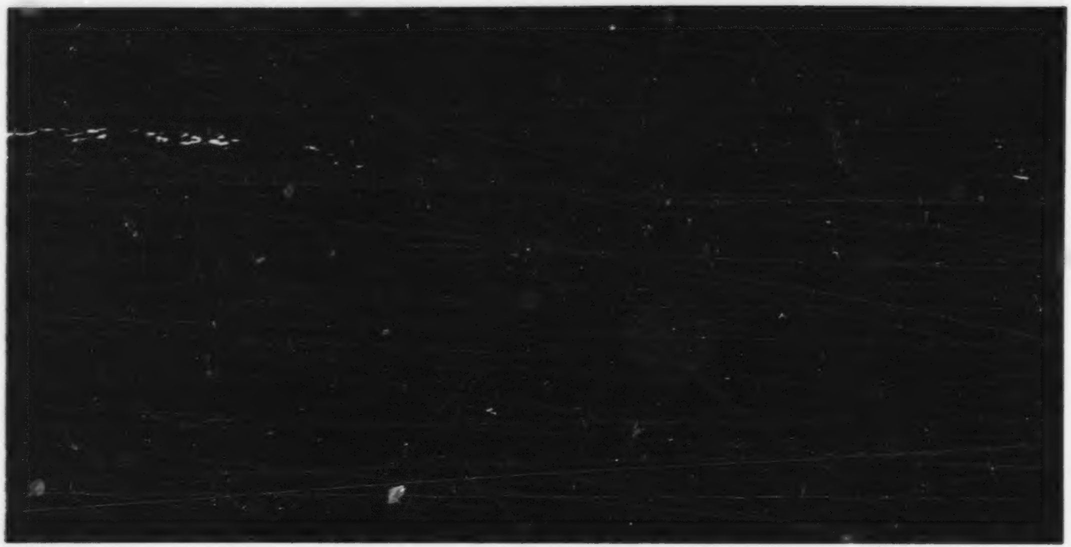

Track #2 (X100)

Track #3 (X100)

Figure 2 (Cont'd)

Track #4 (X100)

Track #5 (X100)

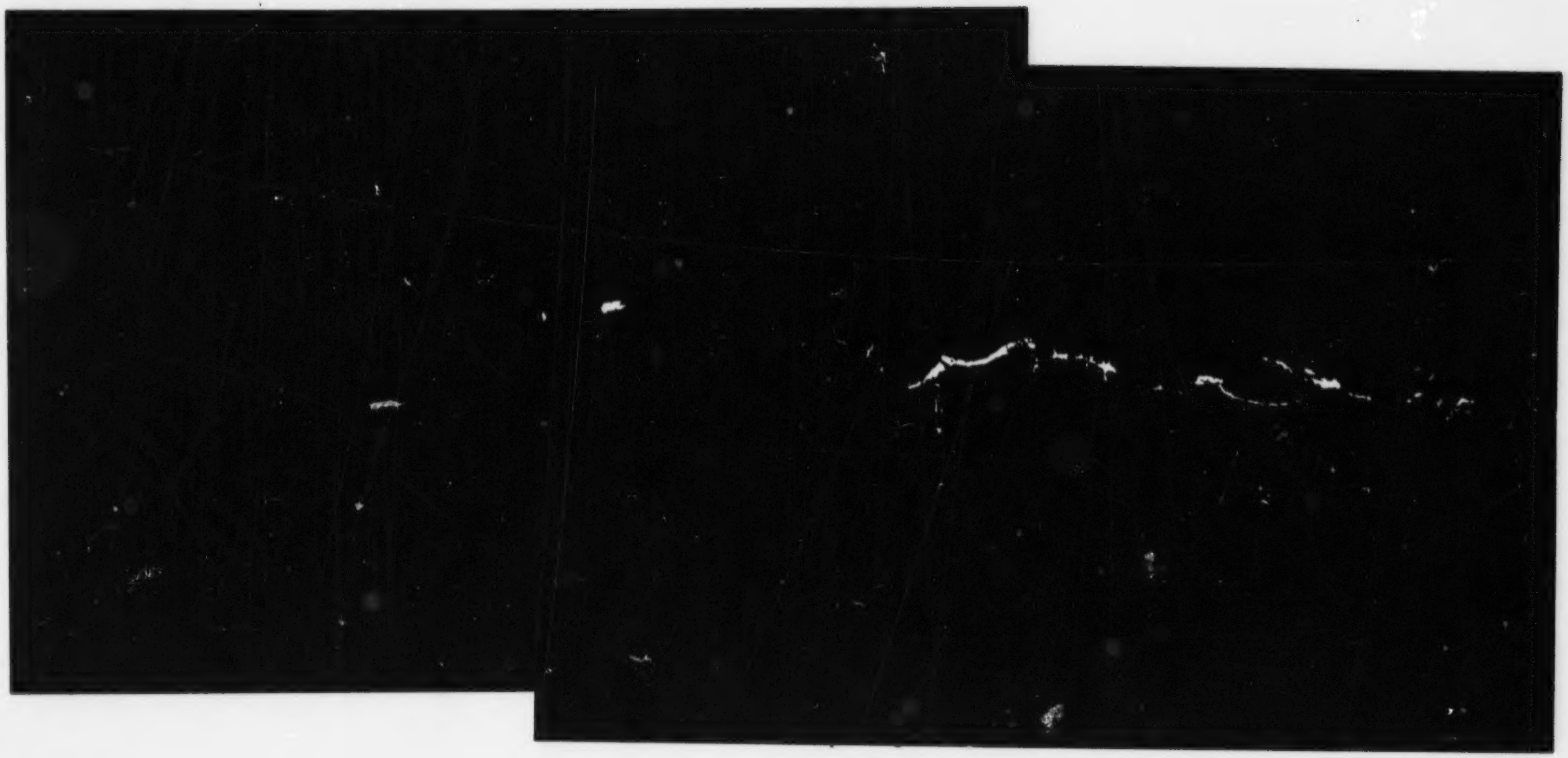

Figure 2 (Cont'd)

Track #6 (X100)

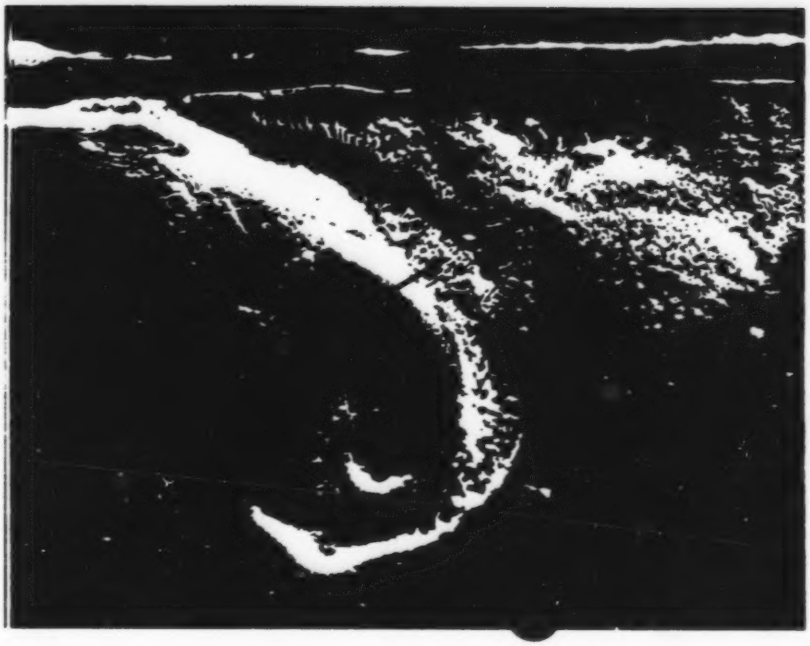

Figure 3; SEM micrograph of swirl in Track #5 of Coupon 610-6

Figure 4
Coupon 610-7
Surface Views

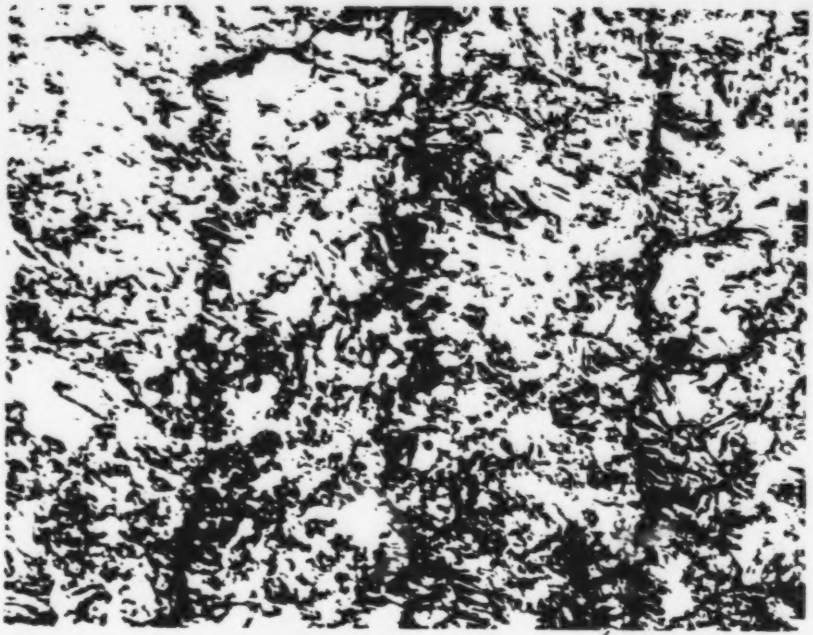

610-7 Area (1)

Area (1) X54

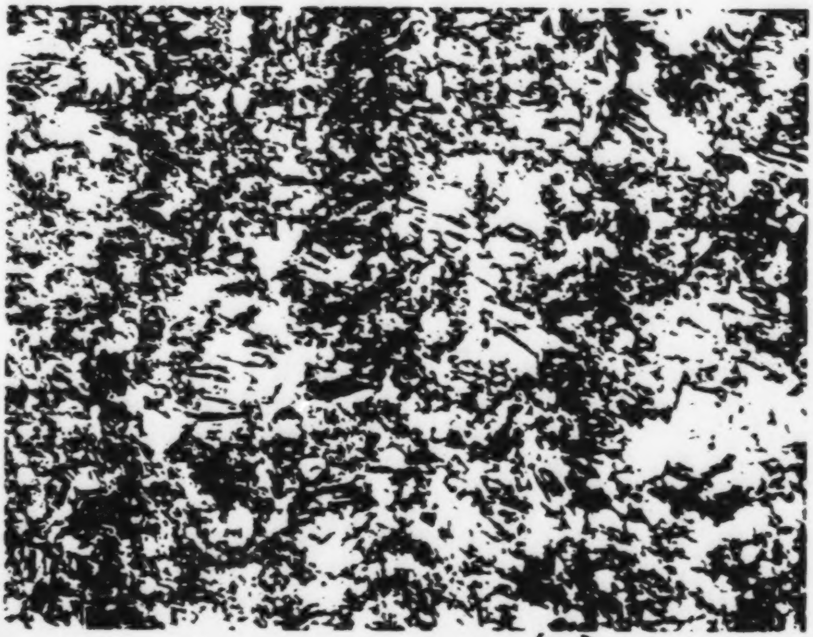

61C-7 Area (2)

Area (2) X54

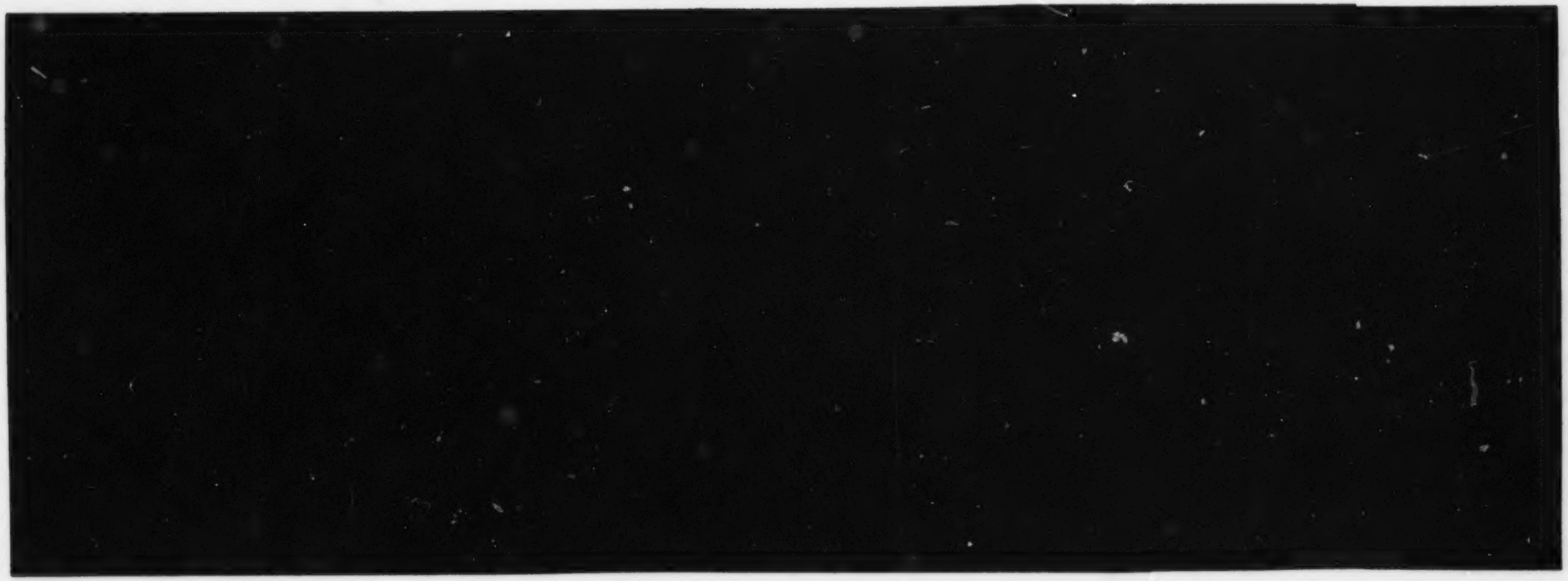

Figure 5; Cross-sectional view of
Coupon 610-7, singly
scanned Area (1), X100

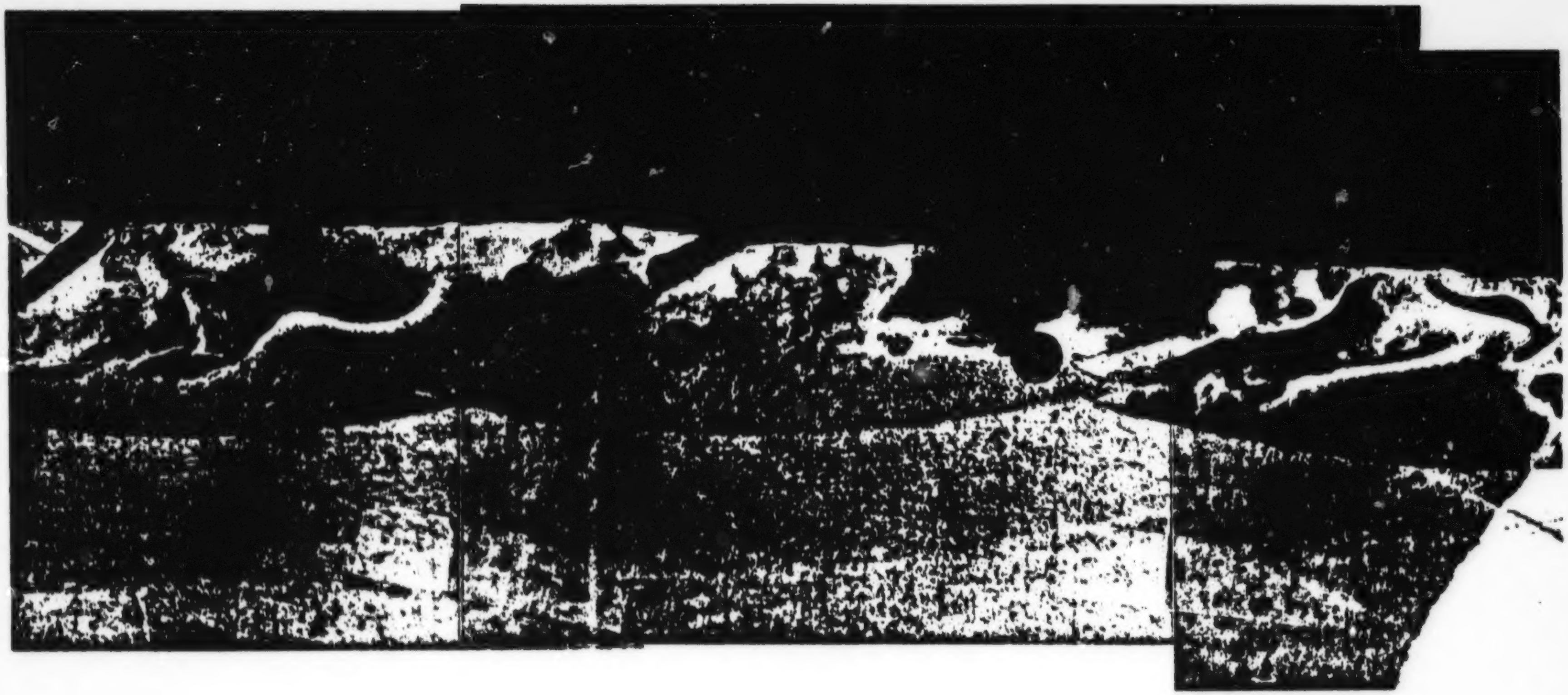

Figure 6: Cross-sectional view of Coupon 610-7, doubly scanned Area (2), X100

Figure 7
Coupon 610-8
Surface Views

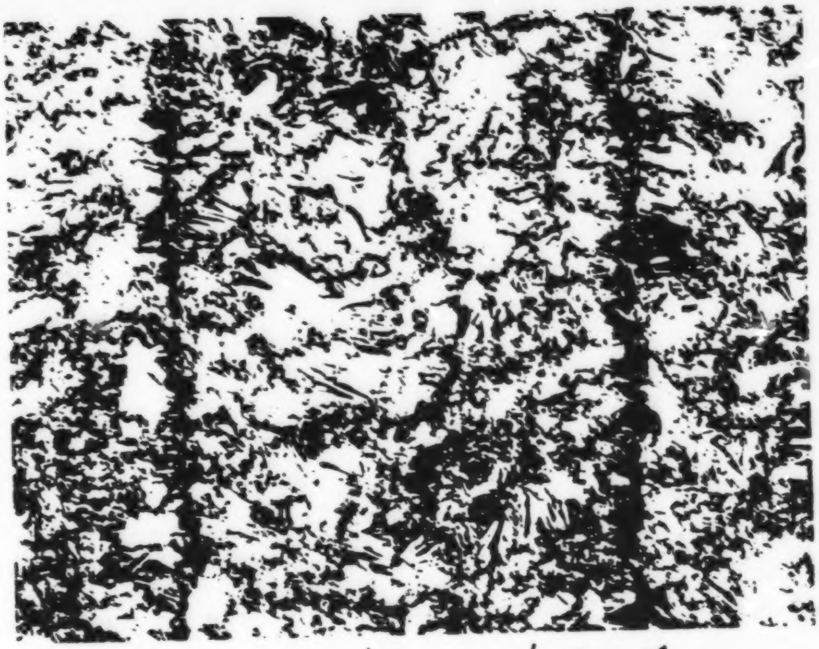

610-8 Area 1

Area (1) X54

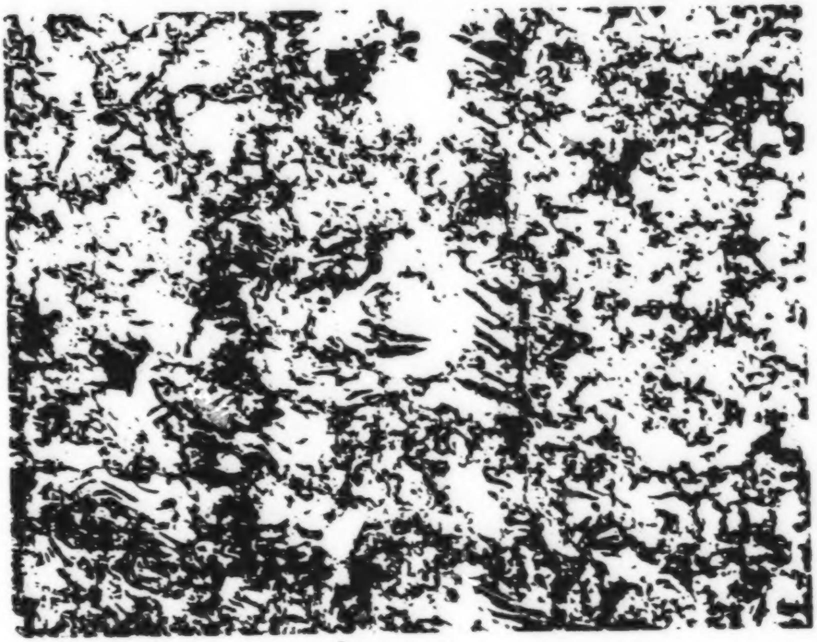

610-8 Area -

Area (2) X54

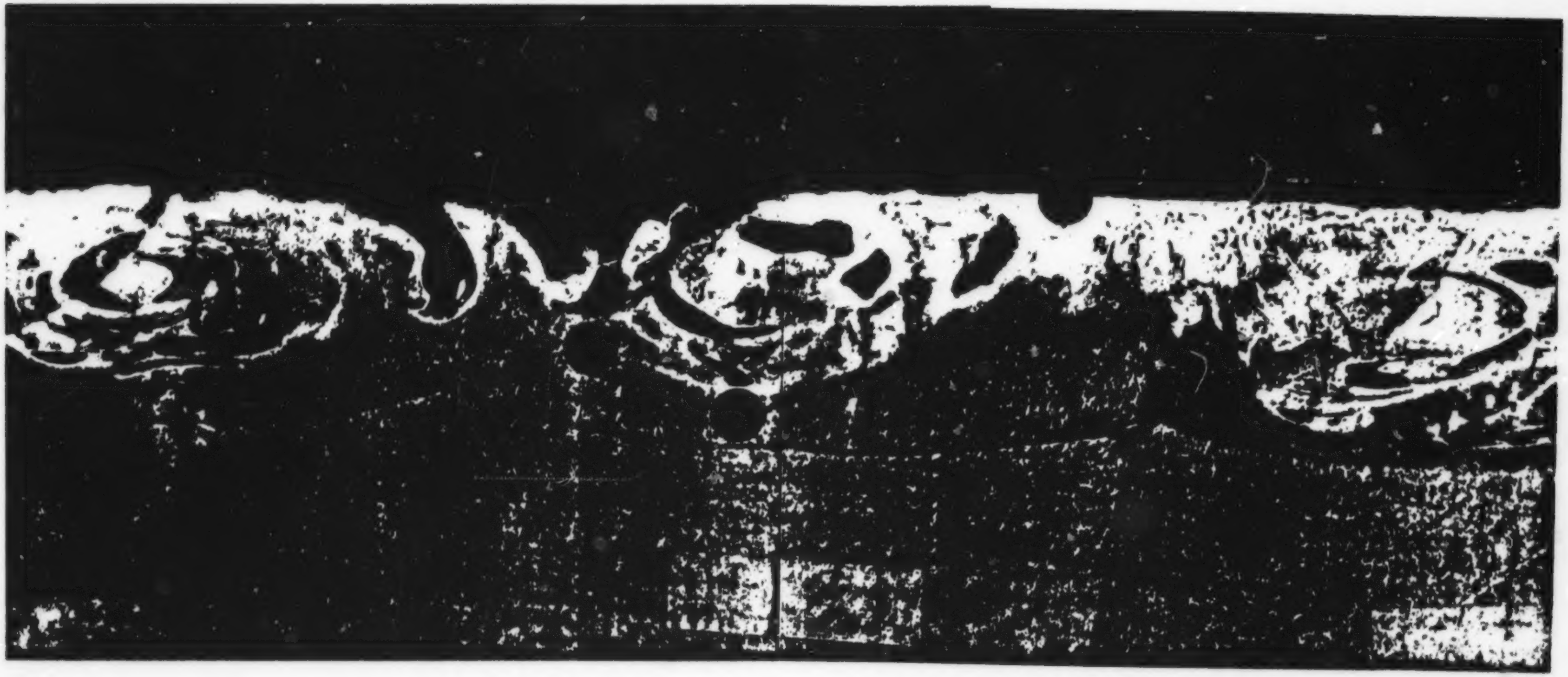

Figure 8; Cross-sectional view of Coupon 610-8, singly scanned Area (1), X100

APPENDIX C

Laser Treatment of Aluminum Bronzes

Progress Report No. 3
Contract No. 67-10908B

Mr. Troy Lassau
Section Manager
Metals and Corrosion Technologies Section

Submitted by:

Dr. T. Kilp
Laser Applications Section
Industrial Materials Technology Centre

April 4, 1989

ORTECH
INTERNATIONAL
2395 Speakman Drive
Mississauga, Ontario L5K 1B3
(416) 822-4111 (800) 268-5390
Telefax (416) 823-1446

ORTECH Corporation

60 Years of Service to Industry

Terms and conditions on reverse.

TABLE OF CONTENTS PAGE

1. INTRODUCTION 1

2. EXPERIMENTAL 1

3. RESULTS 1

4. CONCLUSIONS 5

1. INTRODUCTION

In Progress Report No. 2 (January 5, 1989), details of laser alloying of electrochemically deposited, as opposed to vapour deposited, iron films into binary aluminum bronze substrates were given. The results indicated that while alloying did occur, the distribution of the iron through the melt zone was highly non-uniform. The current report outlines changes in laser processing parameters which have been made in an attempt to produce thin surface layers having relatively uniform distributions of iron.

2. EXPERIMENTAL

As with the studies outlined in previous progress reports, laser treatment of the coupons was carried out using a Photon Sources Turbolase T3000 continuous wave carbon dioxide laser located at the National Research Council of Canada in Ottawa. The laser was operated at 2350 watts total output power, the maximum available from the unit on the particular day processing was carried out.

All other experimental details were as outlined in previous progress reports. The processing conditions used for each coupon here are outlined in Table I.

3. RESULTS

Previous attempts to alloy iron into the coupons had resulted in highly non-uniform distributions of the element throughout the melt zone. Processing methodology changes were clearly required.

For the current samples, alloying was accomplished by the use of an initial area scan using high (63.5 mm/s to 84.6 mm/s) beam traverse rates. It was hoped that this would result in a pre-alloying of the iron into a very shallow surface layer. Subsequent scans, using much lower beam traverse rates and/or reduced heights of beam focal point above the coupon surfaces to increase energy densities (see Progress Report No. 1) were then used to further homegenize the melt layer and to drive the iron deeper into the coupons. Coupon processing details are listed in Table I.

Figure 1 illustrates the surface view of Coupon 610-11 in Area 1. The latter was only rapidly scanned (84.6 mm/s) to achieve pre-alloying of the iron. The melt tracks are narrow and irregular as expected. There are small regions of intact iron coating between successive scan melt tracks.

Figure 2 depicts the surface of Area 3 on Coupon 610-11. In addition to the light pre-alloying scan, a subsequent scan at 12.7 mm/s was used here.

Relatively clean, well defined melt tracks are now seen having the classical overlapping swirls. It will be recalled (Progress Report No. 2) that the swirls were not seen in previous alloying attempts. Their presence is indicative of good turbulence in the melt puddle which is essential to effective dispersal of the iron.

In Figure 2, the dark material edging the melt tracks is most likely comprised of various oxides. These features are more clearly seen in Figure 3, an SEM micrograph of Area 3 on Coupon 610-11. Figure 4, a back scattered electron image of the same area as in Figure 3 shows the edges of the melt tracks as containing lighter (hence darker in the image) elements as compared to the metals in the alloy itself. Hence, oxides are the most probable explanation.

Figure 5 is again a backscattered electron image taken in a region close to an edge of the coupon. Slight undulations which, as expected, deepen as the edge is approached are clearly visible.

Figure 6 is a cross-sectional view of Area 1 in Coupon 610-11. The rapid processing rate used can be seen to have generated a melt depth of only about 70 μm to 80 μm.

Figures 7, 8 and 9 are cross-sectional views of the melt zone in Area 3 of Coupon 610-11. This area received a slower, more intense scanning in addition to the light pre-alloying (Table I). Various metallurgical features are noted, the interpretation of which are beyond the expertise of the present author. The dark undulating feature in Figure 7 is a microcrack formed along the boundaries of the rather large grains in the binary alloy. These cracks are opened up during the initial rapid pre-alloying scan but then, as seen in Figure 7, are resealed on the slower second scan.

Figures 10 to 24 are cross-sectional views of the remaining areas on Coupons 610-11, 610-12 and 610-13. Processing conditions resulting in the observable features are listed in Table I. The wide variety of metallurgical structures shown require evaluation by a qualified metallurgist.

In general, the cross-sectional views seen in the Figures indicate melt zones that are much more uniform in appearance than were achieved previously (Progress Report No. 2). It is noted, however, that none of the photographs provide unambiguous evidence for the presence of an amorphous RST layer on the outer surface of the melt zone. This suggests that following alloying an additional high speed scan might be required to generate an RST layer.

Evaluation of the uniformity of iron distribution in the melt zones was carried out using SEM/EDXA. Results are listed in Table II.

Figure 25 is a cross-sectional SEM view of Area 1 (only lightly treated for pre-alloying) on Coupon 610-11. Figure 26 shows an elemental line scan for iron across this area. It can be seen that the bulk of the iron is located at the surface (7.83%, Table II) and decreases to background within 10-15 μm towards the sample interior.

Figure 27 shows the line scan for iron in Area 2 of Coupon 610-11. This area was processed at 8.5 mm/s (Table I) in addition to the rapid 84.6 mm/s pre-alloying scan. Iron is now seen to be at about an 8% level near the surface (Table II) and decreasing smoothly to background over a distance of about 40 μm into the sample interior.

Figure 28 illustrates the iron line scan for Area 3 on Coupon 610-11. The line scan is not believed to indicate a highly uniform level of iron as Table II indicates only low amounts of this element are present. The Figure is only included here as it illustrates some interesting metallurgical features.

Figure 29 shows an SEM view of the cross-section of Area 2 on Coupon 610-12 and Figure 30, the corresponding iron elemental line scan. The latter indicates a remarkably uniform distribution of iron has been achieved. This is supported by the point analysis data listed in Table II. Iron levels are consistently between 4% and 6% to a depth of over 135 μm.

Figures 31 and 32 are backscattered electron images of Area 2, Coupon 160-12 and Area 2, Coupon 610-13, respectively. They are included here only for the interesting features which are observable.

4. CONCLUSIONS

The foregoing and in particular, the data listed in Table II indicates very successfully alloying was achieved in Coupon 610-12. Treatment here consisted of two high traverse rate pre-alloying area scans followed by a third slow traverse rate fully alloying area scan. The resultant iron levels are found to be quite consistent at between 4% and 6% to depths of 135 μm.

The use of one rapid -pre-alloying area scan followed by a much lower traverse rate full alloying a scan as was done with Coupon 610-13 resulted in fairly uniform but lower level iron distributions (Table II). The lower levels of iron in this case probably reflect some loss by volatilization on the second scan due to incomplete surface coverage on the first pre-alloying scan (see Figure 1 and discussion above).

It would appear that an appropriate process methodology has now been established. It remains necessary to introduce an RST layer to the alloyed melt zone. This will be accomplished by a fourth scan carried out at very high traverse rates and is the objective of the treatment of the next set of coupons.

M. M. Hoffbauer
Project Scientist

T. Kilp, Ph.D.
Section Manager

TABLE I

Laser Processing Conditions

Coupon	Area	Scan #	HF* (mm)	Rate (mm/s)	Jog/Scan** (mm)
160-11	1	1	12.7	84.6	0.38
	2	1	12.7	84.6	0.38
		2	12.7	8.5	0.38
	3	1	12.7	84.6	0.38
		2	9.5	12.7	0.38
160-12	1	1	12.7	63.5	0.64
		2	12.7	63.5	0.64
		3	9.5	16.9	0.38
	2	1	12.7	63.5	0.64
		2	12.7	52.9	0.64
		3	9.5	16.9	0.38
610-13	1	1	12.7	84.6	0.38
		2	9.5	21.2	0.38
	2	1	12.7	84.6	0.38
		2	9.5	16.9	0.38

* Height of laser beam focal point above top surface of coupon

** Distance laser beam moved between successive line scans

TABLE II

SEM/EDXA Analysis of Coupon Cross-sections

Coupon	Area	Depth (μm)	Weight % Element		
			Cu	Al	Fe
610-11	1	5	86.54	5.63	7.83
		20	97.46	1.25	1.29
		60	98.71	1.29	--
		80	98.76	1.24	--
610-11	2	5	82.73	9.26	8.00
		45	96.58	1.85	1.57
		135	97.72	1.97	0.31
		180	98.86	0.85	0.29
610-11	3	5	95.89	0.97	3.14
		45	98.17	0.94	0.89
		135	97.66	--	--
		180	99.99	--	--
610-12	1	5	92.97	2.65	4.38
		45	94.74	1.15	4.11
		135	94.01	1.38	4.61
		180	93.87	0.71	5.41
		200*	98.61	0.90	0.49
610-12	2	5	92.44	3.55	4.01
		45	92.72	1.26	6.02
		135	93.96	1.03	5.02
		180	97.96	0.94	1.10
610-13	1	5	93.11	4.40	2.49
		45	96.04	0.86	3.10
		135	95.38	1.71	2.91
		180	97.73	1.17	1.10
610-13	2	5	96.34	1.33	2.32
		45	94.98	0.66	4.35
		135	97.32	0.77	1.91
		180	98.54	0.85	0.61

* Measurement taken below laser melt region

Figure 1: Coupon 610-11, Area 1, Surface View, X50

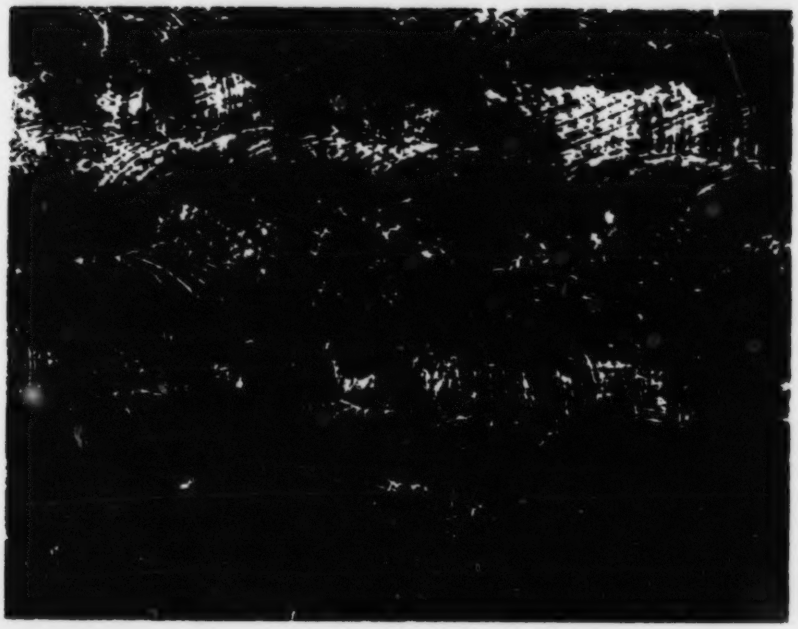

Figure 2: Coupon 610-11, Area 3, Surface View, X50

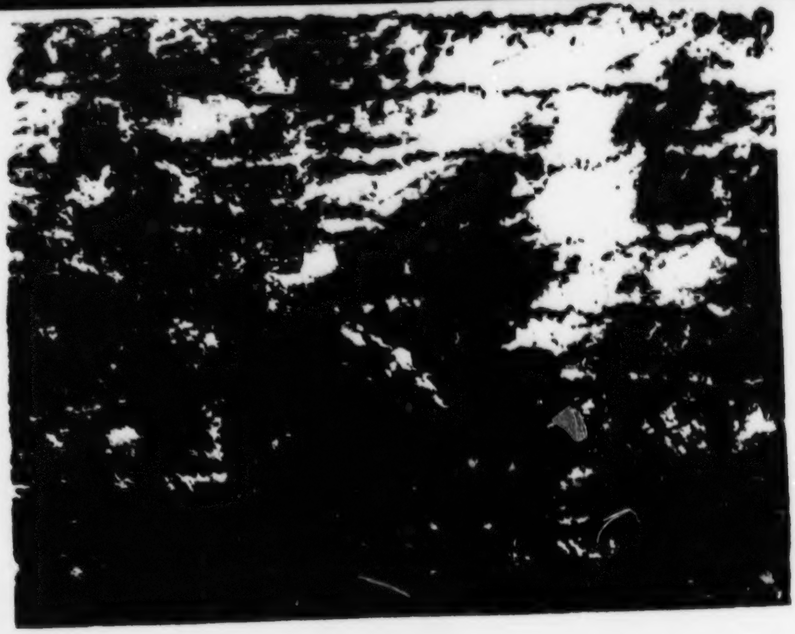

Figure 3: Coupon 610-11, Area 3,
SEM Surface View

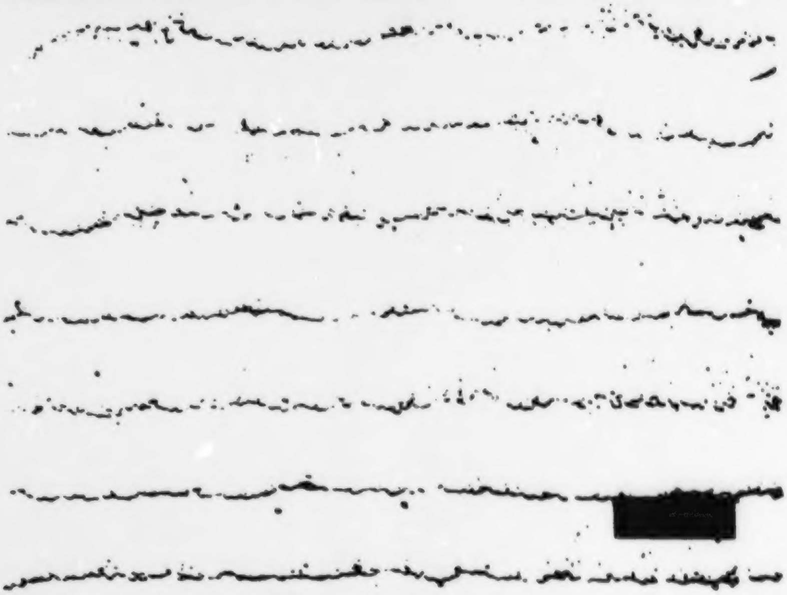

Figure 4: Coupon 610-11, Area 3,
SEM Surface View,
BSE mode

Figure 5: Coupon 610-11, Area 3,
SEM Surface View,
BSE Mode, Near Edge

Figure 6: Coupon 610-11, Area 1, Cross-section, X400

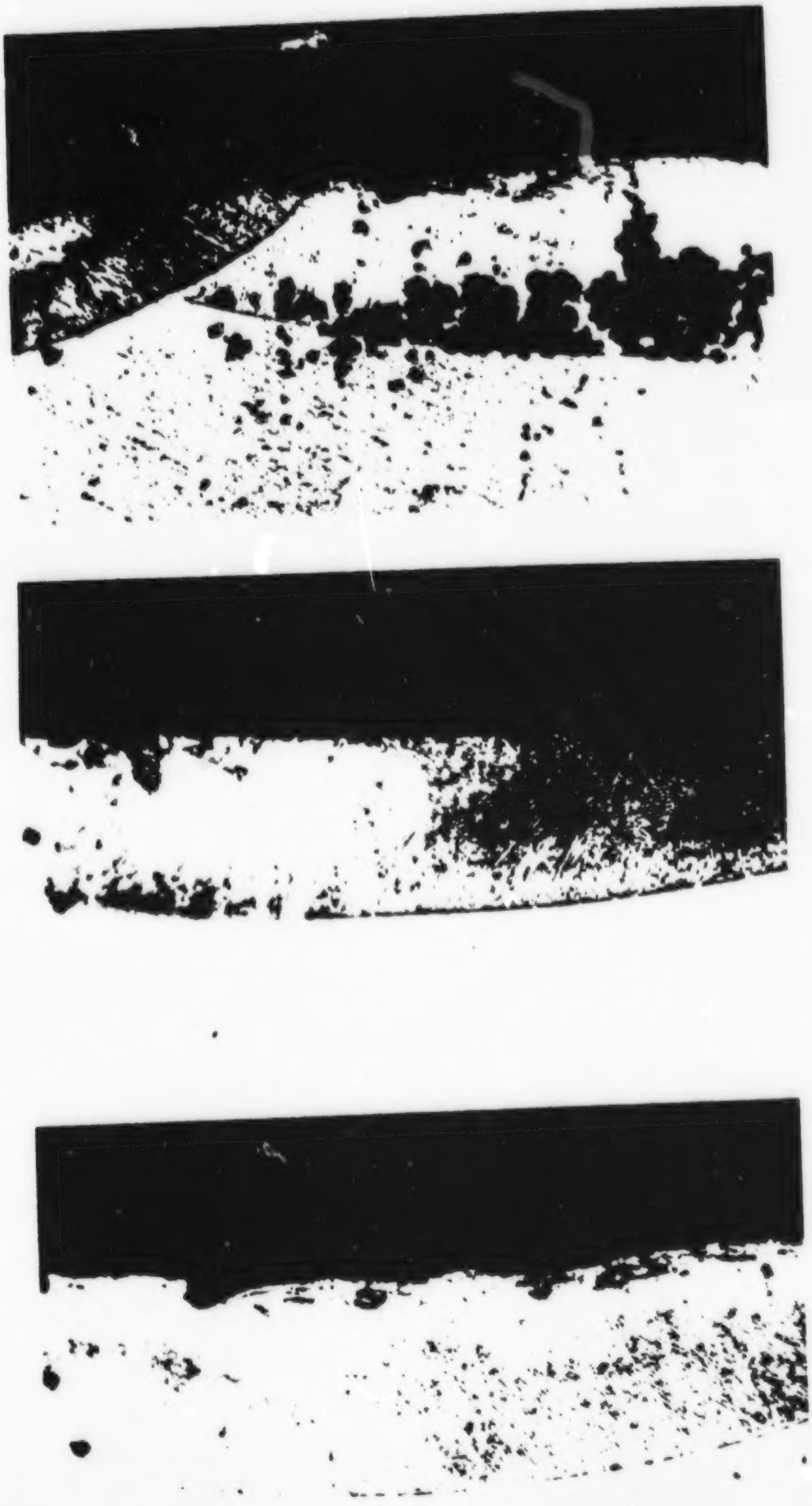

Start

Middle

End

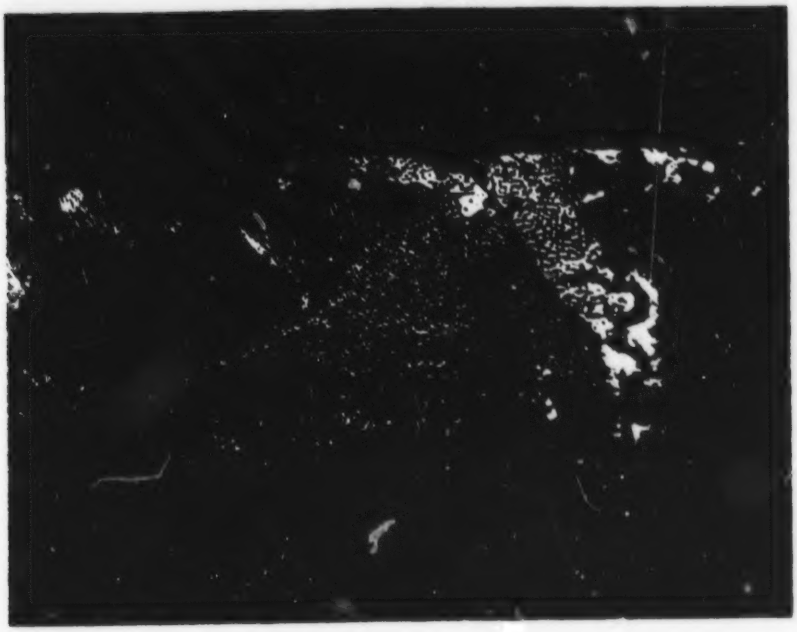

Figure 7: Coupon 610-11, Area 3 (middle), X200

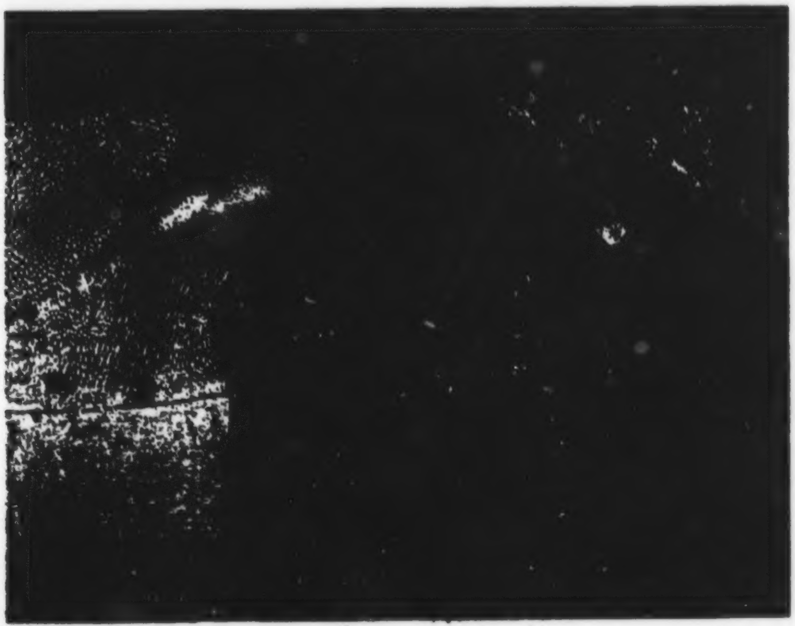

Figure 8: Coupon 610-11, Area 3 (end), X200

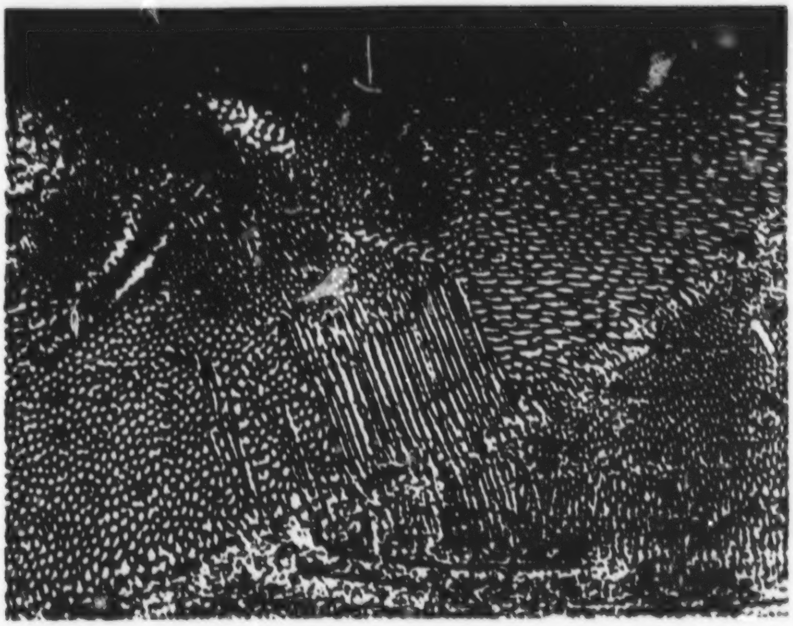

Figure 9: Coupon 610-11, Area 3 (middle), X400

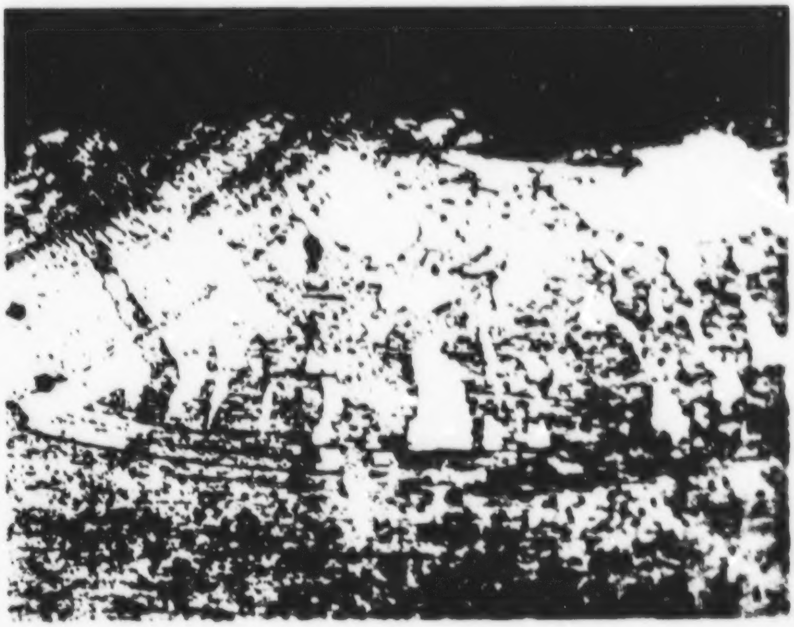

Figure 10: Coupon 610-11, Area 2 (start), X400

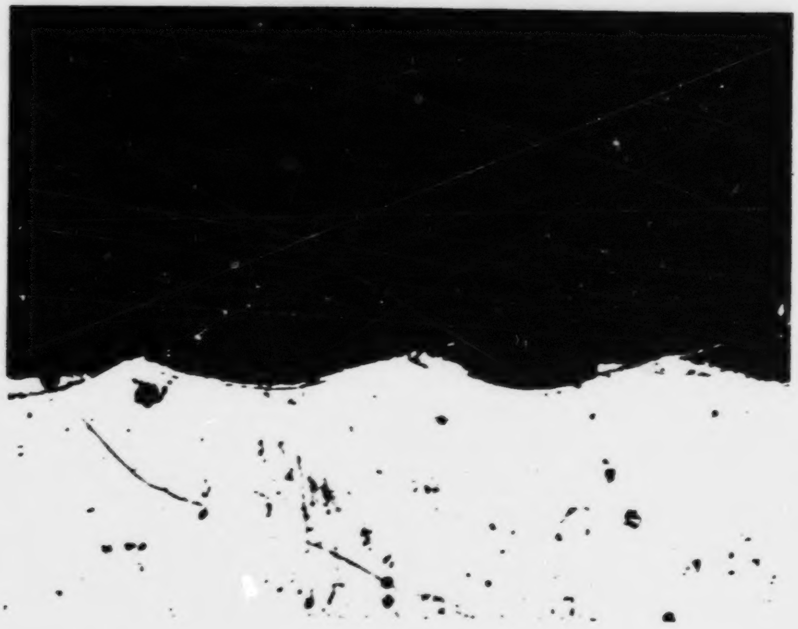

Figure 11: Coupon 610-12, Area 1 (start), X100

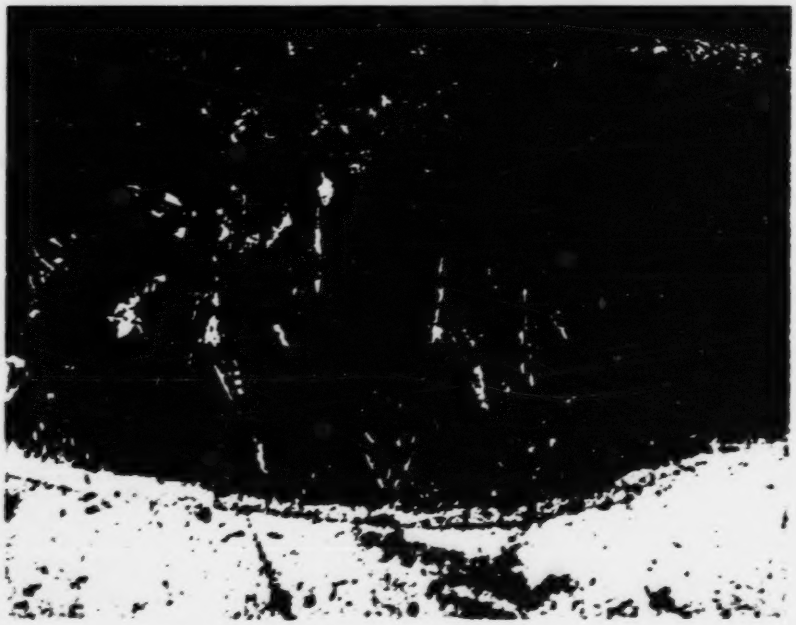

Figure 12: Coupon 610-12, Area I (start), X400

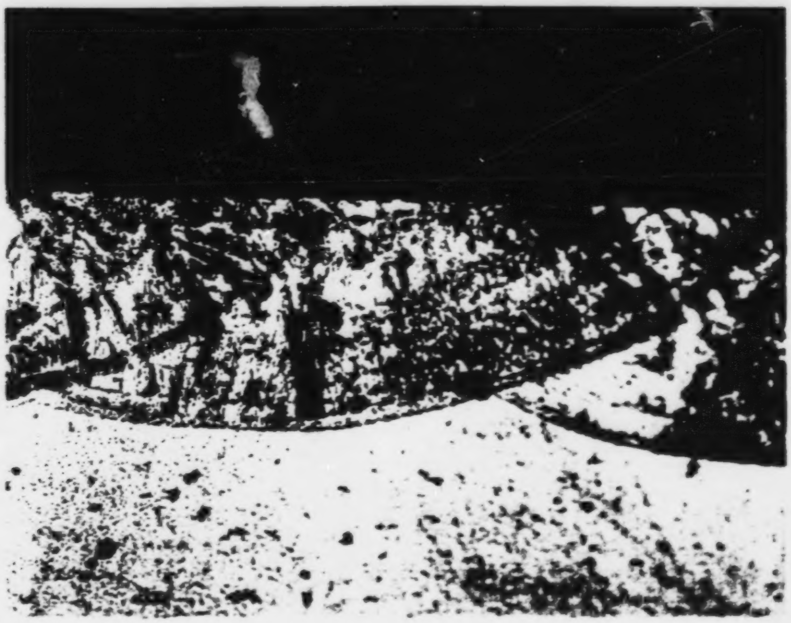

Figure 13: Coupon 610-12, Area 2 (middle), X200

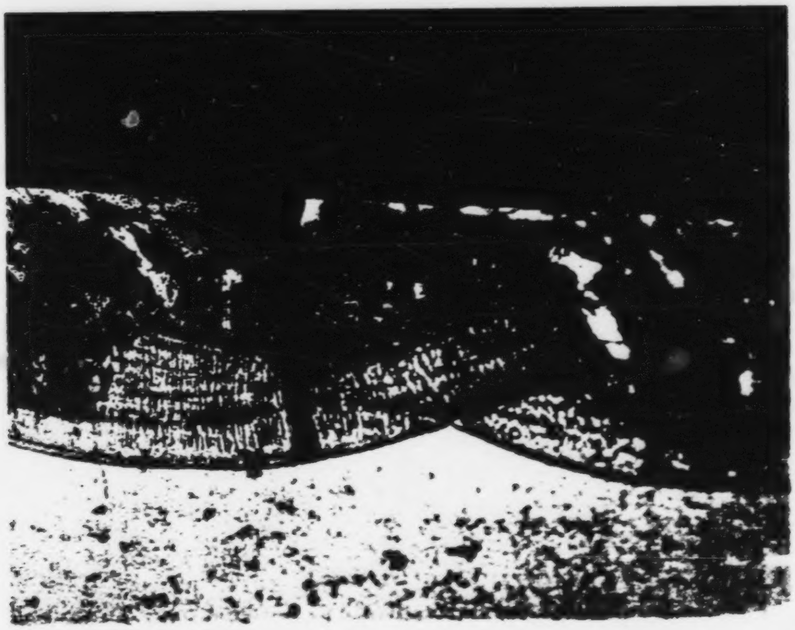

Figure 14: Coupon 610-12, Area 2 (end), X200

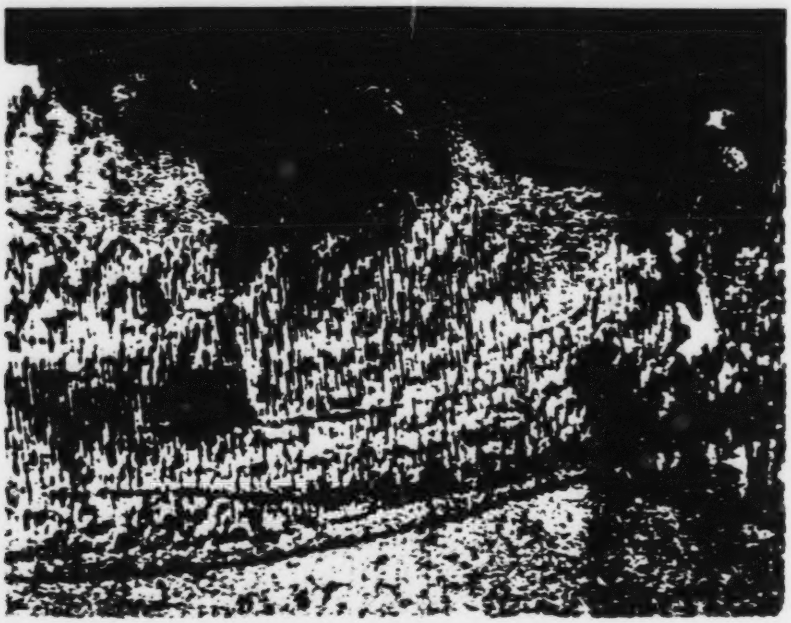

Figure 15: Coupon 610-12, Area 2 (middle), X400

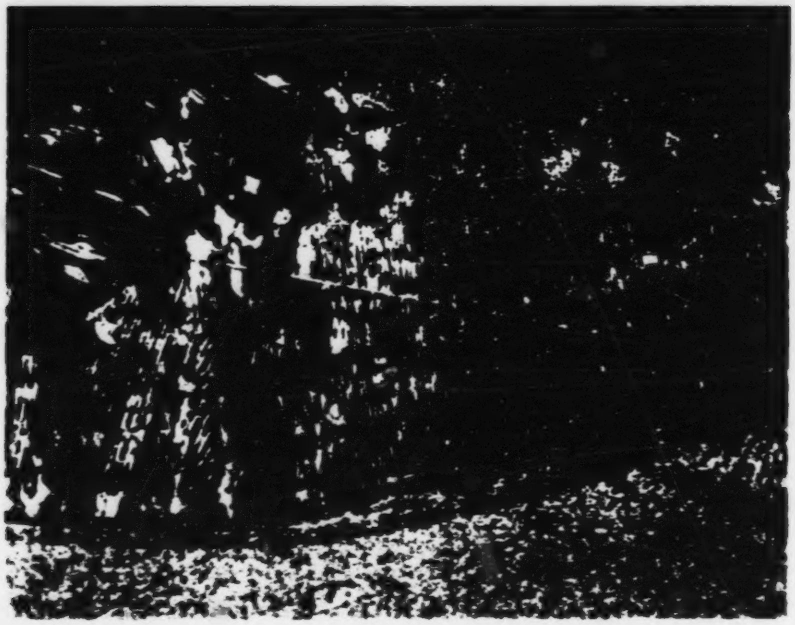

Figure 16: Coupon 610-12, Area 2 (middle), X400

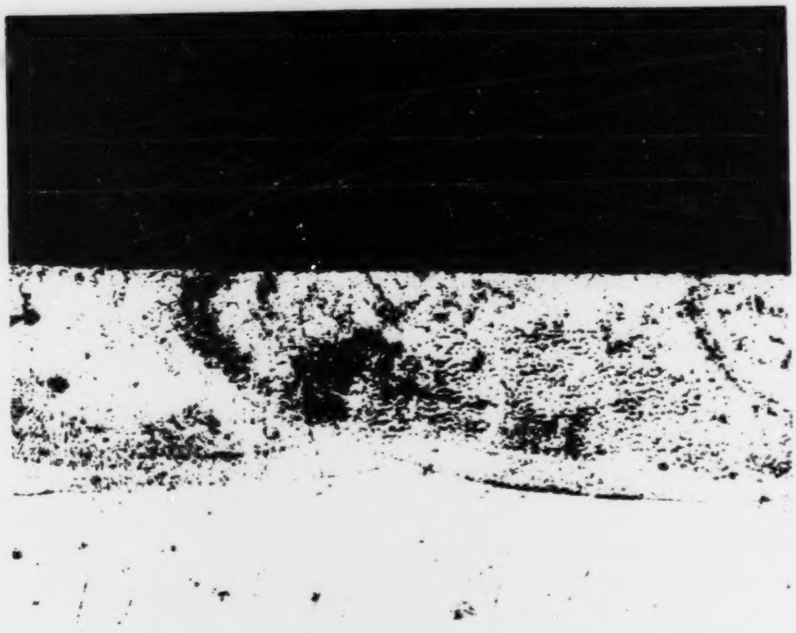

Figure 17: Coupon 610-13, Area 1 (start), X200

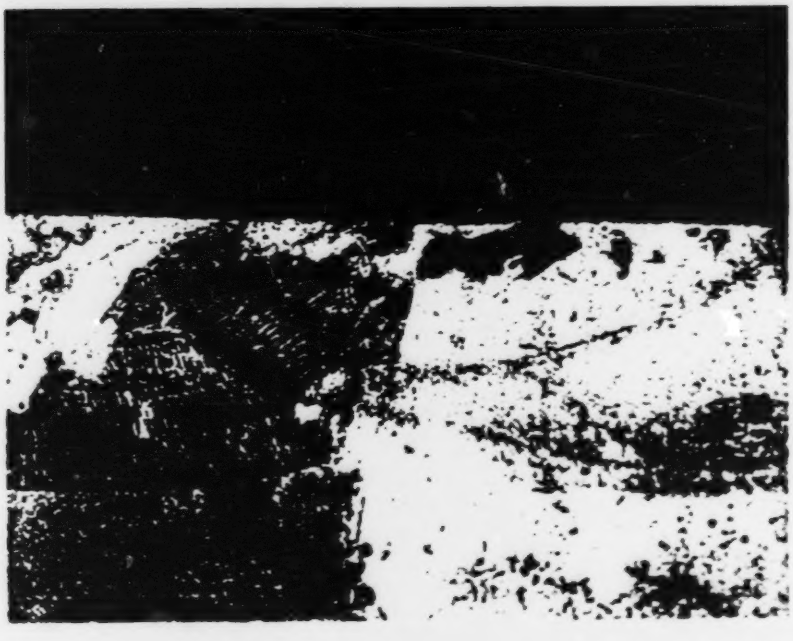

Figure 18: Coupon 610-13, Area 1 (end), X200

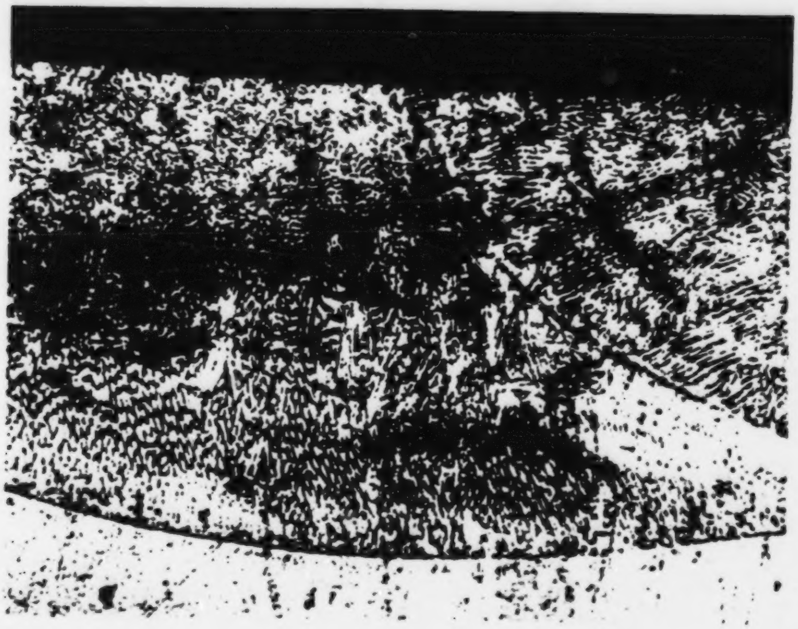

Figure 19: Coupon 610-13, Area 1 (start), X400

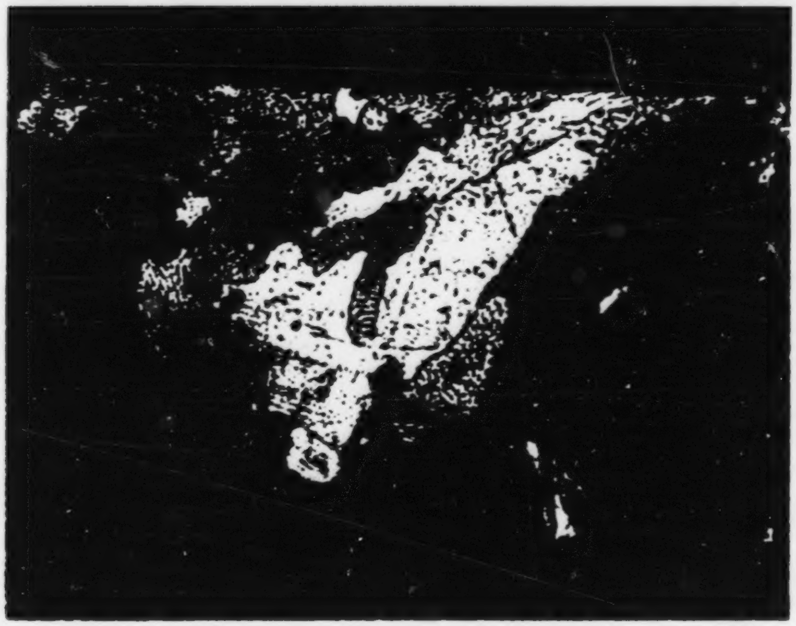

Figure 20: Coupon 610-13, Area 1 (end), X400

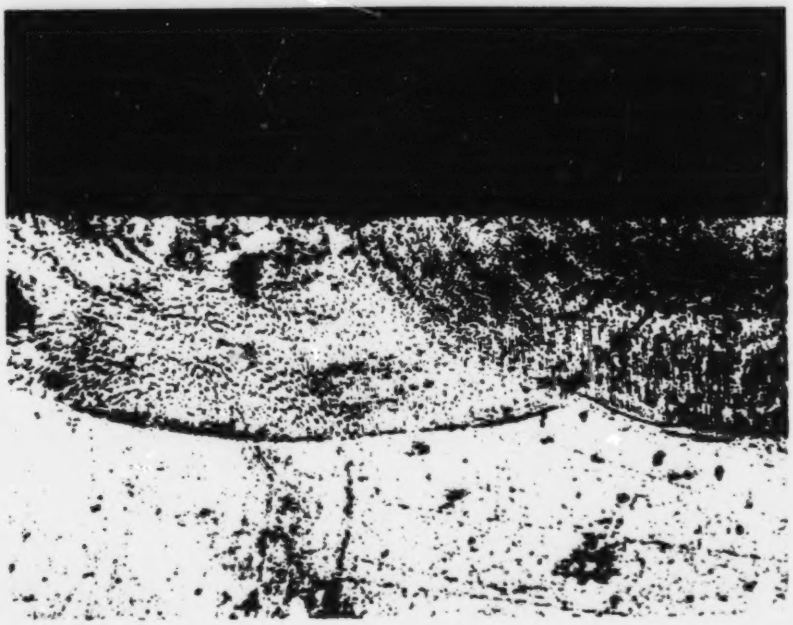

Figure 21: Coupon 610-13, Area 2 (start), X200

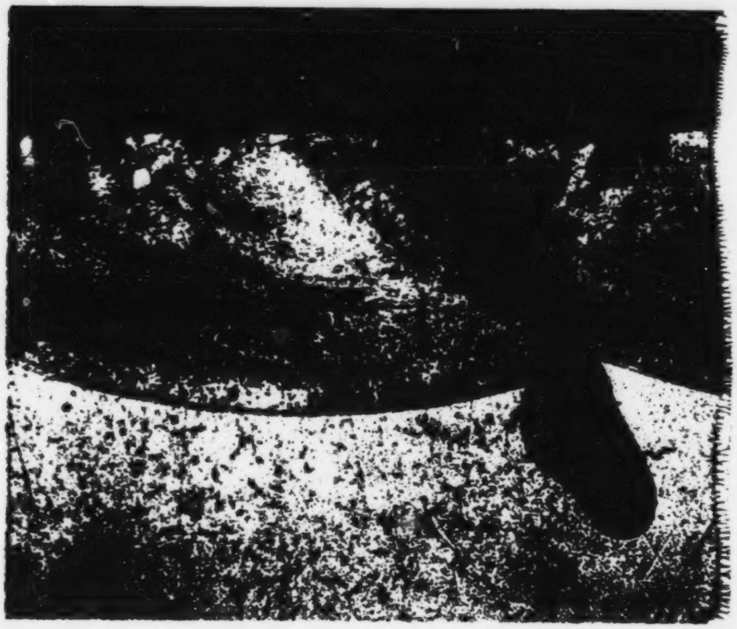

Figure 22: Coupon 610-13, Area 2 (middle), X200

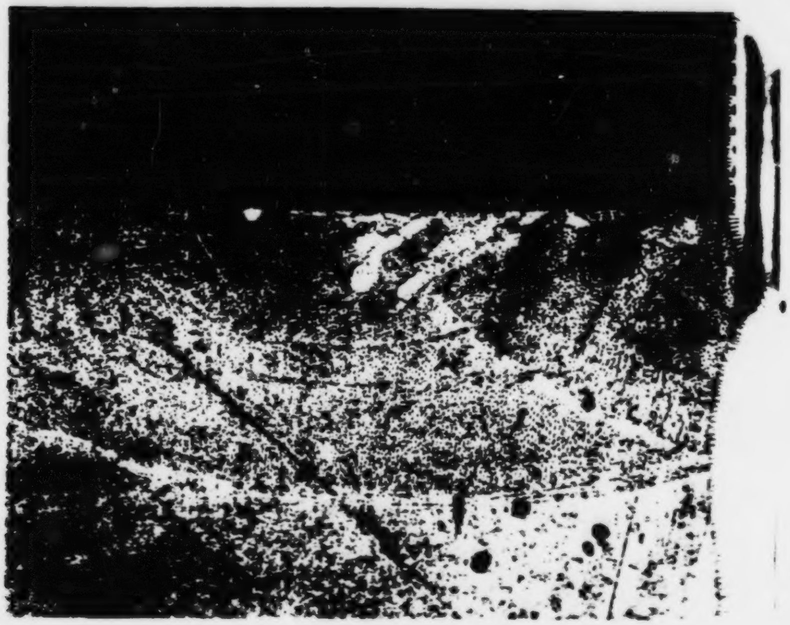

Figure 23: Coupon 610-13, Area 2 (end), X200

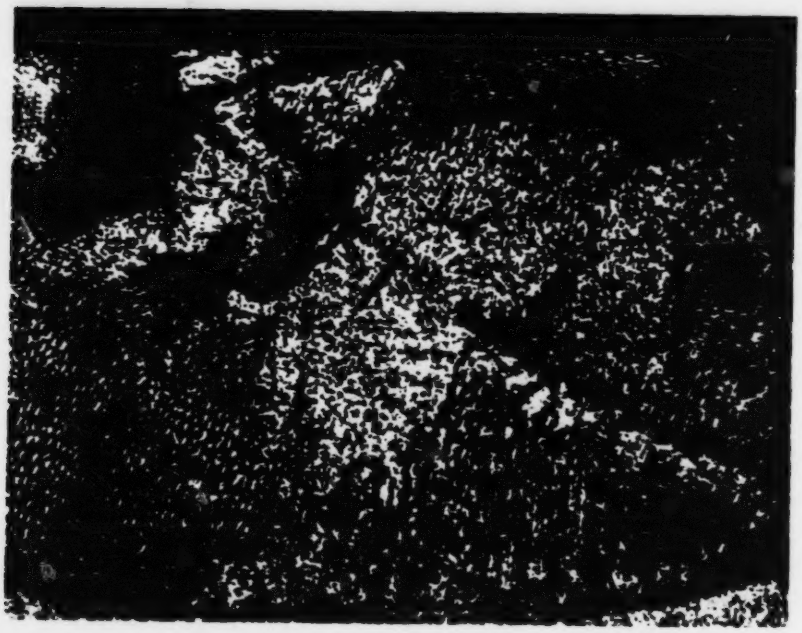

Figure 24: Coupon 610-13, Area 2 (middle), X400

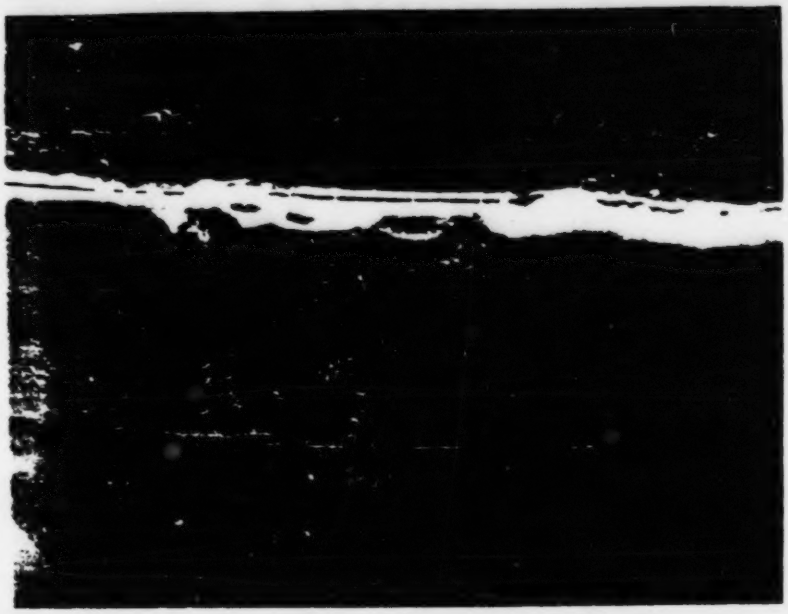

Figure 25: Coupon 610-11, Area 1, SEM view

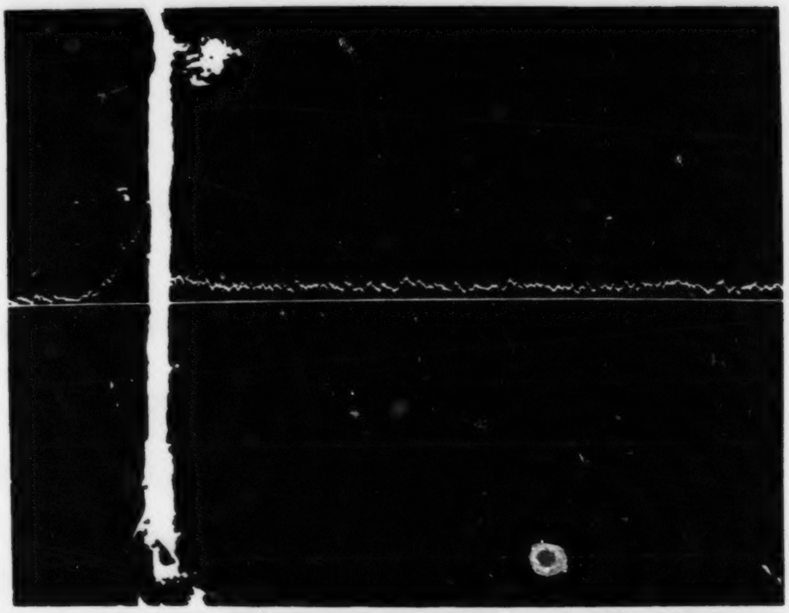

Figure 26: Coupon 610-11, Area 1, Fe line scan

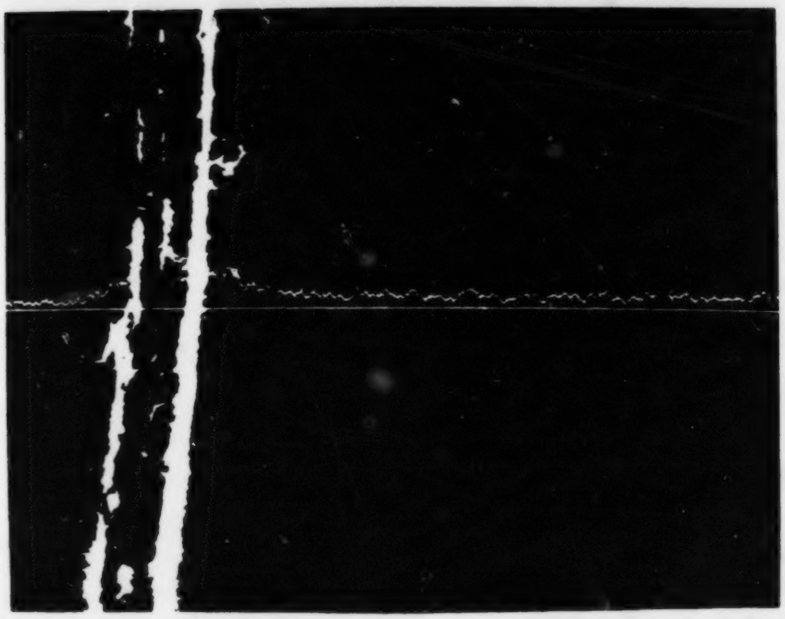

Figure 27: Coupon 610-11, Area 2, Fe line scan

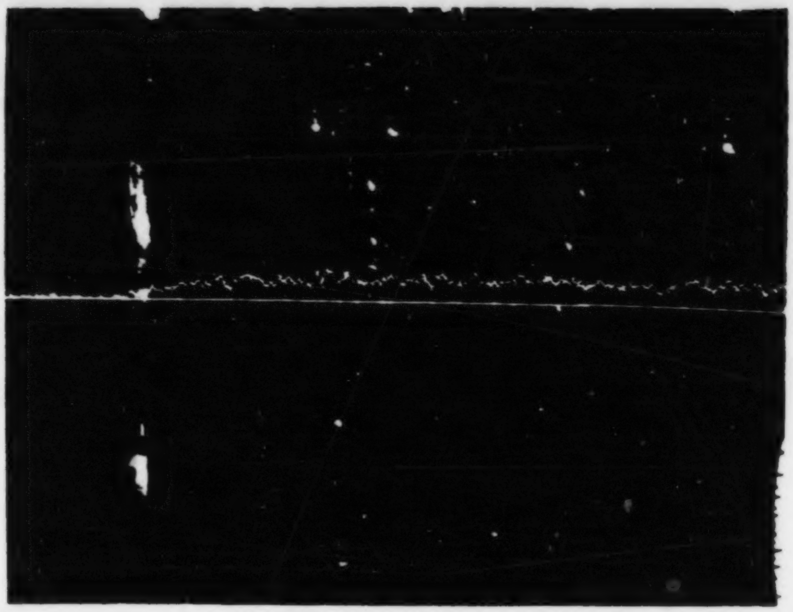

Figure 28: Coupon 610-11, Area 3,
Fe line scan

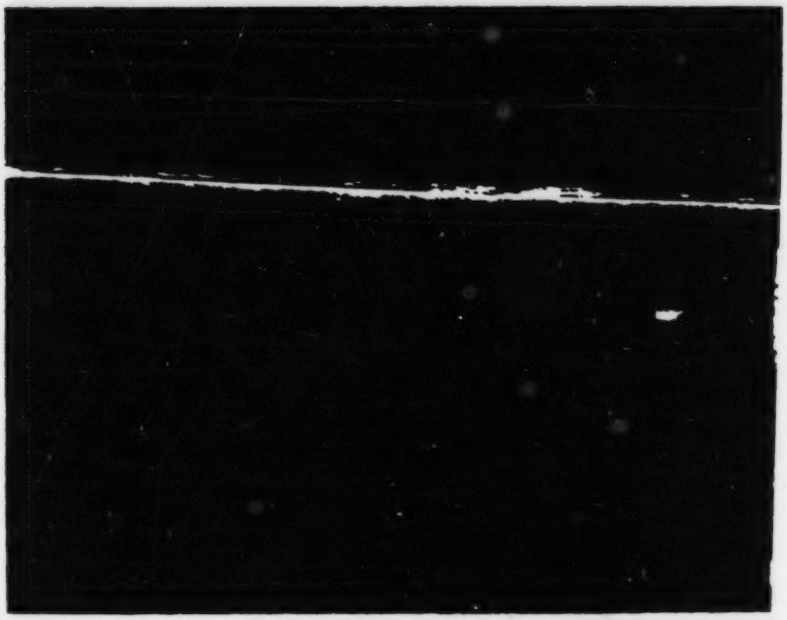

Figure 29: Coupon 610-12, Area 2,
SEM view

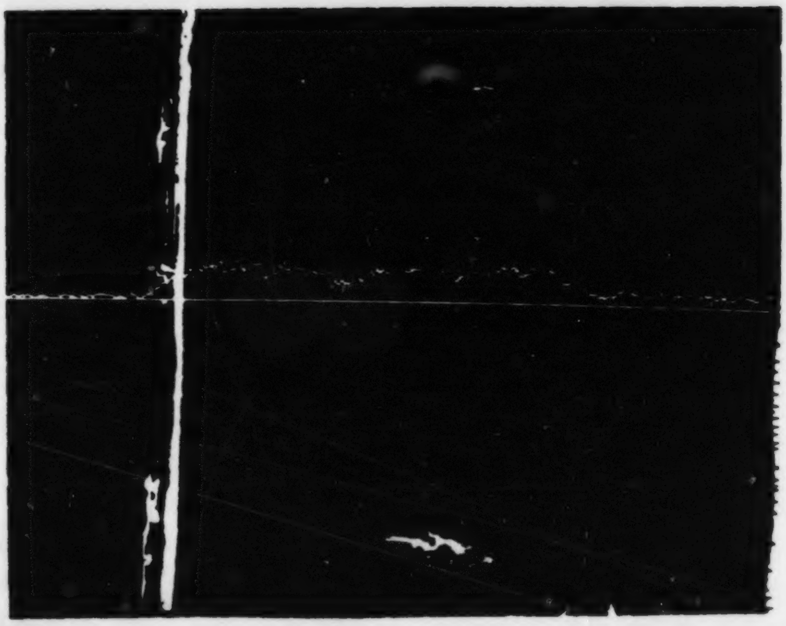

Figure 30: Coupon 610-12, Area 2,
Fe line scan

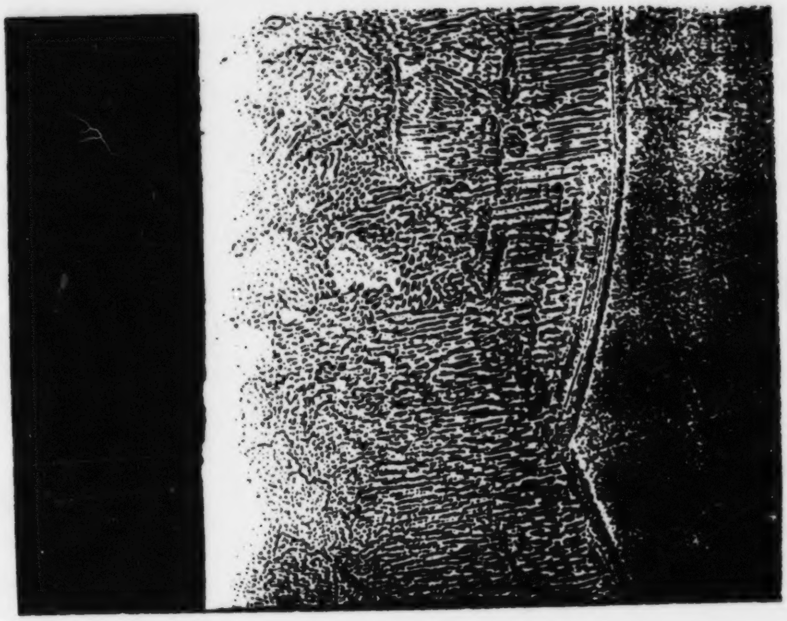

Figure 31: Coupon 610-12, Area 2,
SEM-BSE image

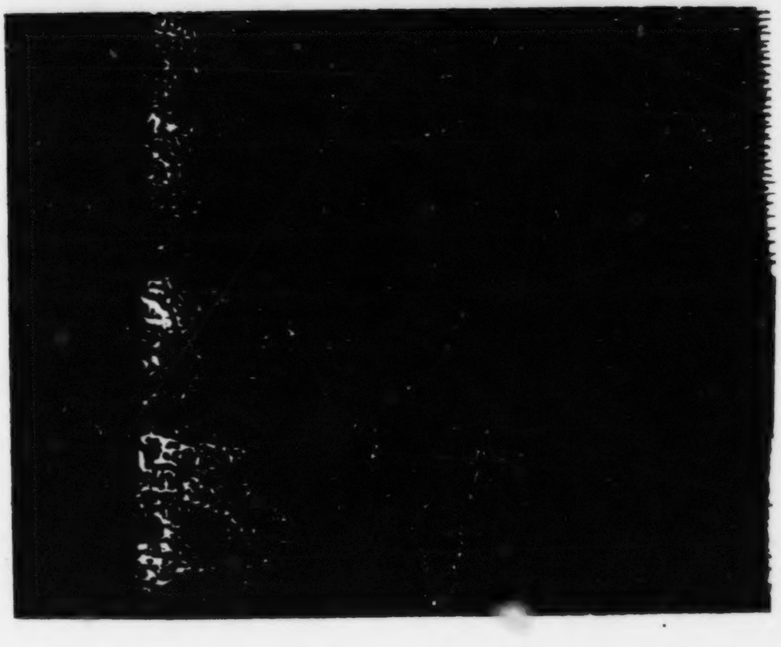

Figure 32: Coupon 610-13, Area 2,
SEM-BSE image